An experimental study of diamond and the nitrogen vacancy centre as a source of single photons

Malehlohonolo Semonyo

Submitted in fulfillment of the academic
requirements for the degree of
Master of Science in the
School of Physics,
University of KwaZulu-Natal,
Westville.

November 2009

Abstract

For applications in Quantum Information and Quantum Key Distribution an on-demand source of single photons is desirable because absolute security is of utmost importance. Photons are quantum systems; hence encoding information onto them offers a secure alternative to classical cryptography as a measurement cannot be performed on photons without altering their properties. The Nitrogen Vacancy (NV) centre in diamond is a good source of such photons. It is photo-stable and its location in diamond offers robustness. It has zero phonon line at 637 nm and its relative short luminescence life-time of about 12 ns makes it suitable for generating single photons. This thesis covers two aspects: Firstly the characterization of defects in diamonds and subsequent selection of diamonds suitable for use in the single photon setup and secondly, the development of the experimental setup for single photon generation.

This thesis sets out to describe the development of a laboratory based single photon source using the NV centre in diamond. For this purpose a suite of diamond samples were selected and subjected to various spectroscopic tests in order to characterize and classify the samples, especially the presence of the NV centres and their concentrations. The characterization of the defects was done through the use of the following spectroscopic techniques: Ultraviolet-Visible-Near infrared spectroscopy, Infrared spectroscopy, Electron Spin Resonance and Photoluminescence. These techniques enabled us to understand the types and origins of crystal defects that were present in the diamond samples used in this study and to use this to select diamonds that are most suitable for use in generation of single photons.

The experimental setup for single photon generation using the NV centre is based on a confocal microscope arrangement. Single NV centres were identified by measuring the second order autocorrelation function of the fluorescence light emitted by the sample when illuminated with a laser. This measurement was done using a Hanbury-Brown Twiss (HBT) interferometer.

Preface

The experimental work described in this dissertation was carried out in the School of Physics, University of KwaZulu-Natal, Westille Campus, Durban, from the period commencing March 2006 to July 2009 under the supervision of Dr. Kessie Govender.

These studies represent original work by the author and have not otherwise been submitted in any form for any degree or diploma to any other tertiary institution. Where use has been made of the work of others it is duly acknowledged in the text.

Declaration

I Malehlohonolo Semonyo, declare that

i. The research reported in this thesis, except where otherwise indicated, is my original work.

ii. This thesis has not been submitted for any degree or examination at any other university.

iii. This thesis does not contain other persons' data, pictures, graphs or other information, unless specifically acknowledged as being sourced from other persons.

iv. This thesis does not contain other persons' writing, unless specifically acknowledged as being sourced from other researchers. Where other written sources have been quoted, then:
    a. Their words have been re-written but the general information attributed to them has been referenced;
    b. where their exact words have been used, their writing has been placed inside quotation marks, and referenced.

v. This thesis does not contain text, graphics or tables copied and pasted from the Internet, unless specifically acknowledged, and the source being detailed in the thesis and in the References sections.

Signed:

Contents

List of Figures

Chapter 1

Introduction

1.1 Quantum Cryptography

Cryptography is the science of keeping messages secure and it deals with all aspects of authentication, digital signatures, electronic money and other applications. Classically, there are two branches of cryptography**: secret key encryption** and **public key encryption**. In secret key cryptosystem, a common key that is used to both encrypt and decrypt the message is shared by the two users. The main problem is the establishment and sharing of the key securely. Public key cryptosystem uses two keys, one made public to encrypt the message and the other (known only to the receiver) for decryption. The security of public key cryptosystem is based on the assumed computational complexity [1]. This assumption has been invalidated by the introduction of Shor's algorithm in 1994 by Peter Shor. This is a quantum algorithm for integer factorization and can be used to break the security of public key cryptosystems on a quantum computer [2].

Such flaws, as in these two systems cannot be tolerated in modern society where secure communications is of utmost importance. A principle in Quantum Mechanics offers a promising solution to this problem. It says that a measurement cannot be performed on a quantum system without altering it. If information can be encoded into such quantum systems, for example, photons, then any attempts to get the information by measuring their properties will cause changes, leading to the detection of any eavesdroppers on the communication [3].

The encoding of data onto orthogonal states of a quantum system is known as Quantum Cryptography and its security relies on the fact that these states cannot be copied. Quantum Cryptography has been an object of strong interest in recent years [4] and has already been

extended into commercial products [5]. The ability to manipulate a quantum state such as the polarization of a single photon, leads to applications that are not achievable in the classical context. One such application is the transmission of an unconditionally secure information using Quantum Key Distribution (QKD) [6]. The first QKD protocol was proposed in 1984 by Bennett and Brassard [7]. It uses four basis states: horizontal $|H\rangle$ and vertical $|V\rangle$ (rectilinear basis) ⊕ and right-circular $|\circlearrowright\rangle$ and left-circular $|\circlearrowleft\rangle$ (circular basis O). The basis states are conventionally assigned a binary value 1 and the binary value 0.

A sender (traditionally called Alice) sends a random sequence of photons chosen from the four orthogonal polarization states. The receiver (called Bob) measures the photons' polarizations in a random sequence of bases: rectilinear ⊕ and circular O and whenever their basis choices are the same, then their results are correlated. During transmission, the two bases are interchanged randomly so that the receiver who uses a wrong basis receives a superposition state (Eqn. 1.1)

$$(|\circlearrowright\rangle = (|H\rangle + |V\rangle)/\sqrt{2}). \qquad (1.1)$$

Therefore, his results will contain a 50 % error. After this Bob tells Alice his choice of basis for each photon received and they keep only those with the same basis choice. However, when the eavesdropper uses a wrong basis in the course of transmission, she has no way of comparing the sent basis and she will thus retransmit 25% erroneous results. The kept data is then interpreted as a binary sequence known as the *sift-key*. The next step is error correction using classical algorithms and privacy amplification [8].

There have been other protocols developed for QKD, for example, using EPR entangled pairs [9] and using phase modulation rather than polarization of the photons [10].

A crucial requirement for the implementation of QKD is the efficient generation of single photons on demand. Single photons present a number of advantages:

a. They are in principle identical and indistinguishable.
b. They are weakly coupled to the environment.
c. They are propagating particles, making transportation of information easy.

Considerable progress has been made in the development of suitable sources of single photons based on variety of systems; quantum dots [11, 12], parametric down-conversion [13], atoms in high-Q cavities [14], single molecules [15], colour centres [16]. A single photon source is a device that produces one and only one photon when triggered as opposed to a bunch of photons produced in a laser pulse. In the next section we will discuss these sources in detail and the details of the statistics are found in Chapter 6.

1.2 Single photon sources

1.2.1 Quantum Dots

Quantum dots are made of semiconducting material in small enough sizes to allow the electron energy levels to be treated as discrete. This situation of discrete energy levels is called quantum confinement and the semiconducting material ceases to resemble bulk but can instead be called a quantum dot. Quantum dots are very versatile compared to the traditional semiconductors and can thus be easily manipulated to achieve desirable outcomes. For example, applying a small voltage on the leads of a quantum device comprising of an array of quantum dots allows one to make precise measurements of the electron spin and other properties therein. This is very useful for applications in quantum computing [17].

The first experimental effort was based on an electrostatic repulsion of single carriers in a semiconductor p-i-n structure. The structure consists of an intrinsic undoped region sandwiched between two p- and n-doped regions. However, the experiment had to be done at milli-Kelvin temperatures and the collection efficiency achieved was insufficient to measure photon correlation function [18]. Since then there has been a significant improvement and one such advancement is the use of quantum dots for multiplexing like that in classical communication levels. In this approach, the occurrence of radiative decay cascades of multi-

particle states is exploited. Photons of different wavelengths are simultaneously emitted and can be encoded independently of each other. There are different methods of separating the photons (with varying successes) such as by using the Michelson interferometer [19].

This cascading feature has been enhanced by placing the quantum dots in a micro-cavity as demonstrated by Benyoucef *et al* [20], main advantage being that emitted photons can be guided into a desired direction. Quantum dots thus offer several advantages as single photon sources; they have large oscillator strengths, long term stability and easy integration into a device structure [21].

1.2.2 Parametric down-conversion

Photon generation by parametric down-conversion offers the prospect of heralded photons in which case the detection of one partner of a correlated pair of photons can be used to effectively create a single photon on-demand. The photon pairs are called heralded because the detection of one announces the presence of the other. This is achieved by pumping a stream of photons into a non-linear crystal which then splits them into pairs. Energy and momentum is conserved in the process, that is, the sum of the energies and the vector sum of the momentum of down-converted photons is equal to that of the incident photon. This indicates that the photon pair should be entangled in the frequency domain, hence detection of one photon indicates the presence of another [22]. The typical rate of pair generation into single mode optical fibers, corresponding to 10 mW pump power is 10^7 pairs per second. The probability of obtaining two pairs instead of one in a time slot of 10 ns is then about 1% as shown in [23].

A source of asynchronous heralded single photons based on this scheme of spontaneous down-conversion has been experimentally realized and characterized [24]. This source exhibits a very low probability of getting more than one heralding photon per signal (reduced by a factor of 500 compared to weak laser source) and thus a good probability of a single photon being produced. Parametric down-conversion photons follow a Poisson distribution, which cannot guarantee emission of just one photon per pulse.

1.2.3 Neutral atoms and ions

Neutral atoms or ions in optical cavities have been used as single photon emitters [25, 26]. The cooled atoms are allowed to fall randomly through a high finesse cavity and are driven by a periodic sequence of laser pulses. Such sources of single photons are spectrally narrow and the photons are emitted into a well defined spatial mode. However, the rate at which the system can emit photons is limited by the cavity. Other approaches have been explored such as trapping a single atom in a tight optical tweezers. In [27] a rubidium atom is trapped and illuminated with short resonant laser pulses and has shown almost perfect anti-bunching in the intensity correlation of the emitted photons, that is photons are observed individually rather than in bunches.

1.2.4 Single molecules

A single fluorescent molecule has been shown to be another source of single photons as it is able to emit only one photon at a time. The emitted light is anti-bunched and tends to consist of single photons separated by a time interval determined by the excited state lifetime and pumping rate. Louis and Moerner [28] were the first to realize the room temperature single photons using the fluorescence of a single terrylene molecule embedded in a p-terphenyl crystal host, however low signal to background ratio resulted in multi-photon detection. There are other approaches which have been taken; replacing the host crystal with a thin polymer film [29] and in other cases improving the photo-stability by working at liquid helium temperatures [30] but these compromises the practicability.

1.2.5 Colour centres

Colour centres are atomic or electronic defects of various types, which produce optical absorption bands in otherwise transparent crystal such as the alkali halides. They are produced by gamma and alpha radiation or by addition of an impurity into the crystal lattice. Colour centres in diamond have been used to demonstrate single photon generation; the

nitrogen vacancy (NV) centre [31], the nickel-nitrogen complex (NE8) [32] among others. A major advantage of diamond is the improved photo-stability due to both the rigidity of the diamond lattice and the protection it offers against highly reactive molecules such as oxygen.

1.2.5.1 NE8 complex

The NE8 complex consists of a nickel atom surrounded by four nitrogen atoms [33]. It is present in small concentrations in natural Type IIa diamonds as well as in High Pressure High Temperature synthetic diamonds where nickel has been used as a catalyst or solvent. The centre can also be fabricated in thin diamond films during Chemical Vapor Deposition synthesis in a controlled way [34]. The centre exhibits striking features at room temperature that make it an interesting candidate for fiber communications. It has a zero phonon line (ZPL) at 800nm, with the excited state having a 2 ns lifetime. It also emits a linearly polarized light [35]. The other advantage it has, as a single photon source, is the narrow emission bandwidth of 1.2 nm at room temperature.

1.2.5.2 Silicon Vacancy

This centre consists of a silicon impurity atom and a vacancy in a diamond lattice structure. It has been shown to exhibit single photon emission characteristics: it has a sharp ZPL at 738 nm with only weak sidebands at room temperature and a very short photoluminescence lifetime of only about 4 ns at room temperature [36]. It has a high photo-stability and narrow emission bandwidth (about 5 nm) at room temperature but its main drawback is the non-radiative transitions which lower the brightness and hence the emission efficiency [37].

1.2.5.3 NV centre

The nitrogen vacancy centre consists of a substitutional nitrogen atom adjacent to a vacant lattice site in a diamond crystal. It can be created in diamonds which already contain nitrogen atom by electron irradiation, this knocks off some of the carbon atoms. Subsequent annealing

at temperatures above 900 ^{0}C causes the vacancies to become mobile and they migrate towards the nitrogen atoms [38]. It has a ZPL at 637nm and an excited state lifetime of about 11.6 ns [39], it exhibits strong photo-stability at room temperature [40] but its main drawback is a broad emission bandwidth of about 120 nm. Its key advantages however are robustness against environmental noise and easy experimental set-ups.

1.3 Research outline

The aim of this thesis is to study the nitrogen vacancy centre in diamond. The main interest is its ability to emit single photons when illuminated with a laser of suitable wavelength without experiencing photochemical destruction of its ability to fluoresce (also known as photo-bleaching). Different spectroscopic techniques were employed to characterize the centre: Ultraviolet-visible-Near Infrared (UV-Vis-NIR), Fourier Transform Infrared (FTIR), Electron Spin Resonance (ESR) and Photoluminescence (PL). These techniques allowed us to select possible candidates for single photon generation from a suite of diamond samples of different types. Thus, this thesis is divided into two parts; the characterization of the NV centre in diamond by use of the fore-mentioned techniques and development of a single photon source using diamonds that have NV centres that are located in different environments.

Chapter 2

Diamond

2.1 Elementary properties

The understanding of the chemistry of diamond relies on the basic knowledge of the carbon element. A neutral carbon (C) is the sixth element in the periodic table and it has six protons and six neutrons in its nucleus balanced by six electrons which orbit the nucleus. The C atom adopts the electronic configuration of $1s^2 2s^2 2p^2$. It has a valence of four, that is, it has two valence electrons in s-orbital and two in p-orbital. If one looks at the electronic configuration of a carbon atom (Figure 2.1), one observes that there are only two unpaired electrons but to form a closed shell, four additional electrons are needed. To explain why carbon is tetravalent instead of divalent as might be expected from looking at the configuration, we look at the theory of Hybridization of Atomic Orbital [41].

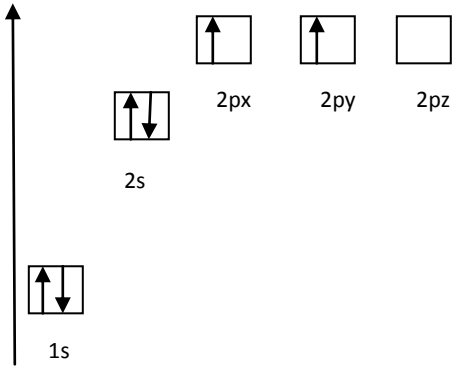

Figure 2.1 The electronic configuration of a carbon atom with the two unpaired electrons. Looking at this, it appears that only two electrons will be needed to form a bond, whereas for diamond four are needed.

This theory says that carbon atoms undergo one of three hybridizations depending on the energy available. If carbon underwent *sp* hybridization, then it would form a triplet bond and a single bond with two other atoms (as in acetylene). If it underwent sp^2 hybridization, it would form one double bond and two single bonds with other atoms (e.g. graphite, benzene, and ethane). Lastly, if it underwent sp^3 hybridization, it would form four single bonds with other atoms (e.g. methane, diamond).

Diamond is made up of repeating units of carbon atoms joined to four other carbon atoms through covalent bonding. Each carbon atom is in an incompressible tetrahedral network where it is equidistant from its neighbouring carbon atoms. This network is very stable and rigid, giving diamond its renowned material hardness. Diamond can only be scratched by another diamond. Diamond is also known for its highest room temperature thermal conductivity compared to any other standard solid.

2.1.1 Crystal structure

The crystal structure of diamond is equivalent to a face-centreed cubic (FCC) lattice with a basis of two carbon atoms at each lattice point as illustrated by Figure 2.2. Its structural unit consists of eight atoms, arranged in a cube. Using this cubic form and its highly symmetrical arrangement of atoms, diamond crystals can develop in a variety of different shapes known as "crystal habits." The octahedron or eight-sided shape that we associate with diamond is its most common crystal habit. But diamond crystals can also form cubes, dodecahedra, and even combinations of these shapes. All of these shapes are manifestations of the cubic crystal system to which the mineral diamond belongs. Two exceptions are the flat form called a macle, which is actually a composite crystal, and etched crystals, which have rounded surfaces and, sometimes, elongated shapes.

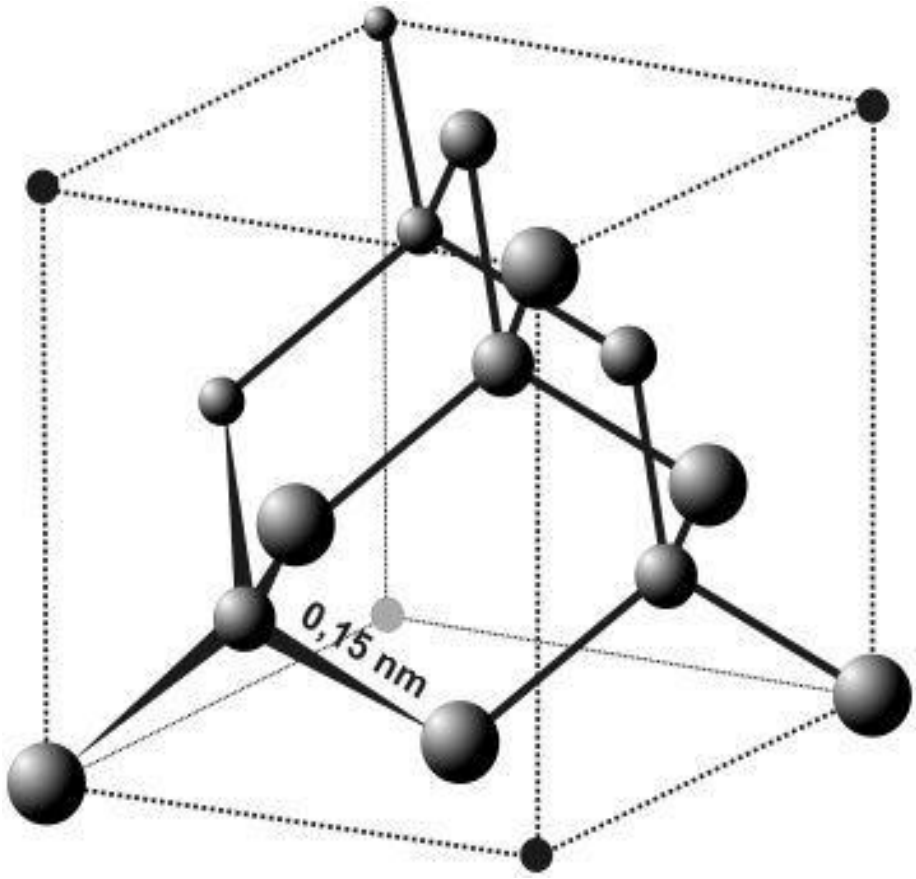

Figure 2.2 The conventional unit cell of diamond. The lattice parameter *a,* has been found to be approximately 0.357 nm [42].

The standard cubic unit cell of a normal diamond has a side length *a* measured to be 0.357 nm (approximately 3.5 Å) at room temperature. The conventional cell consists of eight carbon atoms; the atomic number density *n* can be calculated using the following formula,

$$n = \frac{N}{V}, \tag{2.1}$$

where N is the total number of atoms and V= a^3 is the volume, hence $n \approx 1.76 \times 10^{23}$ cm^{-3}. The density of a perfect diamond is given by $\rho = nA/N_0$, where N_0 is Avogadro's number

(6.023×10^{23} mol^{-1}) and A (12.0107 u) is the mean atomic mass of carbon. The experimental value of the density of diamond differs somewhat from the theoretical value because of the presence of impurity atoms and crystal imperfections.

2.1.2 Defects

It is not uncommon for the regular patterns of the atomic arrangement in the crystal lattice of a diamond to be interrupted by crystal defects. These may be present in the form of vacancies (these are unoccupied sites in the lattice which are normally occupied by an atom), interstitials (atoms which occupy a site at which there isn't usually an atom) as well as impurities (these are foreign atoms that are incorporated at a regular atomic site in the crystal).

The most common impurity atoms in diamond, which are incorporated as substitutional atoms, that is, they replace the carbon atoms, are that of nitrogen (as identified by Kaiser and Bond in 1959) [43] and boron. These are responsible for the colouring (boron gives diamond a blue tint while nitrogen is responsible for the yellow colour) and are also used in the classification of diamond. Nitrogen also dominates the optical properties of diamond, giving rise to strong absorption bands at the visible, infrared and ultraviolet wavelength and these properties will be investigated in Chapter 3. There are other substitutional impurities that can be found in diamond such as silicon and oxygen, which is believed to be in inclusions or within a few atomic layers of the surface [44].

2.1.3 Classification of diamond

Nitrogen is the dominant impurity in diamond therefore diamonds are classified according to the amount of nitrogen they contain [45]. Diamonds that contain nitrogen in high concentrations are classified as Type I and represent almost all natural diamonds. Those that contain a significantly low concentration of nitrogen are classified as Type II.

These types are further subdivided as follows:

- **Type I**: Contain nitrogen atoms in high concentrations.

➢ **Type Ia**: Nitrogen atoms appear as clusters of substitutional atoms, that is, the presence of these nitrogen atoms does not have a significant effect on the density of diamonds. They appear in concentrations of approximately 2500ppm.

➢ **Type IaA**: Nitrogen atoms are normally found in aggregates where their electrons tend to pair up, thus this centre consists of two paired nitrogen atoms.

➢ **Type IaB**: The B centre has a highly aggregated form of nitrogen. It appears as four nitrogen atoms tetrahedrally sited about a vacancy.

➢ **Type Ib**: Nitrogen exists as single substitutional atoms, homogeneously dispersed throughout the diamond sample. Nitrogen can absorb light in the blue end of the spectrum, bringing out the yellow colour that is complementary to blue. Diamonds of this type are therefore usually yellow in colour. Almost all synthetic diamonds are of this type.

- **Type II**: Contain no nitrogen or significantly low concentrations of nitrogen atoms.

➢ **Type IIa**: The A centre, B centre and single nitrogen concentrations are below 1 – 2 atomic ppm, too weak to detect using conventional infrared (IR) instrumentations. This type is not a semiconductor.

➢ **Type IIb**: Absorption bands due to the presence of nitrogen in the IR absorption spectra are also undetectable but the presence of boron atoms give this type semiconducting abilities.

2.2 Synthetic diamonds

Synthetic diamonds are diamonds that are produced through physical and chemical processes under laboratory conditions which are similar to those at 140 km to 200 km below the surface of the earth where natural diamonds are formed. These synthetics are made up of carbon with physical properties and crystallographic structure just like natural diamonds. There are two methods of synthesizing diamond, namely, High Pressure High Temperature technique (HPHT) and Chemical Vapor Deposition (CVD).

2.2.1 High Pressure High Temperature (HPHT)

This is a synthesis technique in which transition to a different phase of material of higher density and often higher coordination numbers of atoms involved occurs. For diamond, this number is four since each carbon atom at a centre of a tetrahedron formed by four other carbon atoms. To recreate the high pressure and high temperature conditions that are found below the earth's surface, a number of HPHT methods have been developed. The two main designs are the Belt press and the Cubic press which are discussed below.

2.2.1.1 Belt press

In the formation of diamond by this process, carbon source, for example, graphite and a metallic catalyst are placed in a hydraulic press under HPHT as shown in Figure 2.3 (typical transformation conditions are P ≈ 13GPa and T ≈ 3000 ^{0}C). The pressure required is supplied by the two anvils that are placed at opposite ends to the prepared sample. The inside of the press is heated by a tube-like graphite heater generating temperatures above 1800 ^{0}C and thus melting the solvent metal. The molten metal then dissolves the high purity carbon source and over a period of a few hours, graphite converts to diamond. That is, coordination of carbon atoms increases from three to four.

The resulting diamonds are usually a few millimeters in size and are often too small to be used as gemstones but are highly useful for industrial applications as drill bits and edges for cutting tools.

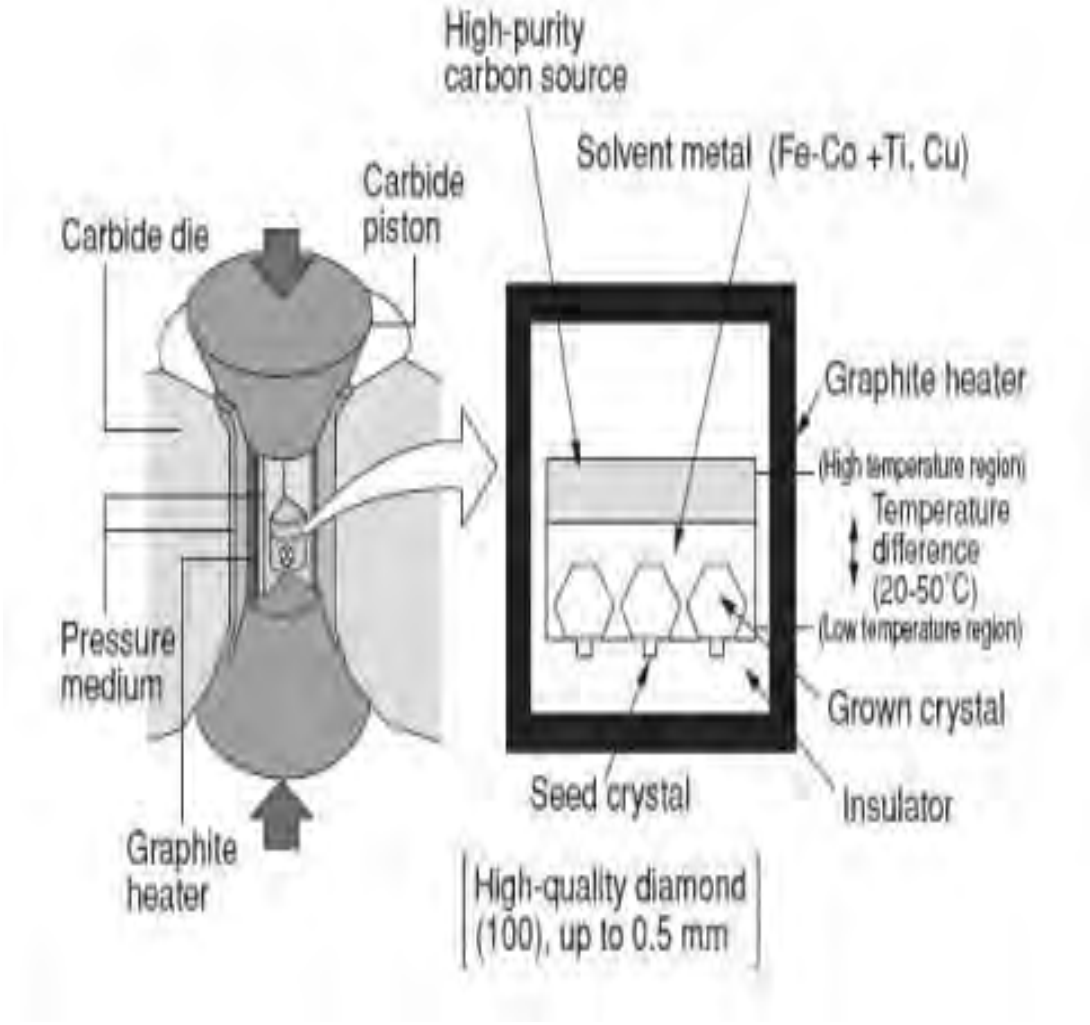

Figure 2.3. Schematic representation of the Belt press HPHT system. The element Ti in the solvent metal is useful for creation of diamond sample with significantly low concentrations of nitrogen (Type II) and Cu is needed to prevent the formation of TiC [46].

2.2.1.2 Cubic press

The cubic press consists of six anvils which provide equal pressure simultaneously to a cube shaped volume. This is usually smaller than a belt press and can achieve the required temperature and pressure necessary for the creation of synthetic diamond relatively faster.

2.2.2 Chemical Vapor Deposition

In this process diamond is produced by energizing mixtures of hydrogen and hydrocarbon gases with heat or electrical energy in a chamber. A region of ionized gas (plasma) drives the complex chemistry which causes diamond to form on objects called substrates placed in the chamber. There are a number of plasma CVD techniques that have been developed over the years, for example, radiofrequency plasma CVD, microwave plasma CVD and remote plasma-enhanced CVD, to name a few. There are also other methods of synthesizing diamonds by CVD that are classified by physical properties of vapor or the operating pressure [47].

All the deposition techniques rely on the ability to set up a dynamic non-equilibrium system in which only sp^3 carbon bonding can survive. This is achieved by the presence of hydrocarbon radicals, and more importantly by large quantities of atomic hydrogen in the deposition gas. The most important role of the atomic hydrogen is to eliminating the sp^2 bonded carbon while stabilizing the dangling bonds of the tetrahedrally bonded carbon sp^3.

Synthetic diamonds are made in a relatively short time and are not kept at high temperature high pressure conditions for long periods of time, therefore the nitrogen atoms trapped in the lattice do not get an opportunity to aggregate. This results in most synthetic diamonds being of Type Ib, yellowish in colour and paramagnetic. Those that are made under conditions where nitrogen is specifically excluded are of Type II and are colourless.

2.3 Nitrogen related impurities

Nitrogen is present in diamonds in many forms and concentrations. In those samples that are synthesized by the conventional high pressure high temperature method, nitrogen impurities occur as single substitutional atoms, while most natural diamonds contain nitrogen in the form of aggregates of substitutional atoms. The nitrogen aggregates that occur most commonly in diamonds are the A centre and the B centre but nitrogen can also be present in diamond in lesser concentrations as aggregates of three substitutional nitrogen atoms neighbouring a vacancy (the N3 centre) [48]. The optical absorption and other material properties of the diamonds with such impurities are highly dependent on the nitrogen content and the way it is configured.

In diamonds that contain vacancies (formed when a sample is irradiated with neutrons or electrons), other centres can be formed when these vacancies become mobile and migrate towards the nitrogen atoms. These centres are described as follows:

- H3 centre – this is the defect that forms when a vacancy is trapped by two adjacent nitrogen atoms (the A centre) [49].
- H4 centre – this centre forms when the B centre traps a vacancy.
- NV centre – a single substitutional atom traps a vacancy for this centre to be formed.

Concentrations of the single substitutional nitrogen centres can be determined accurately by Electron Spin Resonance and that of the A and H4 centres can only be detected by infrared (IR) or ultraviolet (UV) absorption[1] [50]. All the nitrogen-vacancy related centres mentioned above also produce zero-phonon lines (ZPLs) in optical absorption and photoluminescence and can therefore be detected with high sensitivity. A detailed description of these pectroscopic techniques used in the characterization of one of the nitrogen related centre, the nitrogen-vacancy centre will be given in the next chapter.

[1] The amount of nitrogen and its configuration in diamond are two factors that are highly influential on optical absorption as well as other material properties of diamond.

2.3.1 The nitrogen vacancy centre

So far, we have seen that diamonds are not just carbon, they also contain various elements (as impurities) at low concentrations, one of which is nitrogen. The crystalline lattice that makes up diamond can also exhibit various defects. When a carbon atom is missing from its place in the lattice, it is called a vacancy. Heating the diamond sample with such vacancies and impurity nitrogen atoms, allows the vacancies to diffuse through the lattice and when they meet a nitrogen atom it becomes energetically favorable for them to remain besides each other, resulting in what is known as a Nitrogen –Vacancy (NV) defect, see Figure 2.4. Focused implantation of single nitrogen atoms in the creation of this colour centre is an important step for the development of single photon generators, and other applications in quantum information processing as well as quantum cryptography.

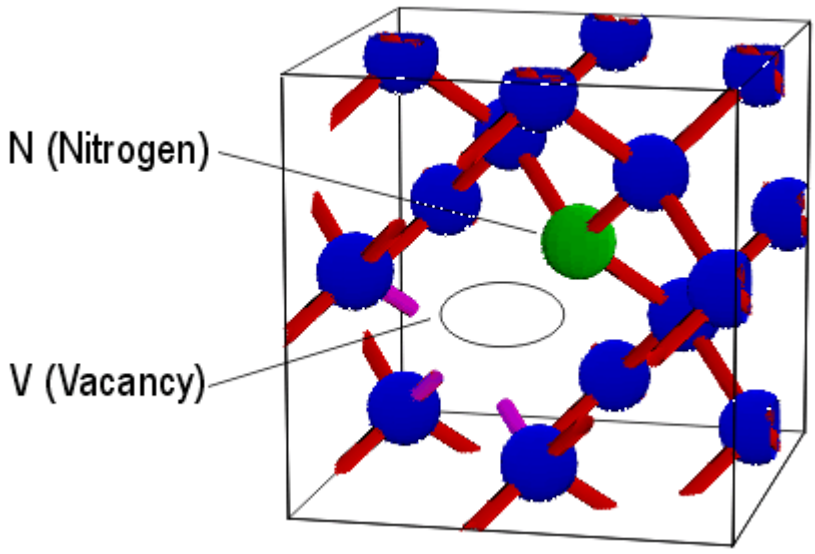

Figure 2.4 Atomic structure of the NV centre. The green ball represents substitutional nitrogen atom and the white ball the vacancy, i.e. the site where there is normally a carbon atom [51].

There are two methods of creating this defect in diamond: (1) vacancy creation in a diamond sample that is rich in nitrogen impurity atoms by ion implantation and (2) implantation of nitrogen atoms in a diamond sample that contains significantly low concentrations of

substitutional impurity nitrogen atoms. Subsequent annealing in both cases at temperatures above 600^{o}C initiates migration of vacancies towards nitrogen atoms, thus creating NV centres.

2.3.1.1 Creation of vacancies

Irradiation of a diamond sample with inert ions (for example helium) can result in the formation of NV centres depending on the pre-existence of nitrogen in the sample. The ions create vacancies by knocking off some of the carbon atoms and subsequent annealing at temperatures above 600^{0}C will cause the vacancies to migrate towards the nitrogen atoms thus forming the NV centre. The resultant concentration of the centres is dependent primarily on the concentration of the native nitrogen atoms in the track of the implanted ion. Irradiation with neutrons, protons and electrons has also been employed for NV centre formation through this method [52]. Since this technique forms NV centres from nitrogen already present in the diamond, it is best suited for creation of small ensembles of centres.

2.3.1.2 Direct implantation of single nitrogen ions

Creation of NV centres by use of this method allows deterministic control of the number of centres created in a given region. This can be achieved by implantation of single nitrogen ions in an ultra pure diamond with very little or no native nitrogen atoms (Type IIa) followed by annealing. It is also desirable that each nitrogen atom implanted creates a single NV centre so that there is no excess. However, this is difficult to ascertain as differentiating between implanted and native atoms is difficult. Meijer *et al* [53] have created an array of NV centres by irradiating a Type IIa diamond with native nitrogen content less than 0.1 ppm with a beam of 2 MeV N^{+} ions with diameter 0.3 μm. They have achieved a regular pattern through raster scanning the beam over the diamond sample, that is, by sweeping the beam horizontally from left to right at a steady rate while increasing the vertical position slowly. To sweep the next line, the beam is switched off as it is returned to the right and the same procedure is repeated.

The difficulty of determining the number of NV centre formed from implanted ions can be overcome by implanting with ^{15}N ions as they have spin ½, hence a different hyperfine spectrum from native ^{14}N ions. The number of nitrogen atoms implanted can be determined from the amount of nitrogen that flows per unit area per unit implantation time [54].

2.3.2 The electronic structure of the NV centre

The electronic structure of the centre as determined from experiments can be summarized using an energy level diagram shown in Figure 2.5. The ground state has been confirmed to be an electron spin triplet state with spin sublevels $m_S = 0$ and $m_S = \pm 1$. Owing to the C_{3v} symmetry of the centre, the $m_S = \pm 1$ sublevels are degenerate with a zero-field splitting from $m_S = 0$ of D_{gs} = 2.88 GHz. The ground state has a group representation of ^3A. The excited state ^3E is also a triplet state with similar characteristics to the ground state. There exists also a third meta-stable state ^1A which is a singlet. From Figure 2.5 we see that there are a number of possible transitions between all these states. The transition between ^3A and ^3E conserves spin as it is a dipolar transition and it gives off photons with a wavelength of 637 nm. There can also be decay from the sublevels of the excited state to the sublevels of the ground state via the meta-stable state with varying probabilities as indicated by the thickness of the arrows.

The probability of decay from the $m_S = \pm 1$ levels of the excited state to the meta-stable state has been determined from experiments and theory to be $0.4 \times 1/\tau$ [55] where τ is the lifetime (11.6 ns) and that from the $m_S = 0$ level to be $\sim 10^{-4} \times 1/\tau$ [56]. There is also a greater probability of decay from the meta-stable state to $m_S = 0$ of the ground state than there is to the $m_S = \pm 1$ level.

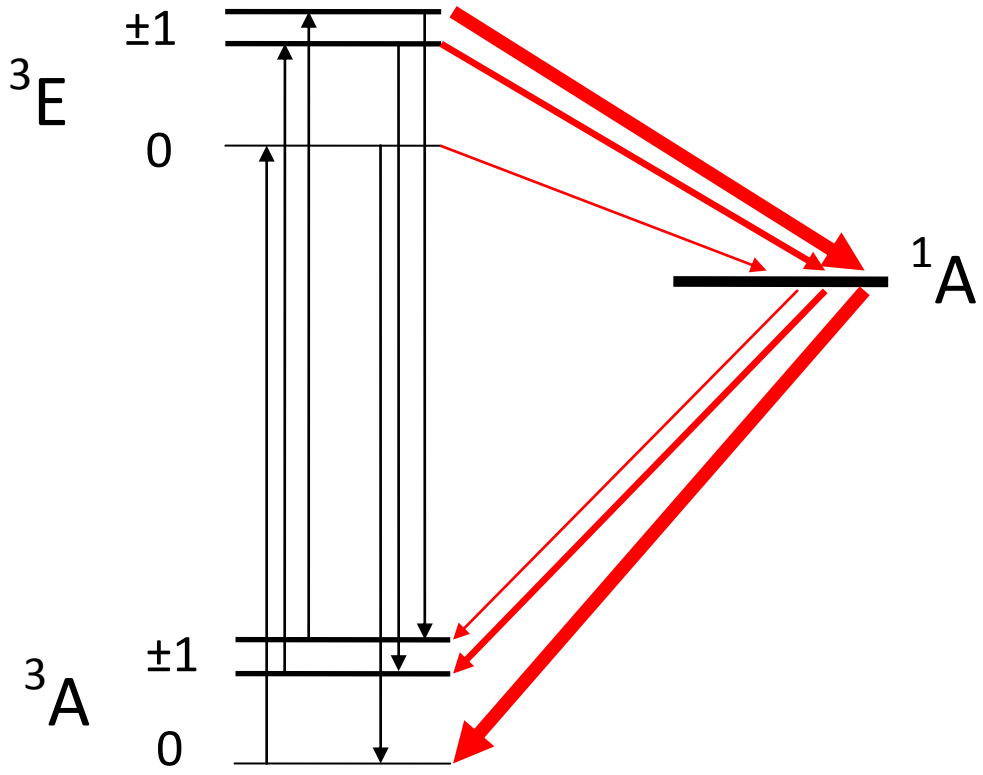

Figure 2.5 Electronic structure of the NV centre. The thicknesses of the arrows to and from the meta-stable state ^{1}A indicate the transition probabilities.

Chapter 3

Characterization of the NV centre: Experimental Techniques

3.1 Introduction

We use spectroscopy to study the interaction of electromagnetic radiation with matter. This interaction can be initiated by application of energy, for example, radiant, thermal or electrical energy. The applied energy excites or energizes the matter and as it relaxes back to ground state it can emit electromagnetic radiation. Another approach would be to examine absorbed frequencies when a continuous radiation is incident on matter.

The resultant spectra from these two approaches are called emission and absorption spectra respectively. The spectrum is mainly a graph of intensity versus wavelength, wave-number or frequency. There are three categories of spectra, (A) line spectrum which is a result of emission (single frequency) from transitions between two energy levels, (B) band spectrum which consists of radiation emitted in groups of closely spaced lines that form bands and (C) continuous spectrum where emitted radiation contains all frequencies within a region of electromagnetic spectrum. Interpretation of these spectra gives useful information about the structure or composition of substances.

Nitrogen is found in diamond in different forms, such as isolated substitutional impurity atoms or various impurity-defect complexes and aggregates. We have studied the presence of nitrogen in its different forms but mainly as an NV centre by use of the Ultraviolet-Visible-Near infrared (UV-Vis-NIR), Fourier Transform Infrared (FTIR), Electron Spin Resonance (ESR) and Photoluminescence (PL) spectroscopic techniques. These are non-destructive and quick techniques to determine the different bonding configurations of

nitrogen as well as nitrogen incorporated in substitutional sites. In this chapter we describe the theory associated with these techniques.

3.2 UV-Vis-NIR spectroscopy

Ultra violet-visible-near infrared spectroscopy is a technique used for qualitative and quantitative analysis of materials. When a sample of an unknown compound is exposed to light, certain functional groups (selection of atoms in a molecule that participate in characteristic reactions) within the molecule absorb light of different wavelengths in the ultraviolet (wavelength range: 200-400 nm), visible (400-800 nm) and near infrared (800 nm-2500 nm) regions of the spectrum. The primary measurement obtained is the UV-Vis-NIR spectrum which is a plot of absorbance versus wavelength. In the identification of diamonds, the peaks in the spectra give information about the colour centres of diamond. This is because many optically active colour centres absorb certain frequencies of light hence most optical colour centres are detected through this technique.

Here we represent the characterization of diamond samples of various types by means of this technique. The experiments were carried at the University of Witwatersrand (Department of Physics), Johannesburg. The main objective of these measurements was to identify and quantify the nitrogen defects in these samples. The UV-Vis-NIR technique is important in the measurement of absorption due to electron defects or trace elements that may cause colouring of the diamonds. The absorption spectra obtained helps with the following:

- Identification of natural and synthetic diamonds.
- Identification of treatment, i.e. heat, irradiation etc.
- Type classification of diamonds

3.2.1 Theory

The classification of the spectra in this instance is divided into two types, namely, emission and absorption spectra. The emission spectrum is obtained by analyzing light emitted by a luminous source, while the absorption spectra is obtained by spectroscopic analysis of the light transmitted by an absorbing medium placed between the light and the spectroscope. During absorption of radiation, there is an energy increase in the sample equal to the energy of the incident photon,

$$E = h\upsilon, \tag{3.1}$$

where h is Planck's constant and υ is the frequency of radiation. The change in energy may be in the electronic, vibrational or rotational energy of the absorbing medium, for example a molecule. If the molecule absorbs energy from a radiation source in the near infrared then both the vibrational and rotational energies of the molecule will change. If the energy is much greater, e.g., in the ultra violet then the changes in the electronic, vibrational and rotational energies of the molecule will take place.

Absorption intensity

The relationship between the absorption and properties of the material through which light is passing is given by the Beer-Lambert law, which states that the fraction of the incident light absorbed is proportional to the number of molecules in the path. That is,

$$A = -\log_{10}\frac{I}{I_0} = \epsilon c l, \tag{3.2}$$

where A is the absorbance, I_0 is the intensity of incident light, I is the intensity of transmitted light, ϵ is the molar extinction coefficient, l is the sample path length and c is the concentration of absorbing species in the material [57].

3.3 Infrared spectroscopy

IR spectroscopy is a technique used to identify compounds and study sample composition. The spectrum required to achieve this is collected by observing the absorption of infrared light as it passes through a sample of interest. Previously a monochromatic beam was used in which wavelengths change over time and the frequencies need to be stated precisely, but modern techniques use Fourier Transform which measures all wavelengths at once which increases accuracy and efficiency. For our study, the technique employed uses the Fourier Transform Infrared (FTIR) method and it was conducted at the Chemistry Department (University of Witwatersrand)

3.3.1 Theory

The infrared region of the spectrum ranges from 750 nm to 1 mm and photons corresponding to these wavelengths are able to excite vibrational transitions in typical covalently bonded solids. These incident photons are in the process absorbed and by plotting this absorption versus wave-number, the vibrational energies can be determined. The amount of radiation that is absorbed is also governed by the Beer-Lambert law (Equation 3.2) where I/I_0 is also known as transmittance *T*. The vibrational mode frequencies are dependent on bond lengths, masses of atoms involved and the type of vibrational mode (stretching or bending). For diamond which is monatomic, defects contribute to absorption and the absorbance (magnitude and frequency) depends on the type of bonds between the carbon atoms and the impurity atoms.

FTIR is based on a Michelson interferometer, illustrated in Figure 3.1. The parallel beam from the IR source is directed to a 50:50 beam splitter (BS) that sends half the radiation to a fixed mirror and the other half to a movable mirror. The two mirrors reflect the beams back for recombination at the BS where the half of the recombined beam goes back to the source and the remainder goes to the sample via a different path. Because the beams travel different

paths as they leave the BS, they will interfere constructively or destructively upon recombination.

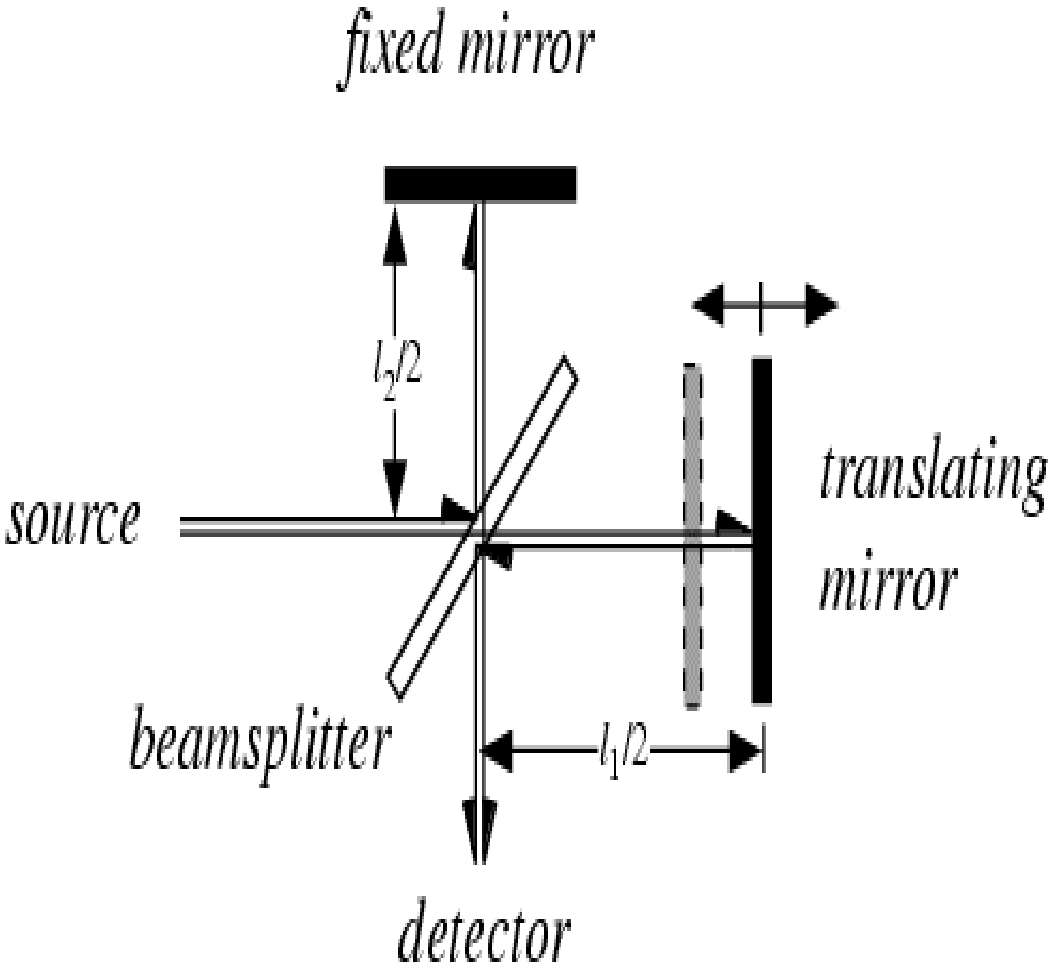

Figure 3.1 Schematic representation of the Michelson interferometer used in the FTIR spectroscopy. A beam of infrared photons with a range of frequencies is directed at a beam splitter, which directs half the intensity to each of the two mirrors. These beams are reflected back and recombine before being directed toward the sample. The transmitted beam is recorded at the detector.

The path difference can be varied by moving the movable mirror and the beam can then be sampled at small intervals and Fourier Transformed to get the beam profile. To obtain the power spectrum $G(\omega)$, intensity is recorded as a function of the path difference. To explain the Fourier Transform spectroscopy used here, first consider the intensity of the sum of two electric fields $\overrightarrow{E_1}$ and $\overrightarrow{E_2}$:

$$\overrightarrow{E_1} = \overrightarrow{E} e^{i\vec{k}\cdot\vec{r}+\omega t} \qquad (3.3)$$
$$\overrightarrow{E_2} = \overrightarrow{E} e^{i[(\vec{k}\cdot\vec{r}+\omega t)+\theta]}$$

where $\theta = kx$ is a phase shift associated with a difference in optical path. The total electric field $\vec{E}$ is given by

$$\vec{E} = \overrightarrow{E_1} + \overrightarrow{E_2}.$$

The intensity *I* is given by,

$$\begin{aligned} I &= |E|^2 \\ &= \vec{E}.\vec{E}^* \\ &= 2|E|^2 + 2|E|^2\cos\theta \\ &= (1+\cos\theta)\,2|E|^2 \end{aligned} \qquad (3.4)$$

The intensity for non-monochromatic light is given by the summation over the complete spectrum and can be written as

$$I(x) = \int_0^\infty (1+\cos kx)\, G(k)\, dk$$

$$= \int_0^\infty G(k)\, dk + \int_0^\infty G(k)\frac{e^{ikx}+e^{-ikx}}{2}\, dk$$

$$= \frac{1}{2}I(0) + \int_0^\infty G(k)\, e^{ikx}\, dk$$

or $$W(x) = 2I(x) - I(0). \qquad (3.5)$$

Where *k* is the wave-number ($\omega = ck$), x is the displacement of the translating mirror and *I (0)* is the intensity at zero path difference. Absorption is then obtained by subtracting the

beam profile from the recorded intensity and to obtain the absorption spectrum, Fourier Transform is performed on $W(x)$ [58].

3.4 Electron Spin Resonance

This is a spectroscopic technique where transitions between spin states of a paramagnetic molecule can be induced. This can be done by applying an external steady magnetic field and then supplying an electromagnetic energy, usually in the range of microwave frequencies.

The absorption spectrum can be obtained by measuring the attenuation versus wavelength or frequency of a beam of electromagnetic radiation as it passes through a sample of matter. Such spectra are known as Electron Spin Resonance (ESR) or Electron Paramagnetic Resonance (EPR) and can be used as an investigative tool in the study of the structure of molecules. Lines in the spectrum represent transitions between energy levels of a molecule, where each line measures the energy separation of two levels. From these lines, an energy level diagram can be constructed if enough data and guidance from theory is given. A selection of diamond samples were studied using this technique at the NMR laboratory in the Physics Department of the University of Witwatersrand.

3.4.1 Theory

A molecule may interact in two ways with the electromagnetic (EM) radiation. Firstly, the electric field component of the radiation may stimulate an electric dipole oscillation in the molecule and secondly, the magnetic component of the field may interact with magnetic dipoles in the field. In magnetic dipolar interactions, a static magnetic field, which can be contributed by the nuclei of the molecule, is required to ensure that absorption of incident EM radiation occurs at different frequencies. In its absence, the energy levels are coincidental. Resonant absorption occurs when the energy $h\nu$ of a quantum in the incident radiation matches the separation between the energy levels ΔE [59].

That is,

$$\Delta E = h\nu = g\mu_B H, \tag{3.6}$$

where ν denotes frequency of incident radiation expressed in Hertz and H is the steady magnetic field, μ_B is the Bohr magneton ($^{e\hbar}/_{2m_e}$) and g is the spectroscopic splitting factor which gives the proportionality between the magnetic field and energy difference between the Zeeman levels. This equation is a fundamental equation as it demonstrates the resonance condition.

Interaction of spin-half particle with external magnetic field

The phenomenon of ESR can be understood by considering a simple case of a free electron. The electron has a spin, according to Quantum Theory and this spin can be understood as an angular momentum leading to a magnetic moment. Spins can interact with the external magnetic field (Zeeman interaction) and with each other (coupling). When the electron is subjected to a steady magnetic filed H in the z direction, the electron's magnetic moment tends to align itself with the field. The relationship between the magnetic moment and the spin vector is given by

$$\vec{\mu}_S = -\frac{g\mu_B}{\hbar}\vec{S} \tag{3.7}$$

In the presence of H, the magnetic moment aligns itself parallel or anti-parallel to the field H, where $m_S = +^1/_2$ (m_S is the spin quantum number) corresponds to the anti-parallel alignment and higher energy state, whereas $m_S = -^1/_2$ corresponds to parallel alignment and lower energy state, as shown in Figure 3.2.

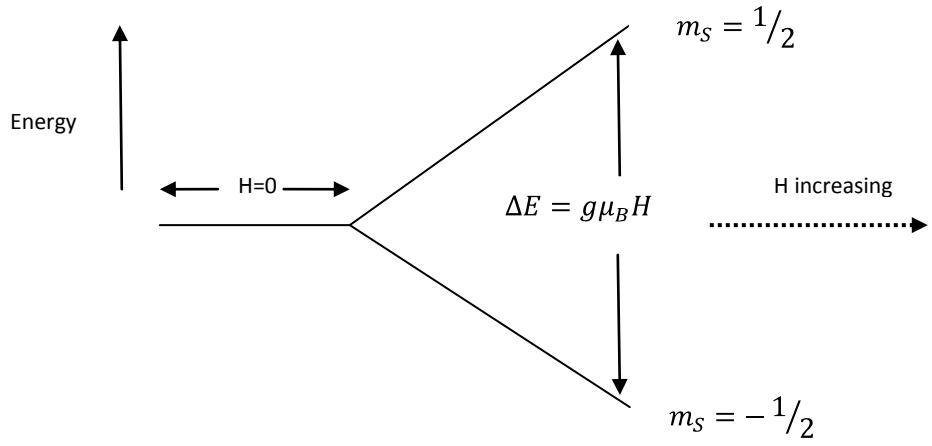

Figure 3.2 Representation of the energy levels for a simple case of a free electron in the presence of a magnetic field H.

That is,

$$\mu_Z = \pm {}^1/_2 \, g\mu_B. \tag{3.8}$$

The ensemble of energy levels then reduces to

$$E_\pm = \pm {}^1/_2 \, g\mu_B H, \tag{3.9}$$

and the energy separation between the two levels is

$$\Delta E = E_+ - E_- \; = \; g\mu_B H. \tag{3.10}$$

If a second, weaker alternating magnetic field H_1, oscillating at a microwave frequency, is applied at right angles to the main field H then the electron spin can be tipped over when the microwave frequency is equal to the precession frequency. The incoming radiation that is absorbed by these free electrons causes them to jump into a higher energy state. This radiation can also be absorbed by electrons in a higher state, causing them to go to a lower energy state (spontaneous emission)[2]. If this happens, one would expect to observe no net

[2] See *The Quantum Theory of Light, 3rd Edition,* by R. Loudon, page 16-19, Oxford Science Publication (2000) for a discussion on Einstein's A and B coefficients.

absorption since the coefficients of absorption and emission are equal. That is, the spontaneous downward jumps with accompanying photon emission and induced upward/downward absorptions/emissions are equal. However, in general, the population in the ground state n_1 is greater than the population in the higher state n_2 and net absorption occurs.

The population ratio of the two states, measured at temperature T, is described by the Boltzmann distribution $n_2/n_1 = e^{-\Delta E/kT}$, where k is the Boltzmann constant. In ESR, it is customary to measure the value of g, and if it differs from 2.0023 (value of g for a free electron), then there are three factors which could contribute to this. Firstly, the electron has gained or lost momentum (through spin-orbit coupling). Secondly, since in this case electrons are associated with atoms, the g factor changes according to the orientation of the paramagnetic atom in the magnetic field. Lastly, if the atom with which the electron is associated has a non-zero nuclear spin, the magnetic field associated with this atom will also affect the electron leading to the phenomenon of hyperfine coupling.

Spin Hamiltonian of a free electron

The spin Hamiltonian for a free electron in a magnetic field H is given by

$$\hat{H} = g\mu_B H\hat{S}_Z \,, \tag{3.11}$$

where g is the g-factor, μ_B is the Bohr magneton and $\hat{S}_Z$ is the component of the spin vector along the z axis.

If the electron is localized at an impurity atom in the lattice of a solid, then it will experience interaction with the nucleus and other electrons. The Hamiltonian in this case then becomes

$$\hat{H} = g\mu_B H\hat{S}_Z + A\hat{I}_Z \cdot \hat{S}_Z \tag{3.12}$$

The first term represents the electron Zeeman interaction. The second term, where $\hat{I}_Z$ and A are the z-component of the nuclear spin vector and hyperfine constant respectively, is due to the magnetic hyperfine interaction.

The measurement of a resonance spectrum of single substitutional nitrogen atoms that are homogeneously dispersed in a diamond lattice were first done by Smith *et al* in 1959 [60]. In their interpretation of the spectra observed, they found that in the case when the external magnetic field is aligned parallel to the $< 111 >$ crystal direction, there appear three lines that are equally spaced and are of equal intensities. They concluded that they are due to nitrogen (I = 1) because the hyperfine multiplicity was 2I + 1=3. In the case when the field is parallel to the $< 111 >$ direction, 25% of the carbon-nitrogen bonds in the lattice were parallel to the lattice, and the spectrum consists of three hyperfine lines of equal intensities. The remaining carbon-nitrogen bonds were at equal angles to the field. A similar interpretation can be applied for the case where the field is parallel to the $< 111 >$ crystal direction.

3.5 Photoluminescence

When a substance absorbs energy in some form or the other, part of that energy may be re-emitted as radiation in the visible region of the spectrum. This is called luminescence and it is a radiative recombination process, that is, the hole in the valence band is annihilated by an electron in the conducting band [61]. If the emission takes place immediately after absorption, then it is said to be fluorescing and if there a relative delay, the process is called phosphorescence. The ability of a substance to exhibit luminescence may be associated with the presence of impurity atoms present in relatively small concentrations in the host material. Colour centres in diamond, also exhibit this behaviour, hence we have studied a suite of diamonds using photoluminescence which is luminescence brought on by incident photons on a material.

3.5.1 Theory

A simple model of the absorption and emission of light at an impurity centre in a crystal lattice enable an understanding of this phenomenon. This model is a qualitative description of the transition processes that occur when a photon is absorbed at an impurity site [61]. Consider the case of allowed optical transitions at zero temperature (0 K) as illustrated in Figure 3.3.

Since only the $n = 0$ vibrational level (represented by horizontal lines) is occupied, transitions will occur only from this level. Because the time taken for an electronic transition is short compared with the period of atomic vibrations, the lattice coordinates do not change during the transition. This is the so-called Frank-Condon principle and leads to the transition being represented by vertical lines in Figure 3.3. Only transitions within these vertical dashed lines are appreciable. Such transitions occur with varying probability from any position consistent with the spatial extent of the $n = 0$ vibrational wave function. Thus, the transition energy varies as the lattice vibrates between the limits set by the horizontal line representing the vibrational level in the diagram.

Immediately after the excited state configuration has been reached by a transition within the absorption band, the lattice relaxes around the defect (i.e. the ions take up new equilibrium positions) to the $m = 0$ vibrational level (in the upper electronic level) by emission of an appropriate number of phonons until the zero vibrational state is reached (part of the excitation energy is transferred to the lattice). This process is represented by the blue curved arrow. Physically it can be thought of as the adjustment of the nearest neighbour nuclei to the changed energy state of the electron. This process has a smaller transition probability than the electronic transition.

Radiative decay from the excited state to the ground state then occurs under the "new" lattice configuration, the peak position corresponding to the maximum probability in the $m = 0$ state is at $Q = \Delta$, where Δ is the average configurational coordinate (normal mode of the lattice) appropriate for the excited state. The ground state is thus not reached immediately. The

electronic transition is instead followed by a rearrangement of the ions into the original configuration. Since energy has then been given up twice to the lattice, the electron recombination energy is less than the excitation energy. Thus since absorption energy E_a is less than excitation energy E_e, in Figure 3.3, it is apparent that there is a shift in energy of the absorption and emission bands; this is usually referred to as the Stokes shift.

Figure 3.3 indicates that the greater the number of phonons excited in a transition, the larger the Stokes shift will be. A further consequence is that the weaker the coupling (fewer phonons), the greater the amount of overlap between the lowest vibrational states $n = m = 0$.

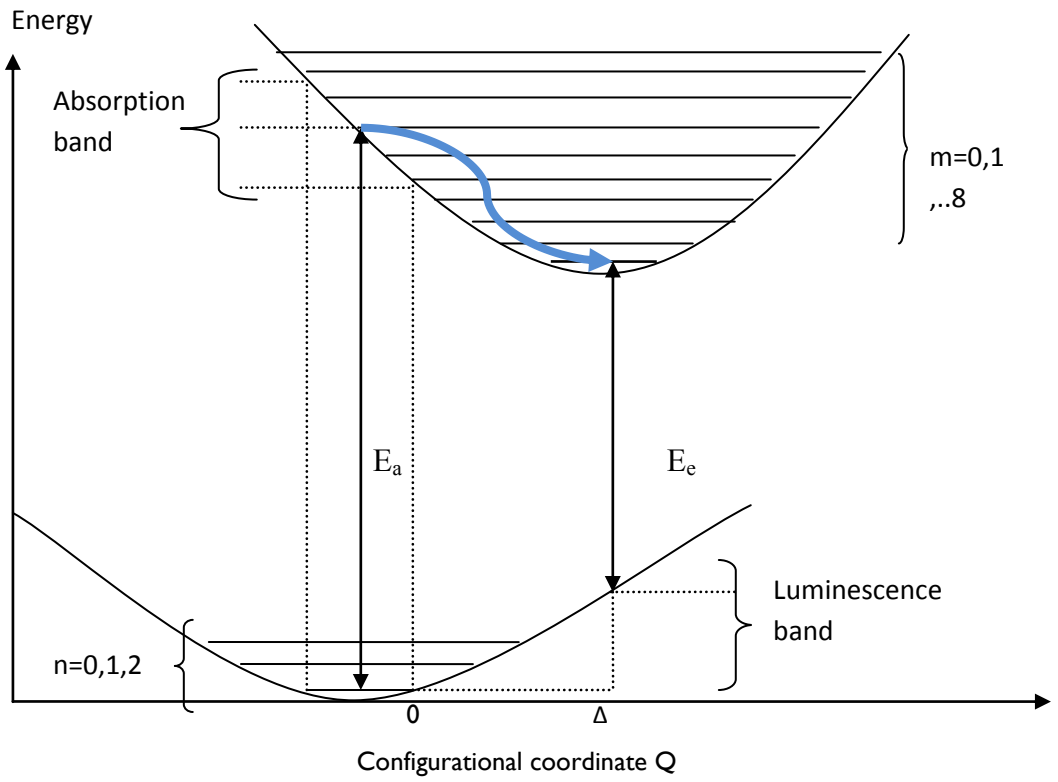

Figure 3.3 Configurational diagram illustrating transitions that are allowed during a photoluminescence process.

The general result for a transition involving *S* phonons being excited at 0 K is

$$P_{nm} = \frac{e^{-S}S^m}{m!}, n = 0, 1, 2; m = 0,1, \ldots, 8 \quad (3.13)$$

Where P_{nm} is the probability of transitions from *n* (lower vibrational state) to *m* (upper vibrational state.)

The optical line shape is defined by a Poisson distribution expressing a discrete number of electronic transitions with phonons. In general when *S* is small, the probability of observing the zero phonon transition is greatest. Increasing *S* effectively increases the intensity in the phonon sidebands (phonon transition contributions from all lattice modes) at the expense of the zero phonon line. When *S* is very large the shape approaches the Gaussian distribution, in which the band peak occurs at *S* = *m*. The ZPL of the NV centre is shown in Figure 3.4.

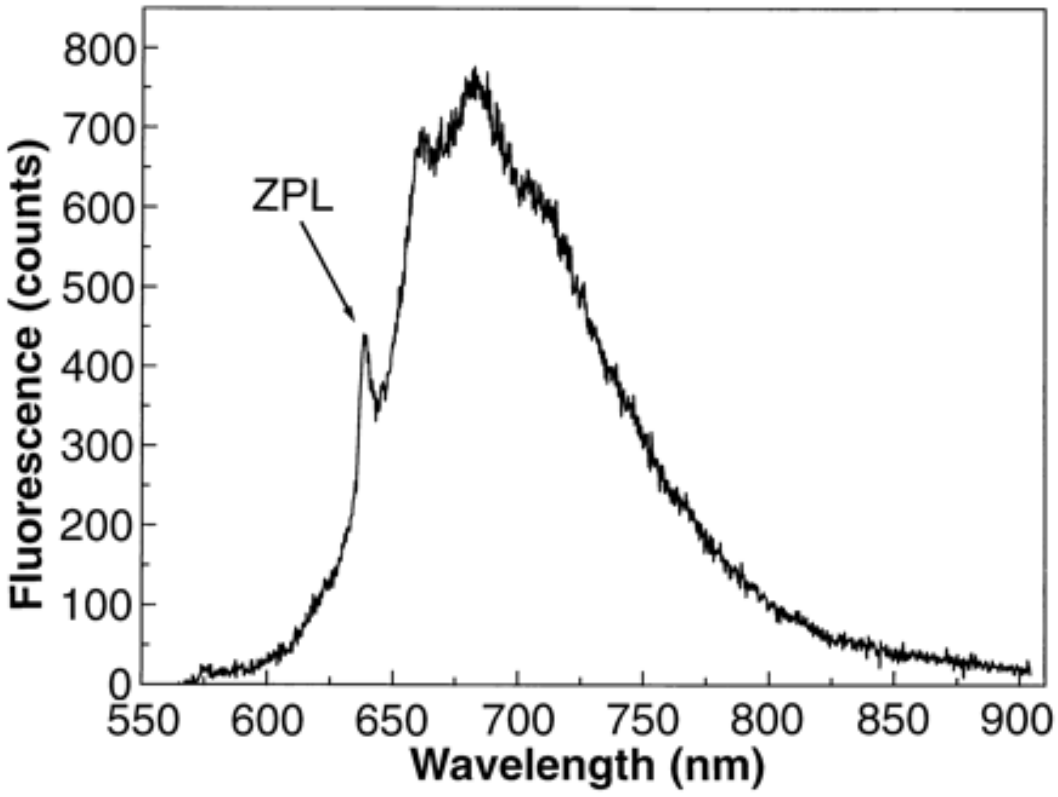

Figure 3.4 Fluorescence spectrum of a single N-V defect centre. The wavelength of the zero phonon line (ZPL) is 637 nm (1.945 eV) [62].

Chapter 4

Characterization of the NV centre: Experimental Procedures and Results

4.1 Introduction

In this chapter we describe the experimental procedures and present the results of the measurements used in the characterization of the NV centre in diamond. The experiments were carried in various laboratories at the University of Witwatersrand in the Department of Physics. To select the diamond samples, we made use of the spectroscopic techniques described in Chapter 3. Each of the techniques involved in the characterization of the NV centre were conducted following the relevant method for each experiment. All of the experiments were non-invasive on the diamond crystals and did not require any irradiation or heat treatment on the diamond samples, that is, we used them as they are. This chapter thus describes briefly the procedures followed in the section processes as well as the results obtained.

The spectra presented in this chapter show that the diamond samples contained a number of different defects. The type of defects in each of the samples is determined by studying the optical behaviour under the spectroscopic experiments. Each of the defects is characterized by an optical band at the relevant wavelength or wave-number. These results enabled us to select a suite of diamond samples to be used in the investigation of the single photon emission properties of the NV centre. The samples selected had to show the presence of nitrogen defects that are substitutional impurity atoms or due to irradiation, annealing or both.

The samples that were selected with the help of these spectroscopic techniques were then sent to another laboratory at the Element Six Headquarters in Johannesburg where they were

viewed with a special viewing technique called Diamond view. A short description of this technique is given in section 4.3 and the resulting images are shown in Figure 4.11. The diamond samples that were used in the spectroscopic techniques have the physical characteristics as presented in Table 1. It includes their given labels (names stated have no special meaning), their thickness in centimeters as well as their colour.

Table 1. Some characteristics of the diamond samples used in the spectroscopic characterization.

Sample	Colour	Thickness (cm)
R2145	Yellow	0.155
M3	Brown-yellow	0.067
M4	Bluish-green	0.079
S1b	Yellow	0.112
Yellowsq1	Yellow	0.136
Yellowsq2	Yellow	0.135
M2	Clear	0.067
clearTria	Clear	0.091
clearHex	Clear	0.088

4.2 Selection of the diamond samples

The studies for characterizing the diamond samples were divided into four experiments and the details of the methods and results are described below. The results are presented in the order in which the experiments were conducted.

4.2.1 Ultraviolet-Visible-Near Infrared

The samples for the study comprised a total of 27 diamonds (as a preliminary step) with a variety of sizes and types (i.e. natural and synthetics). A Varian Cary 500 Scan spectrophotometer with a wavelength ranging from 200 nm to 3000 nm and 0.01 nm precison (see Figure 4.1) was used to record the UV-Vis-NIR spectra at room temperature. A baseline spectrum was first taken with the two sample holders empty to be used during baseline correction. The measurements were then taken by placing a sample in one of the holders. In the UV-Vis-NIR measurements, characteristic absorption bands give details of the type of treatment (if any), that a diamond may have undergone and the characteristic absorption wavelengths are given in [63].

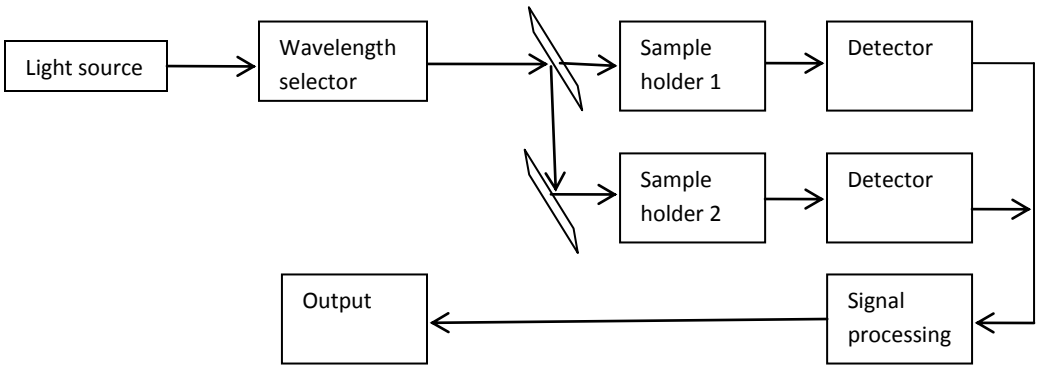

Figure 4. 1 Block diagram of the UV-Vis-NIR spectrophotometer. Only one of the samples holders was used during the acquisition of data, the other holder was kept empty. The output obtained is in the form of a spreadsheet with baseline correction already performed.

Figures 4.2 to 4.4 show the UV-Vis-NIR spectra for a selected few diamond samples. The plots were obtained by using Origin 6.1 software. In Figure 4.2 we observe that the sample has been irradiated because it shows the presence of the absorption around 393 nm. The defect that absorbs at this wavelength is the negatively charged vacancy which is a result of missing carbon atoms which were knocked out during irradiation. Another defect that we observe which is also as result of irradiation is the general radiation (GR1) centre, with an absorption around 741 nm in Figure 4.2. The GR1 centre is associated with a neutral vacancy.

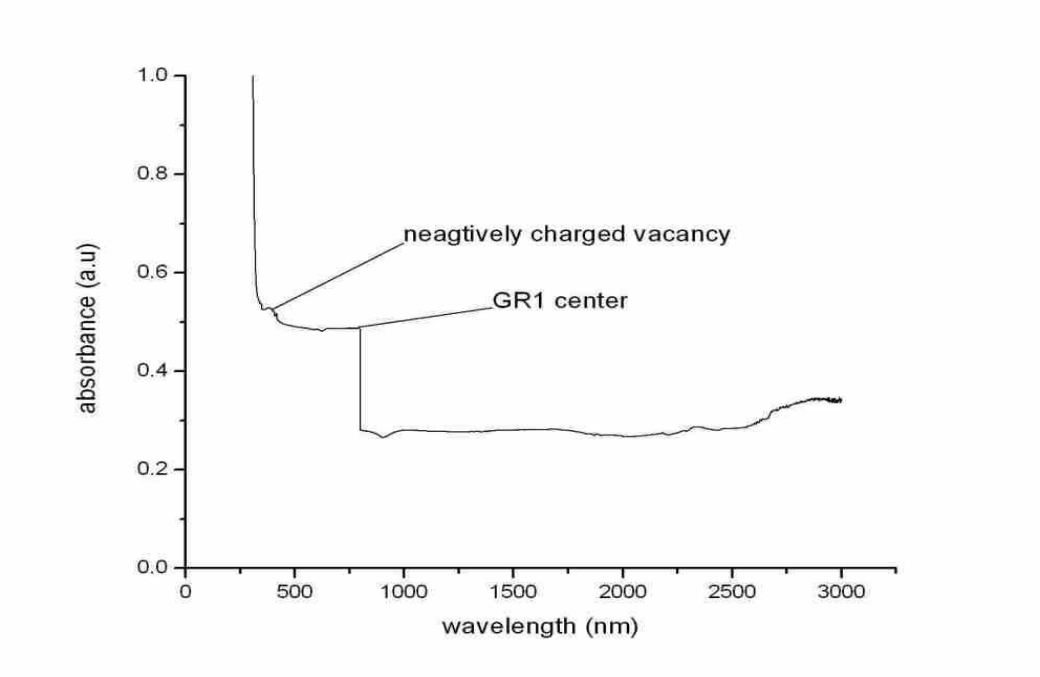

Figure 4.2 The UV-Vis-NIR absorption spectrum of a type IIa diamond (M2). From observations on the spectrum, the sample appears to have been irradiated but not annealed, as it shows the GR1 centre, and the vacancy which is a result of carbon atoms having been knocked out.

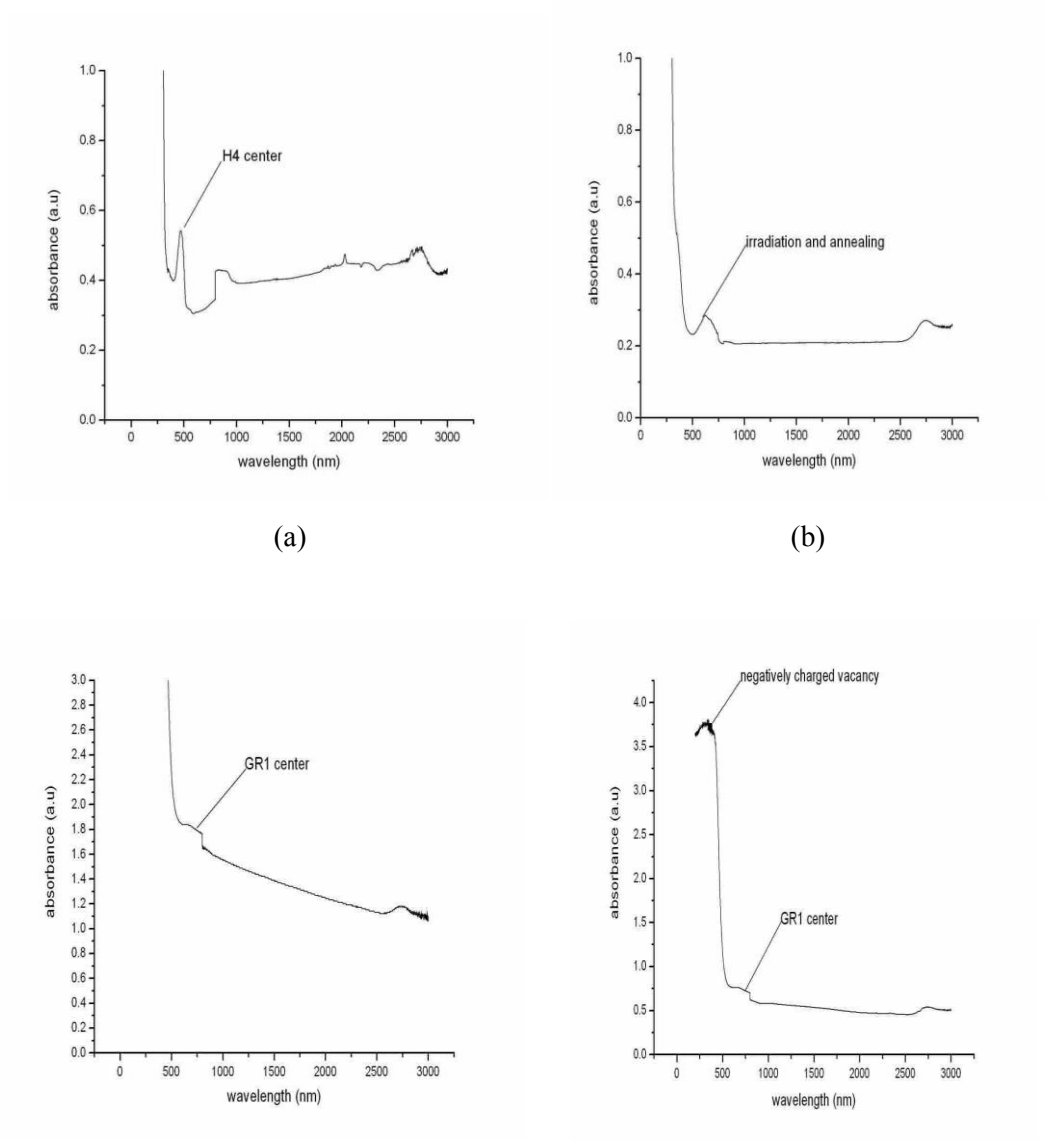

Figure 4.3 UV-Vis-NIR spectra of four different diamonds taken at room temperature. The spectra show that the samples underwent different heat treatments and irradiation processes.

From Figure 4.3 in the above we see that the diamonds have a number of different defects and treatment histories. In Figure 4.3(a) we observe that the diamond has an absorption band in the vicinity of 495 nm. This is due to the H4 centre, which is a vacancy trapped at the B-

aggregate and is observed after irradiation and heating. Figure 4.3(b) shows a peak at 595 nm and this indicates that the sample was annealed after irradiation. Figure 4.3(c) and (d) both show the GR1 absorption band at 741 nm and that tells us that the sample was irradiated. The diamond whose spectrum is shown in Figure 4.3(d) shows the presence of both the negatively charged vacancy as well as the neutral vacancy.

While Figure 4.4(a) indicates that sample R2145 has been irradiated and annealed as the spectrum shows an absorption peak at 637 nm. This tells us that the carbon vacancies after annealing migrated towards the nitrogen atoms to form the nitrogen-vacancy centres. The same seems to apply to Figure 4.4(c). The spectrum in this figure also shows an absorption band at 637 nm. In Figure 4.4(b) we observe that clearTria has been irradiated as it shows an absorption peak at 393 nm. This is due to the presence of a negatively charged carbon vacancy. Figure 4.4(d) also shows that the sample was irradiated, which also resulted in a negatively charged vacancy.

The results of this experiment gave us an insight into the histories of the diamonds. That is, if they were irradiated or irradiated plus annealed and the type of defects that were present in different forms. This assisted us in narrowing the search for diamonds that have the NV centres for use in the study of the single photon emission behaviour of these centres.

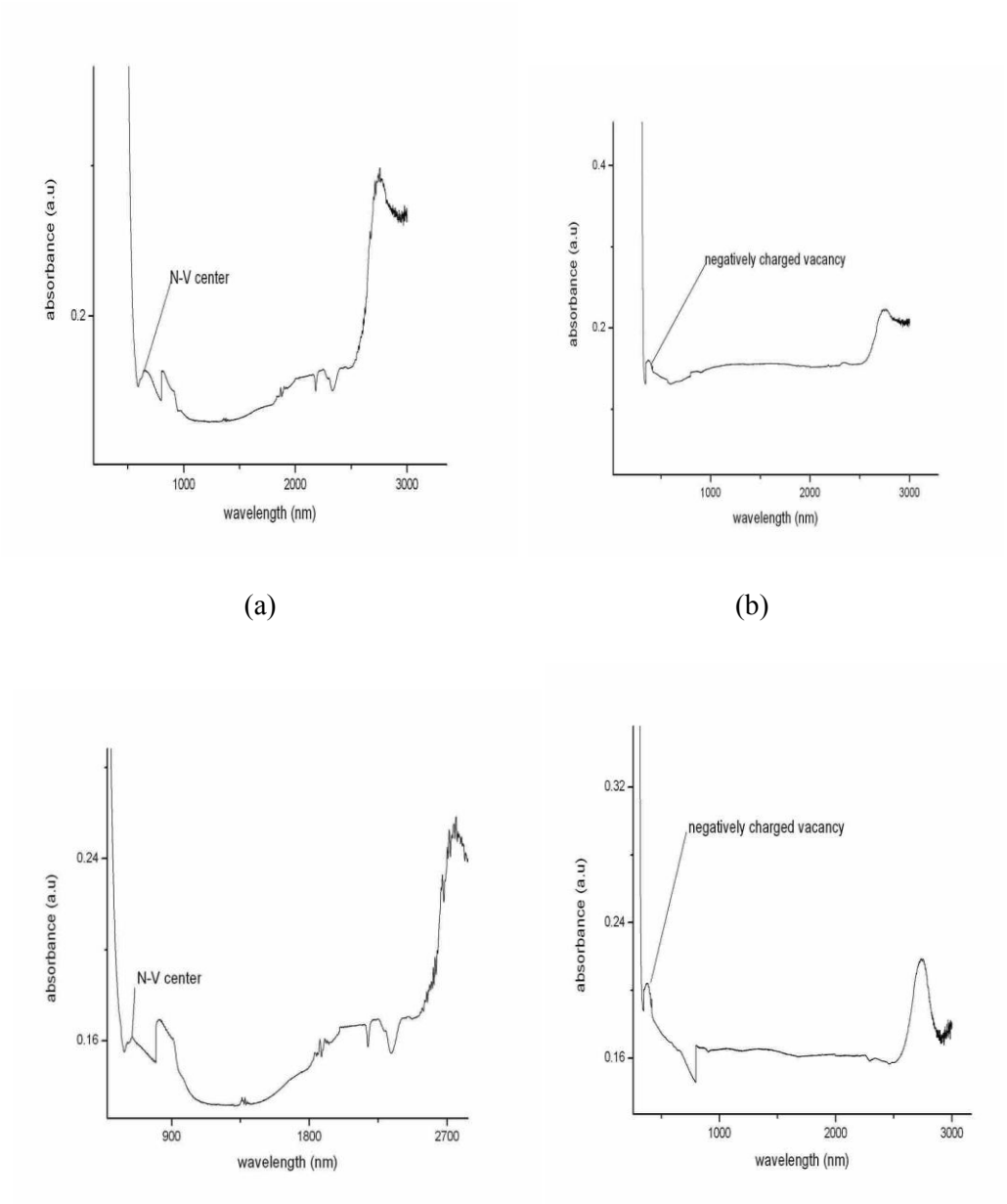

Figure 4.4 The UV-Vis-NIR spectra of four different diamonds, also taken at room temperature. (a) R2145, which is a type Ib that has been electron irradiated and annealed. (b) clearTria, also a type Ia that has been irradiated and as we see an absorption band at 393 nm; (c) S1b, this is a type 1b that has also been irradiated and annealed (d) clearHex, a type 1a diamond that has been irradiated.

4.2.2 Infrared

A suite of nine diamond samples of various types were investigated on a Varian 800 FTIR machine at room temperature to determine their nitrogen content. The setup consisted of a Michelson interferometer (see Figure 3.1) and computer for data processing. A background spectrum was first collected with the sample holder empty for use in the correction of absorption spectra of the samples and we plot absorbance against wave-number in cm^{-1}. Infrared absorption spectrum of diamond has two-phonon absorption in the region between 1700 and 2700 nm and the resulting absorbance is proportional to the thickness of the sample [64]. Hence we first standardize the absorption spectra of the samples according to their thickness, given in Table 1. That is, we divide the absorption coefficient in the spectrum of each sample by the thickness of the sample.

Other absorption bands that are attributed to the presence of defects resulting from the presence of nitrogen in diamond occur between 1000 and 1400 cm^{-1}. The collected spectra in this region were analyzed using the Diamond Trading Company Excel program (IRspec-CAXBD97.XLS) which was used to estimate the concentration of different forms of nitrogen in parts per million in the samples.

The spreadsheet decomposes the single phonon region of a diamond IR spectrum in order to obtain the concentrations and uses the solver tool of excel spreadsheet to fit the data and select the constraints. The results are shown in the next chapter and the fits are as shown in Appendix A. Nitrogen as a single substitutional atom gives a characteristic absorption peak at 1130 cm^{-1} and the A- and B-aggregates give peaks at 1282 and 1175 cm^{-1} respectively. The N-V centre gives an absorption peak at 1332 cm^{-1} and a peak due to platelet nitrogen appears at 1370 cm^{-1} [65, 66]. The spectra presented in Figures 4.5 and 4.6 show these characteristic peaks and the different concentrations of the impurities for the diamonds studied.

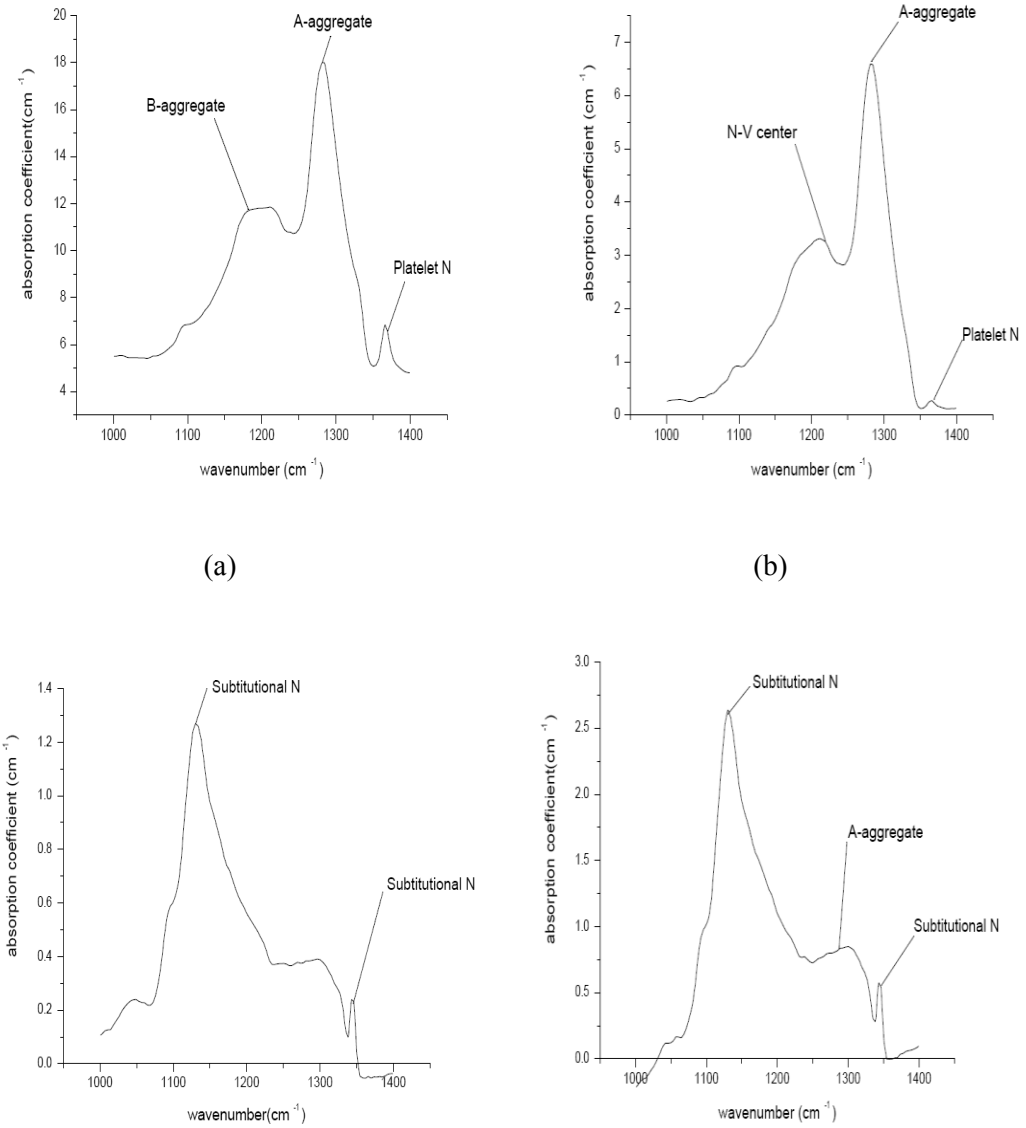

Figure 4.5 Infrared absorption spectra of the diamond samples of different types. The spectra give detailed information about the type of nitrogen defects that are present in each sample as well as their concentrations. In (a) and (b) which are M3 and M4 there appears to be a high concentration of the A-aggregate defect whereas S1b (c) and yellowsq1 (d) appear to have the single substitutional nitrogen (N) atom in high concentrations.

In Figure 4.5, the spectra labeled (a) and (b) are of two samples that were both treated by irradiation with electrons and annealed. Both show similar characteristics in that both have high concentrations of the A-aggregate defect and platelet N in small concentrations. The two samples were selected for further studies in the single photon set-up to investigate if the annealing resulted in the formation of NV centres or not.

In (c) and (d) we observe that the samples have high concentrations of single substitutional nitrogen atoms in high concentrations. The two samples were both Type Ib and the presence of substitutional nitrogen may mean that if the sample was exposed or treated with temperatures above 550^0 C, then this may result in the formation of NV centres. Thus the two samples were also selected for further investigation in the single photon set-up described in detail in Chapter 5.

In Figure 4.6, we observe that in both spectrum (a) and (b) there are high concentrations of single substitutional nitrogen atoms. This is keeping with the fact that both samples are of Type Ib. they also show the presence of the A-aggregate defect, although in smaller concentrations. We observe different behaviour in (c) and (d). The two samples have the A-aggregate as the dominant impurity, which means that the nitrogen atoms are not distributed in the diamond as single atoms but they have paired up. The total concentrations of A-, B-aggregates and single N atoms for the four samples are $[N_A]$ =494.1ppm, $[N_B]$ = 132.2ppm and $[N_C]$ = 143ppm respectively.

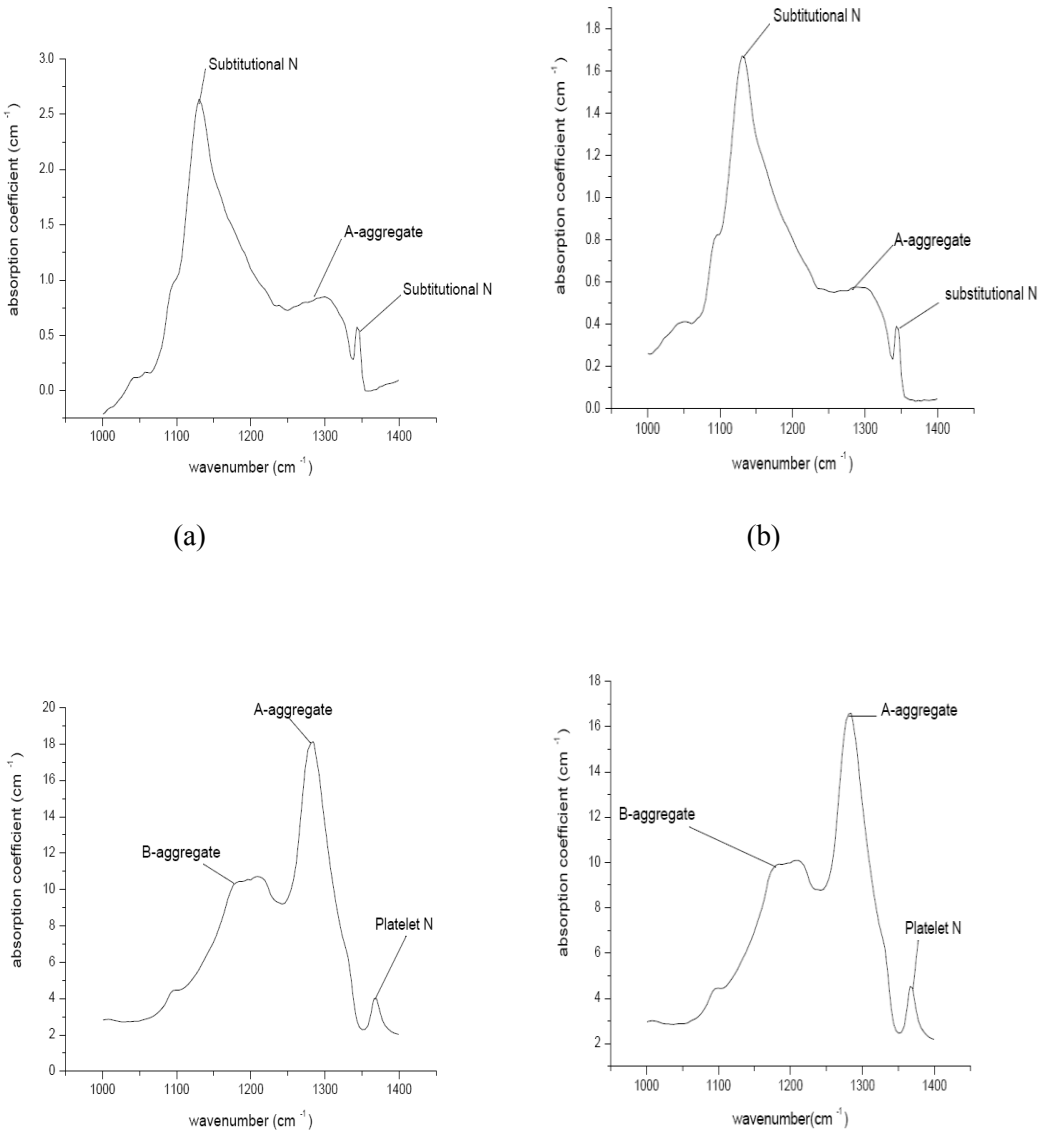

Figure 4.6 Infrared absorption spectra of the diamond samples of different types. The spectra give detailed information about the type of nitrogen defects that are present in each sample as well as their concentrations. Both (a) and (b) which are yellowsq2 and R2145 have substitutional nitrogen atoms as defects and the concentration is higher in (a). The A-aggregate defect dominates in clearTria (c) and clearHex (d) while B-aggregate occurs in small concentrations.

4.2.3 Electron Spin Resonance

A selection of seven diamond samples was studied using the electron spin resonance machine (BRUKER ESP 300 E,) under continuous wave. The frequency was kept constant at approximately 9 GHz while the magnetic field was swept over a certain range. The samples were oriented in four different directions, namely, 0^0, 45^0, 90^0 and -90^0 and spectra recorded.

The samples were illuminated with ultraviolet (UV) light to enhance the ESR signal. The reason being if we refer to Figure 2.5 in Chapter 2, we note that the transitions between the ground state, excited state and the meta-stable state occur with varying probabilities. Hence it is important to illuminate the diamond sample with the UV light to excite the NV centres in the diamond. After a number of excitations and de-excitations, all the NV centres that are in the sample will be polarized to be in the $m_S = 0$ level of the ground state. This effectively enhances the spin resonance between $m_S = 0$ and $m_S = \pm 1$.

To be able to get the crystal orientations right (to get maximum signal, the magnetic field must be parallel to the [111] plane since there is no mixing of levels in this direction). In order to determine the crystal orientation of each sample, the diamonds were taken for Laue measurements using the facility at Ithemba Labs (Gauteng) and the results are presented in Appendix B. The number of samples was reduced to three potential candidates for single photon generation and their spectra are shown in Figures 4.7 to 4.8.

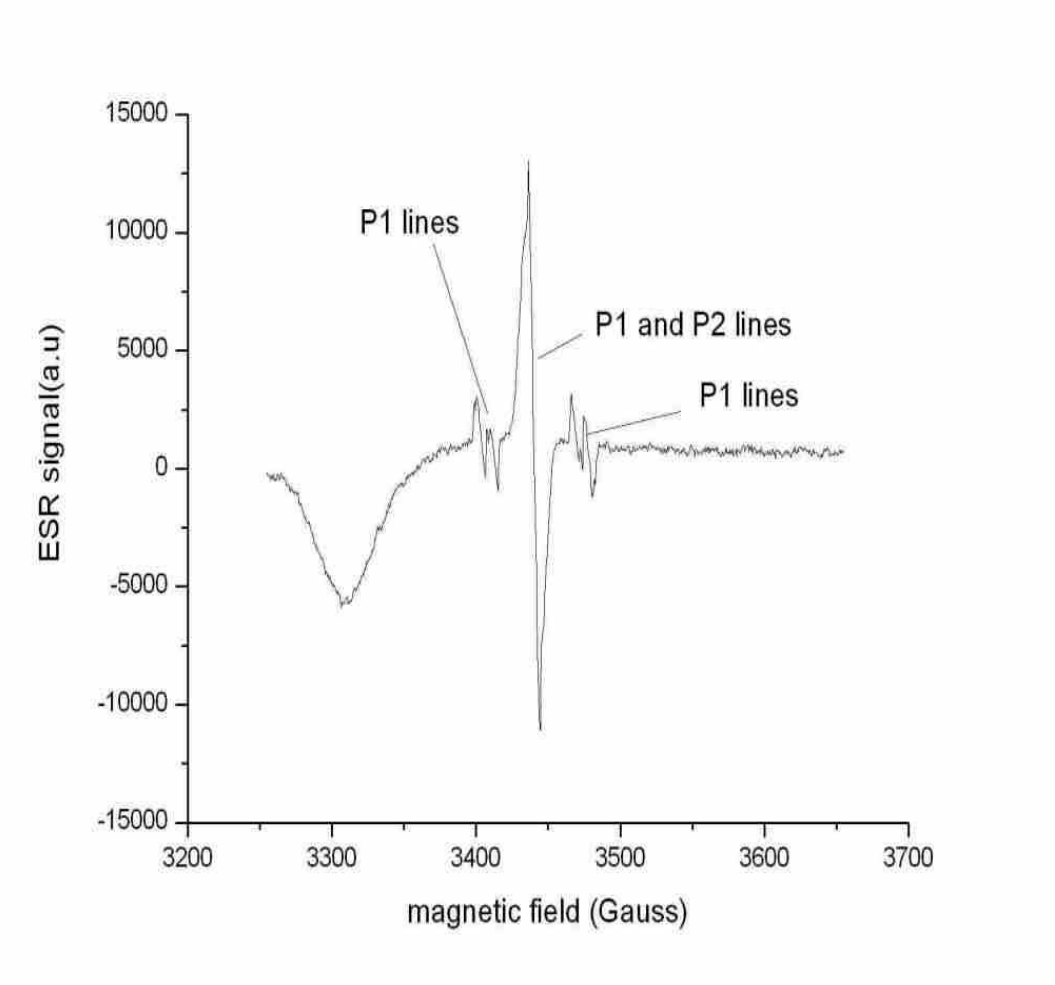

Figure 4.7 Electron Spin Resonance spectrum of a type Ia (clearHex) diamond. The three resonance lines in the spectra are due to the presence of single substitutional nitrogen atoms (P1 lines) and due to the presence of a vacancy around three neighbouring nitrogen impurity atoms, known as the P2 centre [67].

Figure 4.7 shows the ESR spectra due to the P1 centre. The reason for the appearance of the three peaks can be explained in the following way. A nitrogen atom can occupy any one of the lattice sites in the tetrahedral structure of the diamond, thus on average there will be equal intensities from each of the atoms. Each nitrogen atom gives rise to three peaks of equal intensities due to the 2I + 1degeneracy.

For the case when magnetic resonance is parallel to the $< 111 >$ direction, 25% of the carbon-nitrogen (C-N) bonds will be aligned with the magnetic field producing three peaks with a particular spacing *K*. the reason for the three peaks is as follows: the unpaired electron from the nitrogen has $m_S = \pm {}^1/_2$ and its energy levels are split when in a magnetic field. When these levels interact with the nitrogen nucleus (which has spin I=1), $m_S = + {}^1/_2$ and $m_S = - {}^1/_2$ each split further into three sublevels. There are three possible transitions between the three upper and lower sublevels corresponding to different magnetic field strengths. The spacing between peaks is governed by $K^2 = Acos^2\theta + Bsin^2\theta$, where *A* and *B* are constants and θ is the angle between the C-N bonds and the magnetic field [68].

The remaining 75% of the bonds will be at equal angles to the field and will also give rise to three peaks but with a different value of *K*. This gives rise to higher intensity central peak (refer to Figure 4.7) and the satellite peaks that are shifted due to the different value of *K* on either side. In Figure 4.8 we observe that although the diamond sample is different from the previous one, their spectra is similar. The main difference is that the satellite peaks are in this case of a higher intensity than those in Figure 4.7 and this may indicate a larger presence of P1 centres.

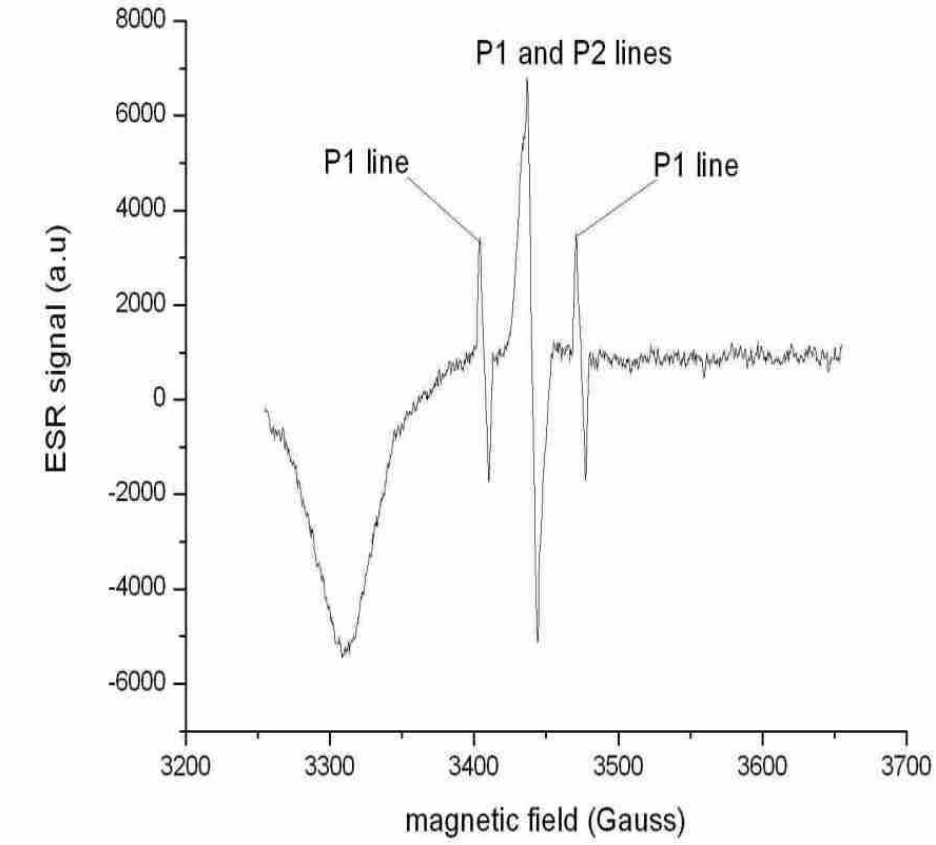

Figure 4.8 Electron Spin Resonance spectrum of a type Ia (clearTria) diamond. The three resonance lines in the spectrum are due to the presence of single substitutional nitrogen atoms (P1 lines) and due to the presence of a vacancy around three neighbouring nitrogen impurity atoms, known as the P2 centre [67].

4.2.4 Photoluminescence

Photoluminescence spectra of 23 diamond samples were recorded in the Raman Laboratory (University of Witwatersrand, Physics Department) as a preliminary step to select samples with NV centres as impurities. The experimental setup consisted of a 514 nm Argon laser used for excitation and a confocal microscope with an adjustable pin-hole to allow only certain volumes of fluorescence from the samples to be collected. The samples were mounted onto an *xyz*-adjustable table controlled by the computer. A CCD (charge coupled device) camera was used for viewing the samples. Inside the microscope the excitation light was separated from luminescence from the sample with the help of a notch filter which allows all frequencies to pass except those in the stop band. The filter also cut-off any Rayleigh scattering that may occur as this type of scattering has the same wavelength as the excitation wavelength and is thus of no interest. It is so intense that if allowed to pass through it would render it almost impossible to see the luminescence light from the sample. A photo of the experimental set-up is shown in Figure 4.9.

A total of seven samples were kept for further investigation of their NV centre concentrations in the photo-luminescence studies. The NV centre exhibits a zero phonon line at 637 nm in the luminescence spectrum and the entire selection of samples had NV centres in different concentrations. The spectra of these samples are shown in Figures 4.10 to 4.12. To obtain the spectrum in Figure 4.10, we chose an area of 100 × 100 microns and did a 100 point scan to map the area. There's a fluorescence peak at 637 nm which corresponds to the zero phonon line of the NV centre as described in the previous chapter. The area showed the presence of NV centres in almost equal concentrations as the fluorescence at each of the points seems to be superimposed on the spectrum. The spectrum has been background corrected to make the peak clearer.

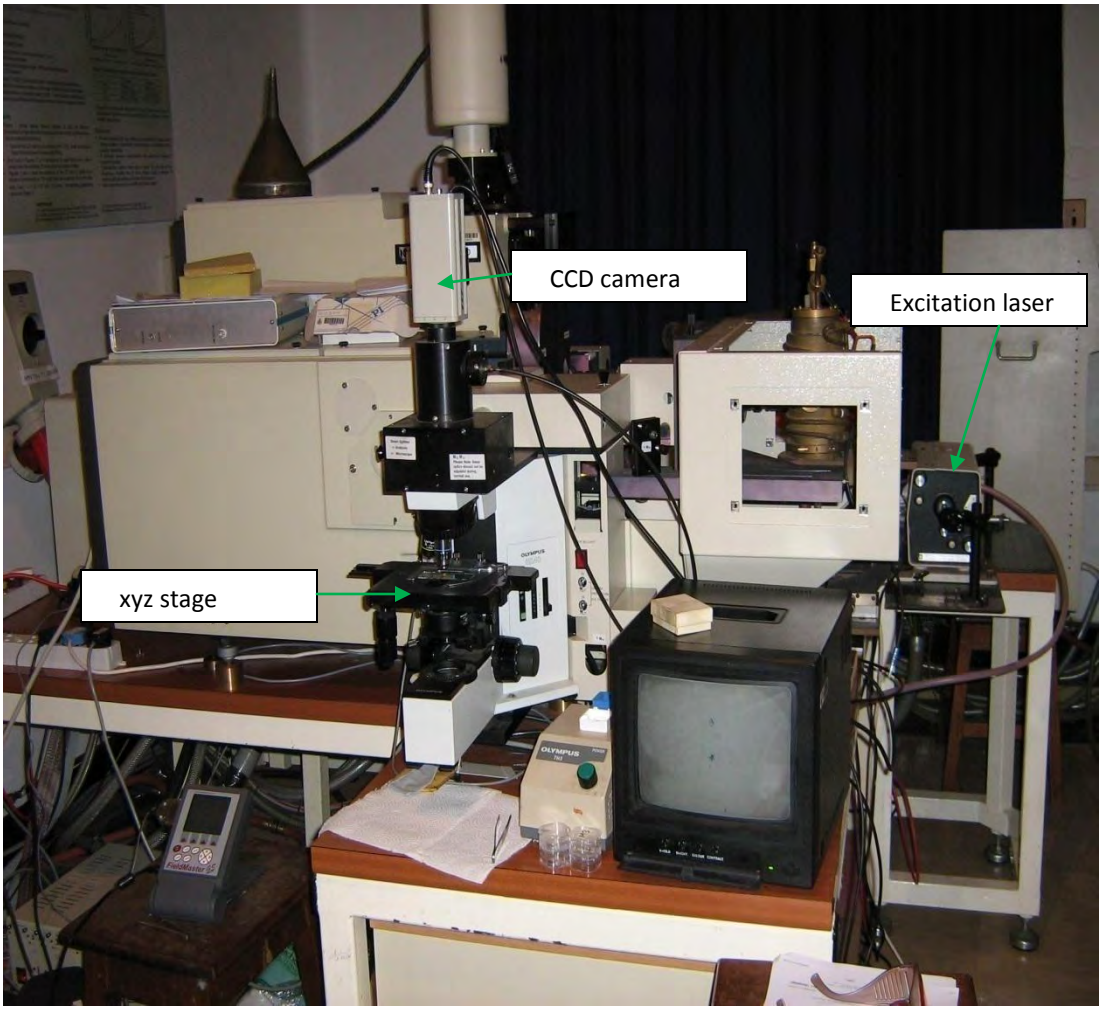

Figure 4. 9 Photo of the experimental set-up used for photoluminescence studies conducted on the diamond samples.

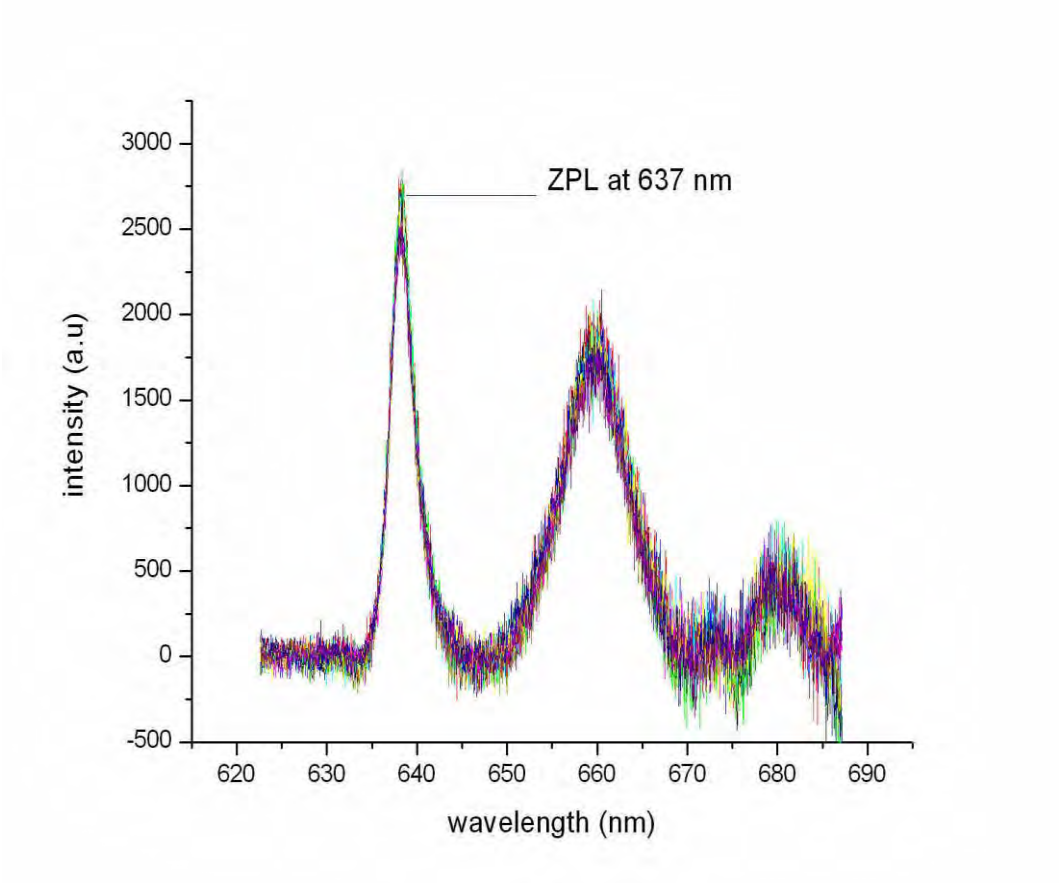

Figure 4.10 Photoluminescence spectrum of M3. An area of 100 microns was selected on the diamond and a 100 point scan done to obtain a map of the area. The NV centre fluorescence showing a zero phonon line (ZPL) at 637 nm which appears as a high intensity peak at that wavelength.

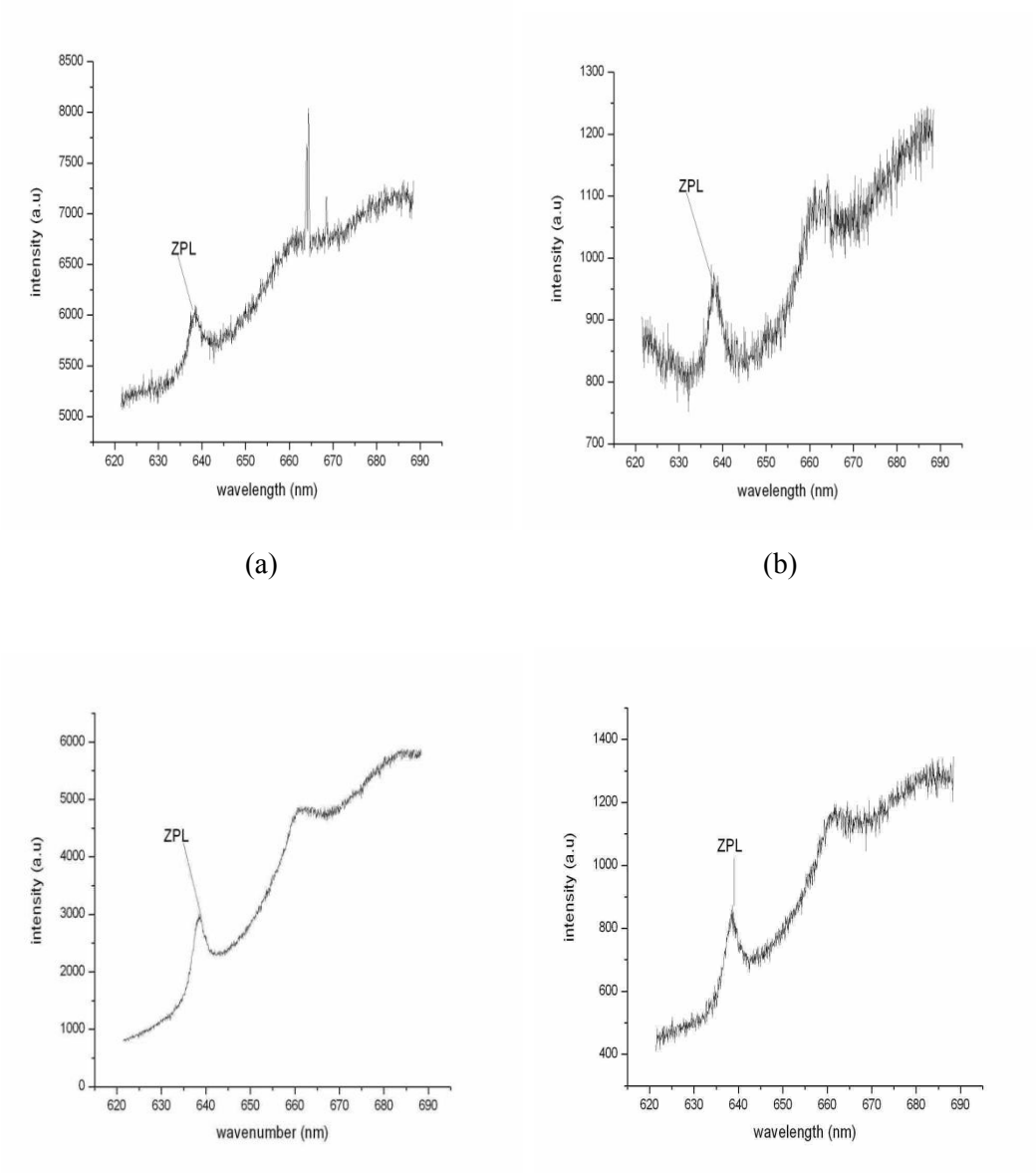

Figure 4.11 Photoluminescence spectrum of (a) M2, (b) M4, (c) R2145 and (d) S1b. All samples have NV centres as they fluoresced with varying intensities at 637nm under laser excitation.

The spectrum in Figure 4.11 (a) was obtained by scanning a 5 × 5 micron area. We did this for the whole surface of the diamond and the spectrum obtained at each of these scans was the same. That could mean that the centres are evenly distributed on the diamond. This diamond has been irradiated as was deduced from the UV-Vis-NIR spectroscopic experiments. Hence, a peak 637 nm on the photoluminescence spectrum means that the NV centre has been formed from the nitrogen atoms that were native in the diamond.

In Figure 4.11 (b-d), we observed the same zero phonon line at 637 nm that is characteristic of the NV centre. The intensities of the fluorescence in each of these spectra are not the same which means that the NV centres present are not in equal quantities or that they are located at different depths in the diamonds. If the latter is true, then the collection of a fluorescent light from deep inside the diamond is hindered by the bulk properties of the diamond. Strong limitation of defect photoemission in diamond arises from the high index of refraction of the bulk diamond material which makes it difficult to collect photoluminescence light efficiently [69]. Refraction at the sample interface leads to a small collection solid angle, limited by total internal refraction, and to strong optical aberrations.

A similar ZPL due to the NV centre under laser excitation is observed in Figure 4.12(a) and (b) and we also conclude from these that the samples contained NV centres with varying fluorescence intensities indicating that they are not present in equal concentrations or they may not be homogeneously distributed throughout the samples.

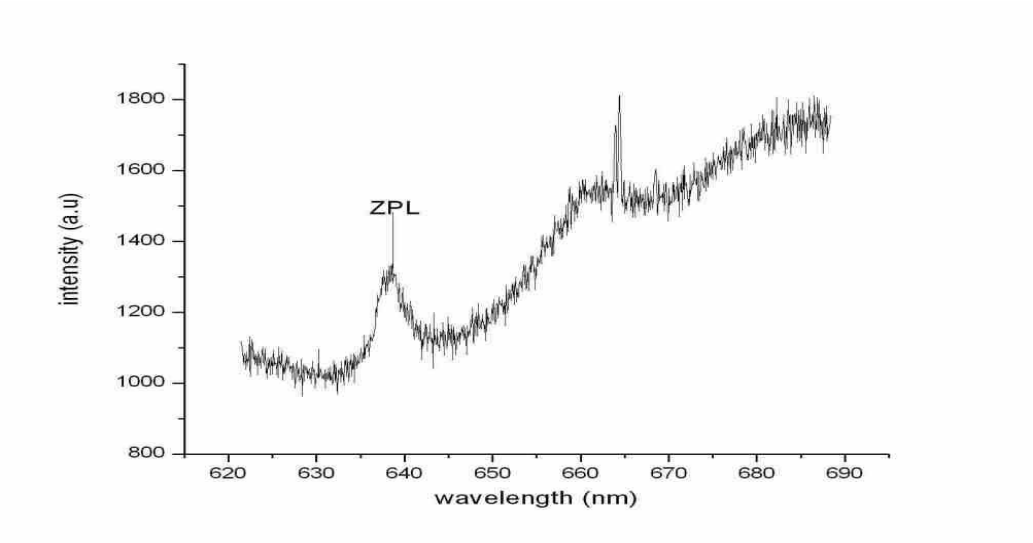

(a)

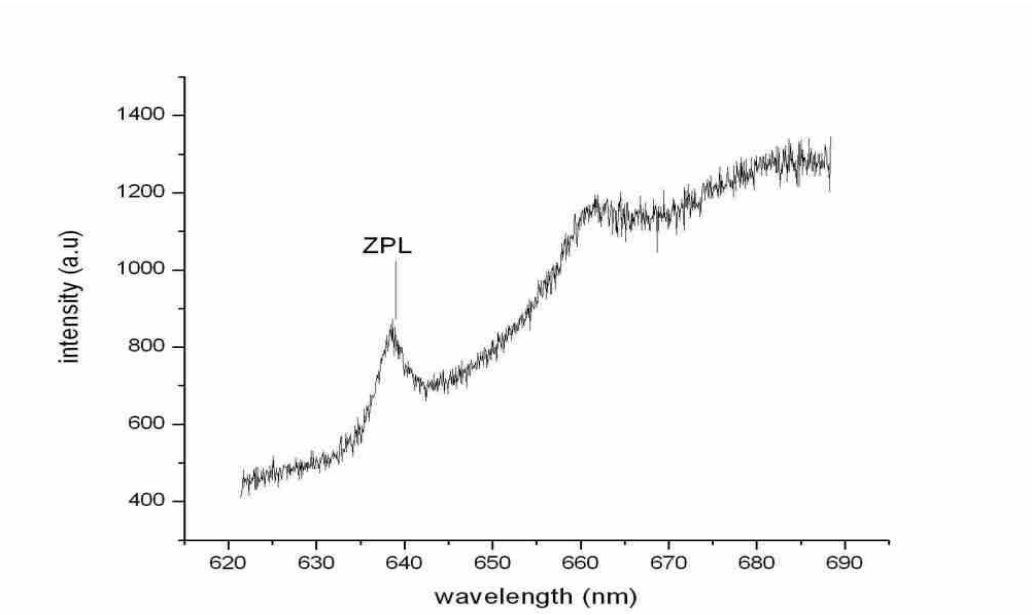

(b)

Figure 4.12 Photoluminescence spectrum of (a) yellowsq1 and (b) yellowsq2. Both samples show the presence of NV centres as they fluoresced with varying intensities at 637nm under laser excitation.

4.3 Diamond View

After the suitable candidates for the development of a single source were selected, these diamonds were then taken to Element Six, Johannesburg, South Africa to be diamond viewed. Diamond View is a procedure developed by De Beers to differentiate between synthetic and natural diamonds. Diamond View reveals some distinguishing feature of synthetic diamonds.

The procedure involves illuminating the diamond with a specialized ultra-violet (UV) light of a wavelength shorter than 230 nm. The resulting fluorescence is confined in the surface of the diamond thus ensuring a clearer and sharper two dimensional image of any fluorescent patterns present in the sample. Once the fluorescence is stimulated, it is viewed by a CCD (charge-coupled device) video camera that is combined with a variable magnification lens with a light source (visible) for focusing.

The resulting UV images of some of the diamonds used in this study are shown in Figure 4.13(a-d) and Figure 4.14(a-d). The samples show different behaviour according to their types. The synthetic ones show the characteristic sector zoning under UV while the natural ones don't show any zones. One sample worth naming in particular is the one whose image is shown in Figure 4.14 (b) in which the zones are clearly visible.

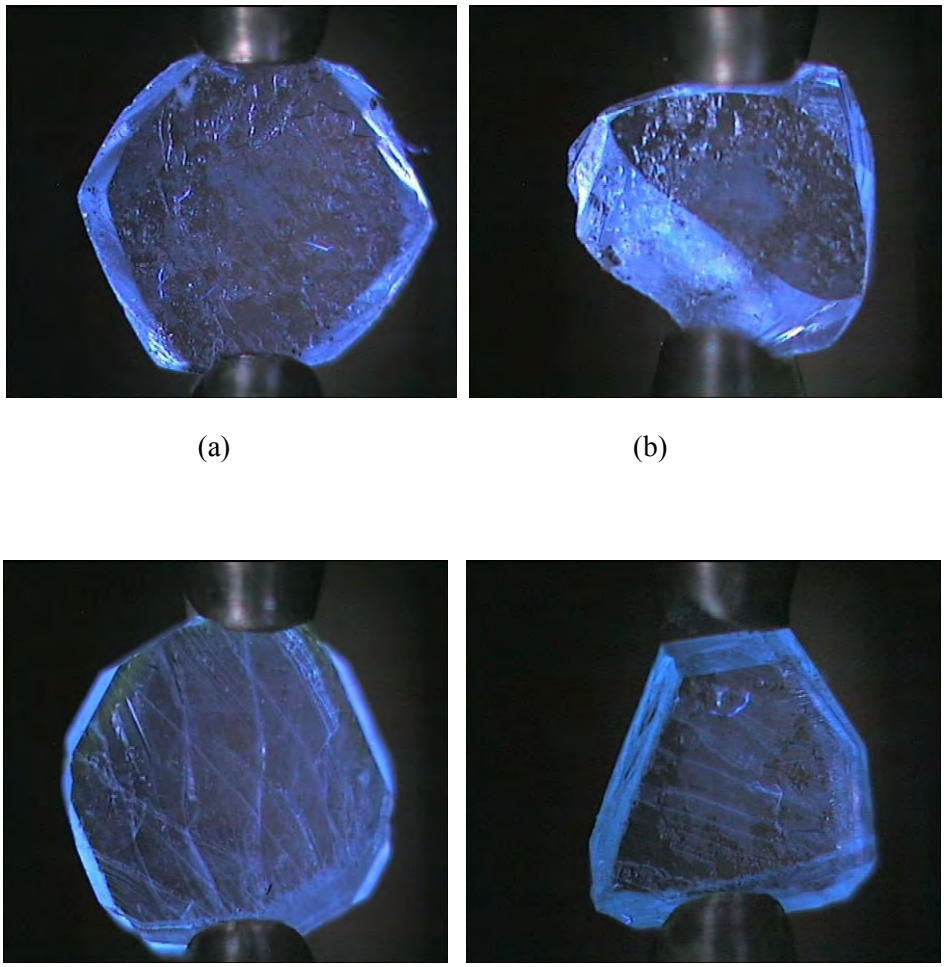

(a) (b)

(c) (d)

Figure 4.13 Diamond View images of some of the diamond samples used in this study. These are all natural Type Ia and IIa diamonds.

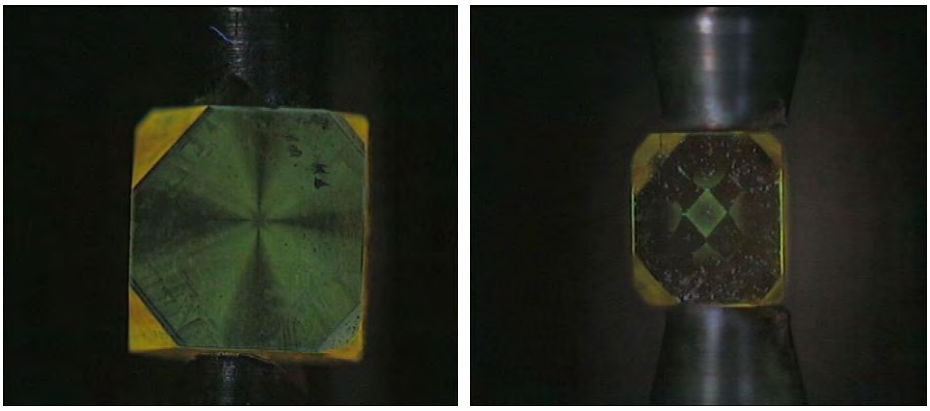

(a) (b)

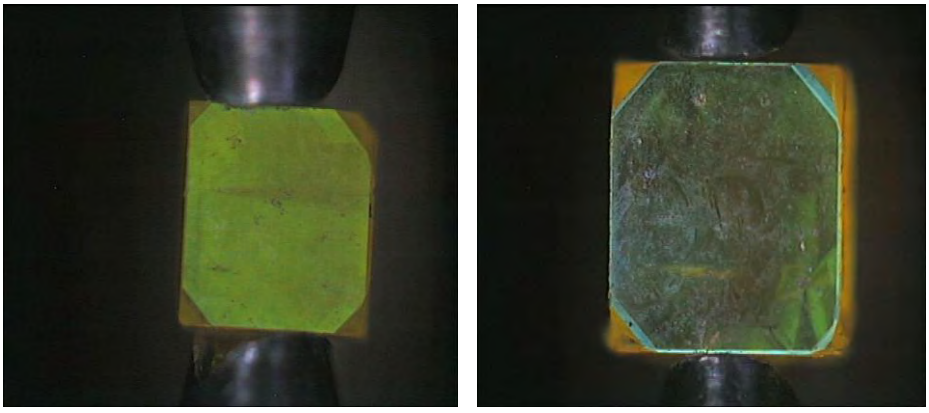

(c) (d)

Figure 4.14 Diamond View images of some of the diamond samples used in this study. All these diamonds are synthetic Type Ib as characterized by the typical yellow tint due to the nitrogen content as well as the distinct sector zoning that becomes visible when synthetic diamonds are illuminated with UV light.

4.4 Summary

A suite of diamond samples of different types were selected for use in the investigation of defects that may be present in the diamonds. The defects were characterized by use of Ultra violet-Visible-Near infrared (UV-Vis-NIR), Fourier Transform Infrared (FTIR), Electron Spin Resonance (ESR) and photoluminescence (PL) spectroscopic techniques. The diamonds showed a number of defects that gave us information about the type of diamonds and the kind of treatment they underwent, i.e. irradiation and/or annealing. These techniques also allowed us to select samples that contained nitrogen related defects, to narrow our search for NV centres.

From the UV-Vis-NIR studies, we were able to observe that a number of samples contained the irradiation induced defect; the GR1 centre. This means that in nitrogen rich samples, these could result in vacancies forming next to nitrogen, thus creating NV centres (see Figures 4.3 and 4.4). The dominant defects observed in FTIR were the A and B- aggregates as well as single substitutional nitrogen atoms.

Electron Spin Resonance investigation also showed the presence of nitrogen related centres (P1 and P2 centres). These two were observed in a spectrum of a Type Ia diamond. To be able to observe the NV centres, the samples were illuminated with a mercury lamp to polarize the centres. The light allows the decay from the excited triplet state to prefer the $m_S = 0$ sublevel in the triplet ground state of the NV centre. None of the diamonds showed any evidence of NV centres possibly due to the low concentration of the NV centres in the samples investigated.

PL studies enabled us to observe the fluorescence of each of the samples which were illuminated with a 514 nm Argon laser. In those samples that have NV centres as a defect, we observed ZPL at 637 nm (1.945 eV). This test was used to further reduce the number of samples to eleven to be used in the investigation of the single photon emission characteristics of the NV centre. This will be conducted by observing the fluorescence of the centre upon laser excitation in a confocal microscopic set-up.

Chapter 5

Single photon source: Experimental set-up

5.1 Introduction

In this chapter the experimental set-up for investigating the emission characteristics of single photons by the NV centre are described. The experiment consisted of three sections: the excitation part, the confocal part, the Hanbury Brown-Twiss (HBT). In the excitation section of the set-up, the diamond sample was illuminated with a laser through a microscope objective to excite the NV centres and the resulting fluorescence was collected and passed through a dichroic mirror to the HBT set-up.

The confocal set-up consists of a few lenses used for magnification and a pin-hole that is used to separate closely spaced point sources of light. In the HBT set-up, the fluorescent light is split using a beam-splitter and each half sent to two detectors. The detector outputs are connected to a time-amplitude-converter (TAC). Each section of the set-up will be described in detail in the next chapter with the function of each of the components explained.

We also describe the detailed search for the NV centres conducted in the lab on all of the diamond samples that were selected in the spectroscopic experiments. The theory behind the ability of the NV centre to emit single photons is also given as well as the statistics used to quantify if a source is really a single photon source (refer to page 74).

5.2 Excitation set-up

In Figure 5.1, the experimental set-up used in the investigation of the NV centre as a source of single photons is shown as a schematic diagram. The apparatus are labeled S: diamond sample; O: microscope objective (numerical aperture =0.50); L: the excitation laser (excitation light is represented by green rays) (wavelength of 532 nm); DM: dichroic mirror; F: band pass filter; F1: Plano-convex lens (focal length(f) =100mm); F2: Plano-convex lens (f=400mm); P-H: pin hole; F3: Plano-convex lens (f=100mm); BS: 50/50 beam splitter; F4: Plano-convex lens (f=125mm); F4: Plano-convex lens (f=125mm); F5: Plano-convex lens (f=125mm); D1: detector (SPCM-AQR) and D2: detector (SPCM-AQR) and TAC: time-to-amplitude converter; MP: multi-port; PC: computer plus an additional mirror M and a CCD (charge couple device) camera.

A continuous wave laser which produces 10 mW optical power at a wavelength of 532 nm was used to excite the NV centres in the diamond sample. The laser light is sent to the dichroic mirror where it is reflected and directed to the microscope objective. The objective, through the lenses that are built in, focuses this light onto the diamond. The objective that we are using has a numerical aperture of 0.50 and it is responsible for focusing the excitation light as well as for collecting the fluorescent light from the diamond.

The diamond is mounted onto a home-made stand that is movable in the x, y and z directions. The collected fluorescent light is separated from the excitation light by the same dichroic mirror and sent to the confocal set-up formed by lens F2, pin-hole (P-H) and lens F3 in Figure 5.1. Additionally mirror M and a CCD camera were added to the set-up to enable us to view the fluorescent spots due to the NV centres in the sample. Once a potential NV centre was observed on the monitor, the CCD camera and the mirror were removed. In Figure 5.2 we show a picture of the actual excitation set-up that was constructed in the laboratory.

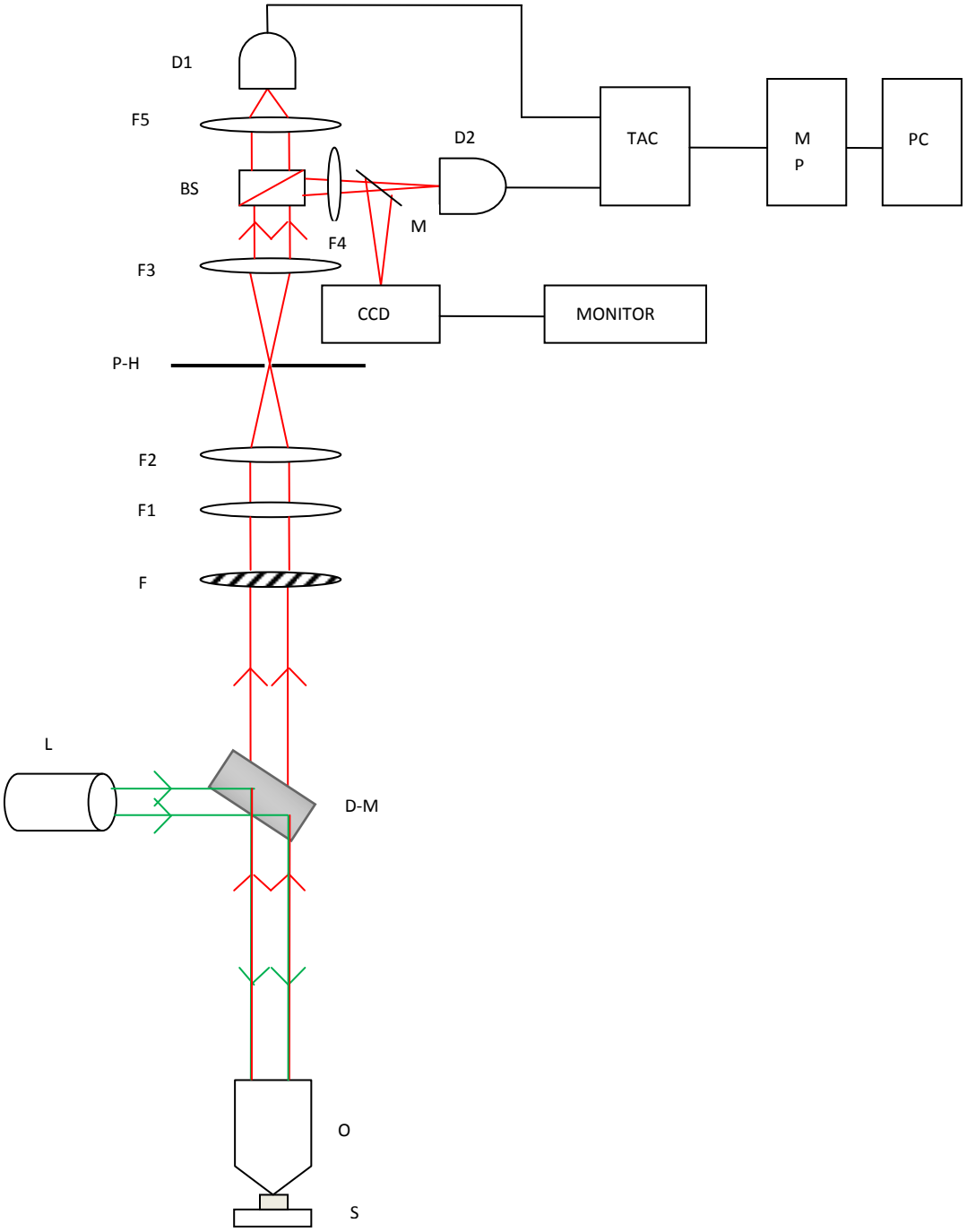

Figure 5.1 Scheme of the set-up used to study the fluorescence (red rays) from the diamond. The symbols used are D1-2: detectors; F1-5: lenses; M-P: multi-port; PC: computer; TAC: time-to-amplitude converter; P-H: pin-hole; F: filter; L: laser; D-M: dichroic mirror; O: objective and S: sample.

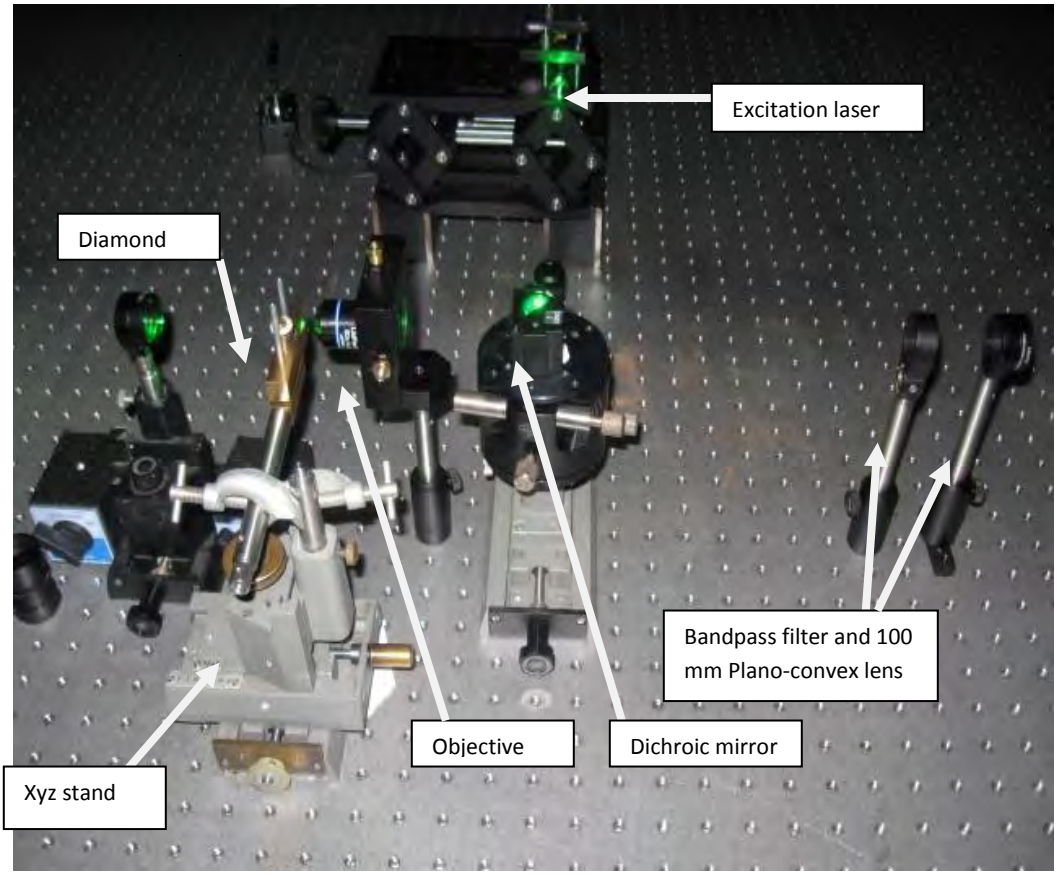

Figure 5.2 Excitation set-up we used in the generation of single photons by exciting the NV centres in diamond. The sample is held by a stand that can be moved in three directions. It is excited by a laser (532 nm) and emitted light is collected by the same objective used for focusing and sent through the dichroic mirror and filter which allows only the fluorescent light to pass through.

5.3 Confocal set-up

A confocal microscope creates sharp images of sample by excluding most light that is not from the objective's focal plane. Unlike in conventional microscopes, it gives images that are less hazy and better contrast. The modern confocal microscope uses the same techniques such as the pin-hole and point to point illumination of the sample as the one first invented by Martin Minsky in 1955 [69].

In our set-up we took the objective out of a standard microscope and used it on its own to focus the excitation light on the sample and also to collect the resulting fluorescent light. The set-up consisted of a band pass filter with central transmission wavelength of 640 nm and a bandwidth of 90 % over 14 nm to help cut-off light of other wavelengths. Then to improve the magnification of our collection area on the diamond, a number of lenses were used. These are labeled F1 (f=100mm), F2 (f=400mm) in Figure 5.1. The lenses were chosen so that we could view a $20\mu\text{m} \times 20\mu\text{m}$ section on the diamond. We ascertain this by removing the diamond from the sample holder and inserting a microscope grating in its place. The magnification was determined by illuminating the grating, which has a set of parallel lines that are spaced $10\ \mu$m apart, with a light and collecting this light as it passes through the objective. The image was viewed using the CCD camera and the two lenses F1 and F2 were changed until we could see the image shown in Figure 5.3. The lines on the grating are $10\ \mu$m apart and therefore the total distance from one end to the other on the figure is $20\ \mu$m.

The pin hole was placed at the focal length of F2 as seen in Figure 5.1 to allow the point of light at this length to be the only one allowed to go through to the detectors. Behind the pin-hole we put another lens to collimate the light before it strikes the beam splitter. The whole alignment of the optical components was done with the help of a HeNe laser that was placed on the same side of the objective as the sample holder with the sample holder empty. The laser beam path was adjusted such that it passes through all the optics at the same height. This was to ensure that the collected fluorescence is directed onto the detectors.

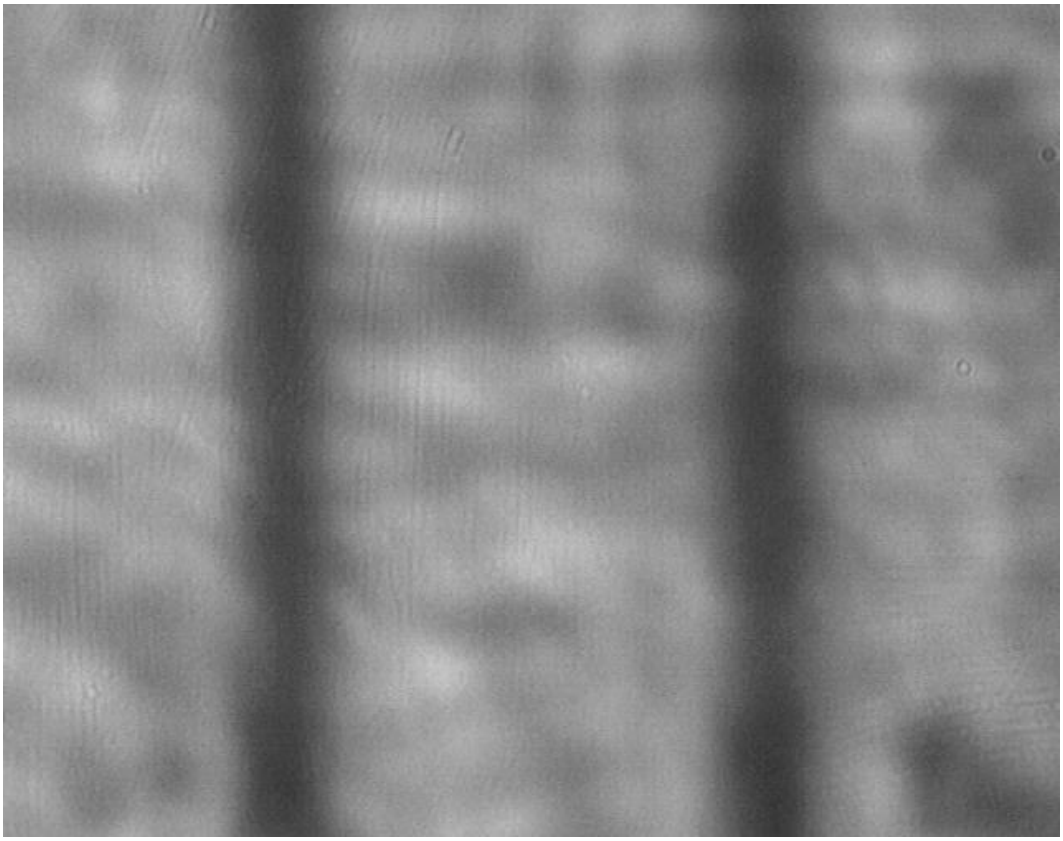

Figure 5.3 Image of the grating lines on the microscope grating slide. Each line is spaced $\mathbf{10}\boldsymbol{\mu}\mathbf{m}$ from the next and through this, only fluorescent light from within the area of $\mathbf{20}\boldsymbol{\mu}\mathbf{m} \times \mathbf{20}\boldsymbol{\mu}\mathbf{m}$ was sent to detection. This reduces the collection of background light from the diamond.

5.4. Hanbury Brown and Twiss set-up

The HBT experiment was first done by Robert Hanbury Brown and Richard Twiss in 1956 [70]. Their set-up consisted of light from a mercury lamp which was collimated, split up by a beam splitter. The intensity of each portion is measured by the two photo cathodes which were placed at the same distance from the beam splitter. One of the detectors could be transversely displaced with respect to the fixed detector for the measurement of the photon correlations[3]. The fluctuations in the outputs of the two detectors are multiplied together in the correlator. Although their measured correlations were within the classical statistical optics, the same techniques have been applied in quantum optical statistics.

5.4.1 Detection

We have used an HBT detection set-up in our experiment (see Figure 5.4); it consists of a 50/50 beam-splitter, two detectors and the TAC (the TAC is not shown in the figure). The beam splitter sends half the fluorescent photons to one detector and the other half to the second detector placed perpendicularly with reference to the first one. The output from these detectors is sent to the TAC. Both detectors are single photon counting module (SPCM-AQR) from PerkinElmer with a peak photon detection efficiency of 65%. They use unique avalanche photodiodes (APDs) which are basically p-n junctions reverse biased at a voltage slightly above the breakdown voltage. At this bias the electric field is high enough to allow a single charge carrier to trigger an avalanche when injected in the depletion layer (this layer is devoid of charge carriers due to the diffusion of electron and holes across the junction causing annihilation of carriers). In order to function as photo-detectors, the diodes must be capable of being switched off and a sufficient time allowed for the current to flow until the avalanche is quenched. This is achieved by removing the bias voltage to stop the avalanche current and restoring bias before another photon can be detected.

[3] Photon correlation gives the number of pairs of photons appearing at each detector as a function of the relative time delay between arrivals of each photon at the detector.

Silicon APDs offer an advantage over normal APDs in that they operate in Geiger mode where reverse voltage higher than the APD's breakdown voltage thus increasing the device's sensitivity to incident photons. This means that when a photon strikes the device an avalanche current is generated. This avalanche can only be stopped by removing applied voltage. In linear mode the gain is not sufficient or is barely enough to detect single photons.

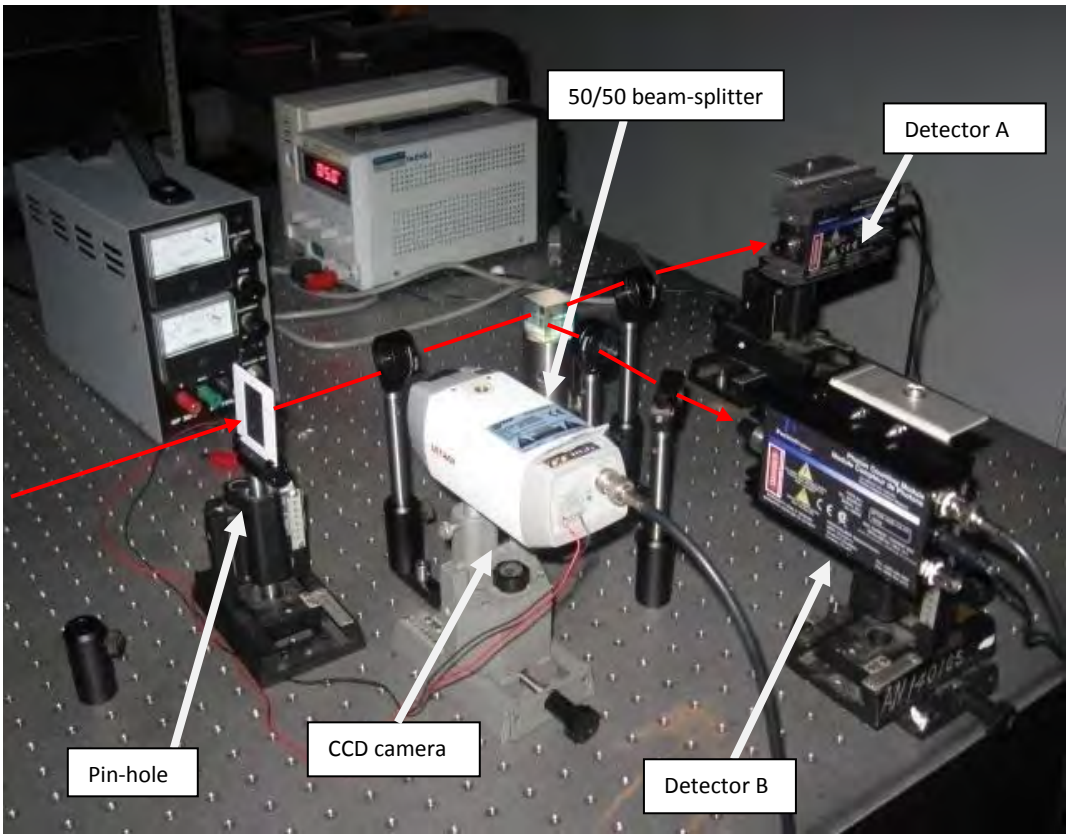

Figure 5.4 Hanbury Brown-Twiss detection set-up. The incoming photons (illustrated with the red line) go through a pin-hole which ensures that all the background light from the diamond does not go to the detectors. They are then focused onto the 50/50 beam-splitter where one half is transmitted and goes to detector A and the other half is reflected and goes through to detector B.

Silicon APDs in these particular modules we are using can achieve peak photon detection efficiencies greater than 65% at 650 nm. The detectors that we use had a dark count of 100 counts per second.

5.4.2 Time-to-Amplitude Conversion

In order to determine the timing properties of the arrival of photons at the detectors, i.e. the coincidences of the photon arrivals at each of the detectors a Constant Fraction Discriminator (CFD, CANBERRA model 2126) was used together with the TAC. This is achieved by feeding a signal from detector A into the TAC (CANBERRA model 2145) via a CFD module. This will be the START signal for the TAC. The output from the detector B is also fed through the CFD and onto the TAC where it will provide the STOP signal. The CFD works by offering timing output signal when a constant ratio of the pulse height is reached. This ratio, once set, is consistent from pulse to pulse thus removing amplitude and rise time errors that arise. The STOP signal is delayed from the START by approximately 64 ns. This delay is set by the Nanosecond Delay (CANBERRA model 2058) which uses a number of switches to select a delay of 0.5, 1, 2, 4, 8, 16 or 32 ns or any combination of these.

The signals that are received from the CFD are used in the TAC to generate an output pulse (voltage) whose amplitude is linearly proportional to the time between the START and STOP input pulse pair. The TAC then selects only pulses that are in the START-STOP interval and rejects any over range time differences. It also rejects START pulses that come before the START. Thus the reason for inserting a delay in one of the detector outputs is that if both detectors receive a photon simultaneously (i.e. there is zero time between the arrivals of photons), we still obtain a pulse of non-zero height from the TAC which can be counted; hence we chose the highest delay time on the module. The outputs from the TAC are then analyzed by another module called the multiport to create a histogram of the pulse height, i.e. a histogram of the time between pulses. The histogram is downloaded onto the computer for display. A true single photon source will not produce a count at $\tau = 64\,ns$, due to the fact that a single photon will choose to go to only one of the detectors at a time (see Section 6.3 for the reason for delay).

5.5 Experimental search for NV centres

All the diamonds that were studied in Chapter 4 were examined using the set-up that was just described for the presence of NV centres. To try and locate the NV centres, an entire surface area of each of the diamond samples was scanned. This was done using the experimental set-up shown as a schematic in Figure 5.1. The diamond was illuminated using a 532 nm continuous wave laser with maximum optical power of 10mW as described in section 5.2.1. The fluorescence of the NV centres was viewed by use of a CCD camera and it appeared as bright spots on the monitor. Magnification was adjusted so that we could view a 20μm $\times$ 20μm section of the diamond sample. We then moved the sample using the xyz control on the sample holder until we saw bright spots on the monitor, which is connected to the CCD camera. Once we have a bright spot in view we removed mirror M and the camera so we can performed the auto-correlation computation. We repeated this for other regions on all diamonds. The collection efficiency was also improved through the use of a band pass filter and a pin-hole as explained in Section 5.3.

The NV centres give photons with a wavelength of 637 nm and thus they appeared as red spots on the diamonds. To be able to see the fluorescent light from the diamond by viewing the diamond directly with the eyes, we used goggles that cut off the green excitation light and allowed us to see only the red fluorescence. Some of the centres were difficult to see with the naked eye on the CCD monitor; therefore we used a digital oscilloscope to show the output pulses from the detectors. Whenever a site containing NV centres was at the focal point of the objective, the detector outputs showed an increase in the number of pulses. The time of arrival of the photons at the detectors was processed as explained in sub-section 5.4.2. The number of counts, i.e. the time between photon arrivals, which were binned into a histogram by the multi port, was so low that it became necessary to collect data over several days in order to obtain a histogram for a single point on a particular sample. After the experiment was performed using a number of diamond samples, only two showed the characteristics of NV centre as a single photon emitter and the results are presented in the next chapter.

Chapter 6

Single photon source: Results

6.1 Introduction

The experimental set-up described in the previous chapter was used to systematically scan the diamond samples for possible isolated single NV centres. Single photon emitters are identified by measuring and plotting the histogram of time (τ) between the arrival of photons at each detector in the HBT set-up. This histogram is proportional to the second order autocorrelation function. Single photon emitters display a dip in the second order autocorrelation plot at $\tau = 0$ [71].

This chapter presents the results of the autocorrelation experiment and relates them to the electronic structure of the NV centre described in the next section. References to the three-level energy diagram will be made to explain the single photon emission. We will also refer to the results of the spectroscopic experiments described previously in our analysis of the data in this chapter. The diamond samples that were found to be suitable for further study from these spectroscopic techniques did not all turn out to be useful samples for applications as single photon sources. Of the eleven samples selected, only two showed characteristic behaviour of NV centres when illuminated with a laser of correct wavelength. The others either did not show any fluorescence or the fluorescent light from the sample was just too much to give us single photons.

The results of the two diamonds which mimic the behaviour of single photon emitters also showed some flaws, thus illustrating that our preliminary experimental set-up needs some improvements.

6.2 Emission of single photons by the NV centre

To understand the single photon emission properties of the NV centre, we look at its electronic structure. The electronic structure of the NV centre consists of a triplet ground state and a triplet excited state as illustrated in Figure 6.1. As the centre is illuminated with a laser of a suitable wavelength, in this case 532 nm, it gets pumped from the ground state into the excited state.

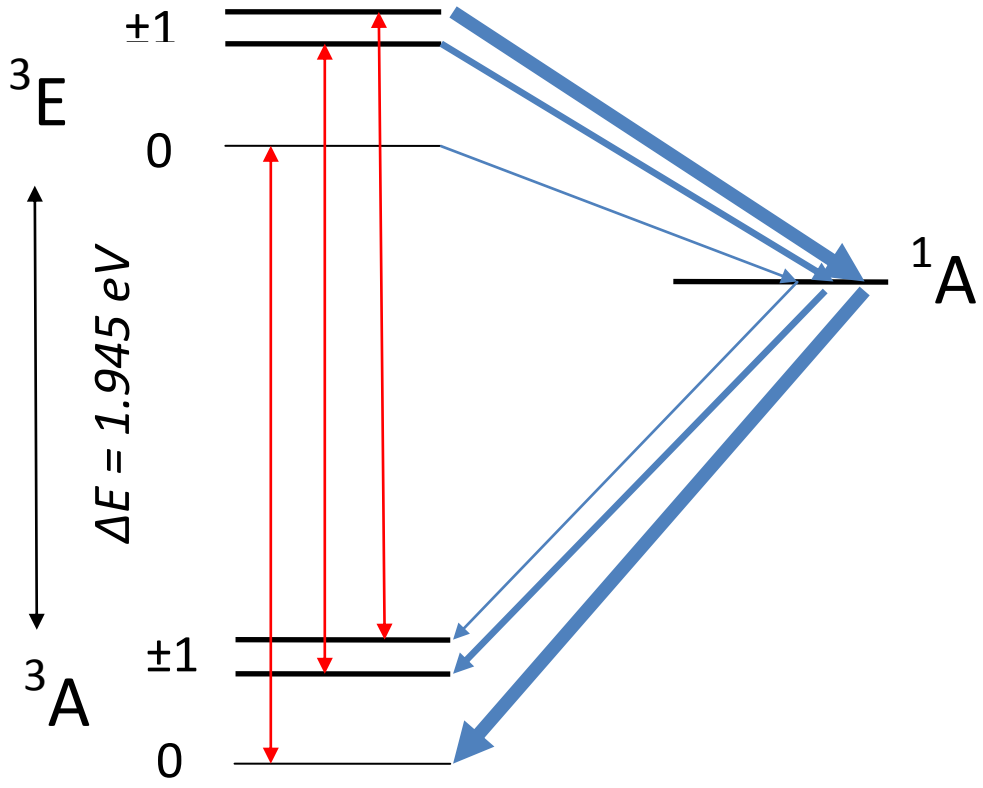

Figure 6.1 Simplified energy level diagram of the NV centre. The ground state ^{3}A is a triplet with m_s= 0, ±1 sublevels. The excited state ^{3}E is believed to be similar [72]. The three red lines indicate the three possible optical transitions between the ground and excited states. Decay rates are indicated by the blue lines with the thickest one indicating a higher rate of decay.

The energy separation between these states is $\Delta E = 1.945\, eV$, therefore as the centre decays back to the ground state it gives off photons with a wavelength of 637 nm which corresponds to this energy. The centre is able to be classified as a source of single photons because it cannot emit more than one photon at a time as it has to decay back to ground, be re-excited and then decay again to give off another photon. Hence the photons come at regular intervals determined by the lifetime of the excited state. There exists a third singlet state in the electronic structure as seen in the figure and if it is populated during excitation, it contributes to the intersystem crossing during optical transitions of the NV centre.

The intersystem crossing transitions between the excited state ^{3}E and the meta-stable state ^{1}A occur with different transition probabilities as illustrated by the thickness of the arrows in Figure 6.1. The decay rate from the $m_S = 0$ sublevel of ^{3}E is smaller than those from $m_S = \pm 1$ levels. The decays from the ^{1}A to the ground state are also with different transition probability with the $m_S = 0$ being the preferred level to decay to. Thus, from this rates we can deduce that after sufficient optical pumping, the $m_S = 0$ level of the ground state will be the most populated and hence most transitions will be from this state. The fluorescence from the NV centre is brightest if the spin is in the $m_S = 0$ sublevel. The total decay rate of the NV centre after excitation has been found to be approximately 13 ns [72].

By illuminating the samples with the 532 nm laser, the NV centres in the diamonds will follow these transitions and emit photons as they decay to the ground state. If the system undergoes transitions from the excited state to the meta-stable singlet state, then the centre will not fluoresce and a dark interval will occur with a time period equal to the lifetime of the meta-stable state. The average number of excitation and emission cycles that is possible depends on the structure of the fluorescing molecule and the local environment. Some molecules photo-bleach quickly after emitting only a few photons while other more robust ones can undergo thousands or even millions of cycles before photo-bleaching. The location of the NV centre in diamond gives it an advantage over this phenomenon in that diamond is very robust against interactions with the environment, thus providing the NV centre with high photo-stability.

6.2.1 Photon statistics

To quantify how good a source of single photons is, we first need to understand the photon statistics. In instances when photons are emitted by such a source, the probability of getting two or more photons should be negligibly small. This can be better described by considering the case of a weak coherent pulse source, for example, an attenuated laser beam. The pulses have a Poissonian distribution given by equation (6.1), i.e. some pulses are empty, and another fraction has only one photon per pulse while some will have two or photons per pulse.

$$p(m) = \frac{<n>^m}{m!} e^{-<n>} \tag{6.1}$$

$\langle n \rangle$ is the average number of photons and m is the number of counted photons.

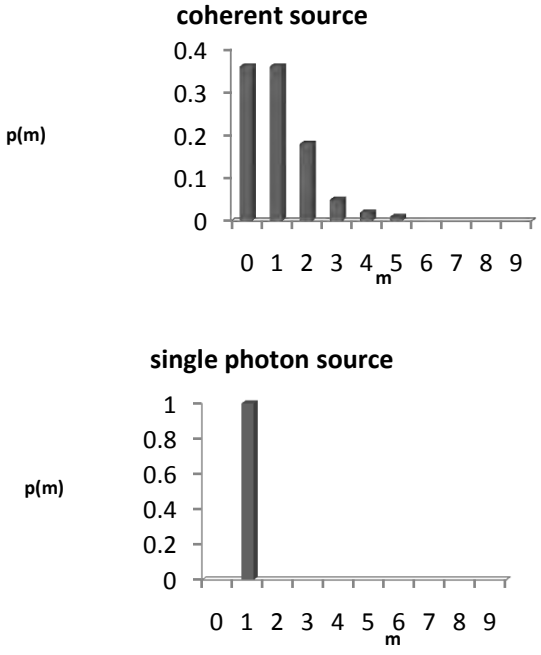

Figure 6.2 The probability distribution of the number of photons for two sources with an average photon number <n>. The coherent light source presents a Poisson distribution with a strong number fluctuations whereas the single photon source delivers a number state with m=1 at regular time intervals.

In a given probability of getting a photon, the probability of getting two or more photons should be very small compared to the Poisson value. Figure 6.2 illustrates the probability distribution of the number of photons per pulse for a weak coherent source and a single photon source. The fluctuations that occur for the coherent source are called particle fluctuations and are due to the discrete nature of the photoelectric process. That is, energy can be removed from the light beam only in whole photons.

6.2.2 The second order correlation function

The normalized second order correlation is used to quantify if a source of photons is indeed giving out single photons at a time. The function is described by the following equation,

$$g^{(2)}(\tau) = \frac{\langle I(t)I(t+\tau)\rangle}{\langle I(t)\rangle^2}, \tag{6.2}$$

where $I(t)$ is the intensity of light at time t. This function is related to the joint probability of detecting a photon at time t and the detection a subsequent photon at some later time $t + \tau$.

For a coherent source, the average intensity of light is independent of time, thus $g^{(2)}(\tau) = 1$ for all values of τ . To illustrate this, consider the electric field

$$E = Ae^{i\vec{k}\vec{r}-\omega t},$$

where A is the amplitude.

If we let $\vec{r}$ be at the origin, then equation (6.3) becomes

$$E = Ae^{-i\omega t}. \tag{6.3}$$

Equation (6.2) can be expressed in terms of intensity of light as

$$g^{(2)}(\tau) = \frac{\langle E^*(t)E^*(t+\tau)E(t)E(t+\tau)\rangle}{\langle E^*(t)E(t)\rangle^2}. \tag{6.4}$$

Substituting equation (6.3) in equation (6.4) yields

$$g^{(2)}(\tau) = 1$$

For light that comes from a single photon source, the pulses come at regular intervals therefore $g^{(2)}(0) < 1$, demonstrating the antibunching effect. For the NV centre, the time interval between the pulses will be determined by the lifetime of its transition between ground and excited states. This ability of the NV centre to emit one photon at a time and at regular intervals has been described in section 6.2.1.

The Hanbury Brown and Twiss experiment depends on the resolution in time of the intensity fluctuations rather than the frequency resolution that is characteristic in spectroscopic experiments.

6.3 Analyzing the fluorescent light

All the samples were illuminated as explained in Chapter 5 to excite the NV centres and the two samples that exhibited the characteristic behaviour of a single photon emitter were M4 and clearTria. This was deduced from the plot of a number of counts of photon arrivals versus the time delay (in nanoseconds).

For a true single photon source, the arrival of photons at the two detectors is never coincidental, that is, there can never be a recorded count in the two detectors at the same time. Thus, at zero delay the number of counts should go to zero. This is due to the fact that, at the beam-splitter there is a 50 percent chance for the photon to either be reflected to one detector or be transmitted to the other detector. A coincidence at zero delay would mean the photon was split-up thus defying the laws of quantum physics. In our analysis, we expect to have a dip at around 64 ns (our delay time) although it may not necessarily go to zero because our diamond have different environments and concentrations of NV centres which may affect this depth of the dip.

From the spectroscopic experiments conducted earlier, the M4 sample showed a weak intensity peak at 637 nm zero phonon line in the PL spectrum. We concluded that the concentration of NV centres in this sample may be weak making it a good candidate for

single photon studies. We kept it under continuous excitation for a number of days and we still got to only about 100 counts per histogram bin. This agrees with the conclusion made earlier that the NV centre concentration is low. The recorded counts of photons from this sample are shown in Figure 6.3. Because we had set our delay at 64 ns, we expected a dip at around this time but due to other factors such as the length of the connection cables, the dip seems to appear in the vicinity of 80 ns. The number of counts binned at this time is about 7 which mean that the fluorescence collected was not from a single NV centre in the diamond but maybe from a number of them. This is because exciting different centres means that they will decay at different times hence the resulting photons will not be separated by the same time interval (equal to the lifetime in the excited state). The presence of other dips at time scales out of the range of the delay we set is due to reasons not yet established.

Figure 6.3 show that the diamond sample has portions which approach the behaviour of a single photon source. To obtain a proper single photon source at this stage is almost impossible as also evident in other papers published. However, a source that approaches single photon behaviour means that every now and then more than one photon is produced. This in turn means that the purity of the source is compromised.

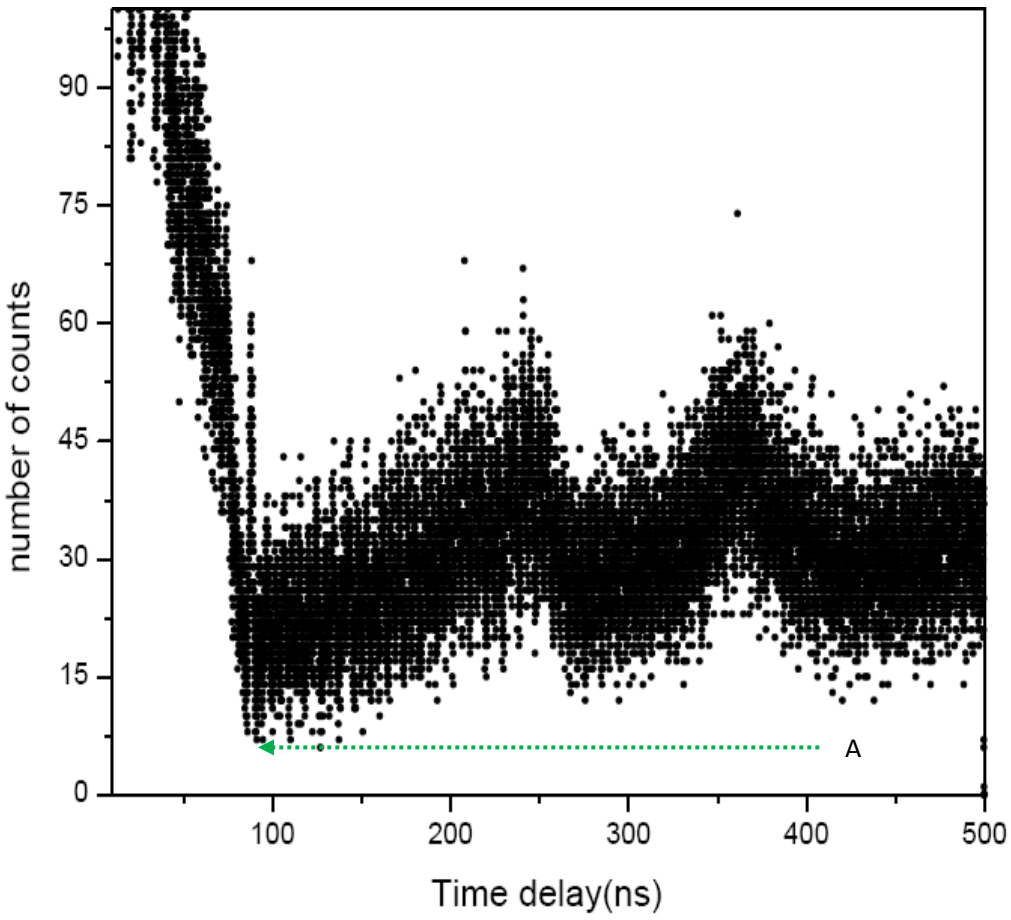

Figure 6.3 The plot of the number of counts of the photon arrivals at each of the detectors versus the time delay in nanoseconds for M4. . Point A indicates a point where the number of counts was the lowest, at around 80 ns (our zero delay was set at 65 ns) therefore the diamond approaches the behaviour of a single photon source.

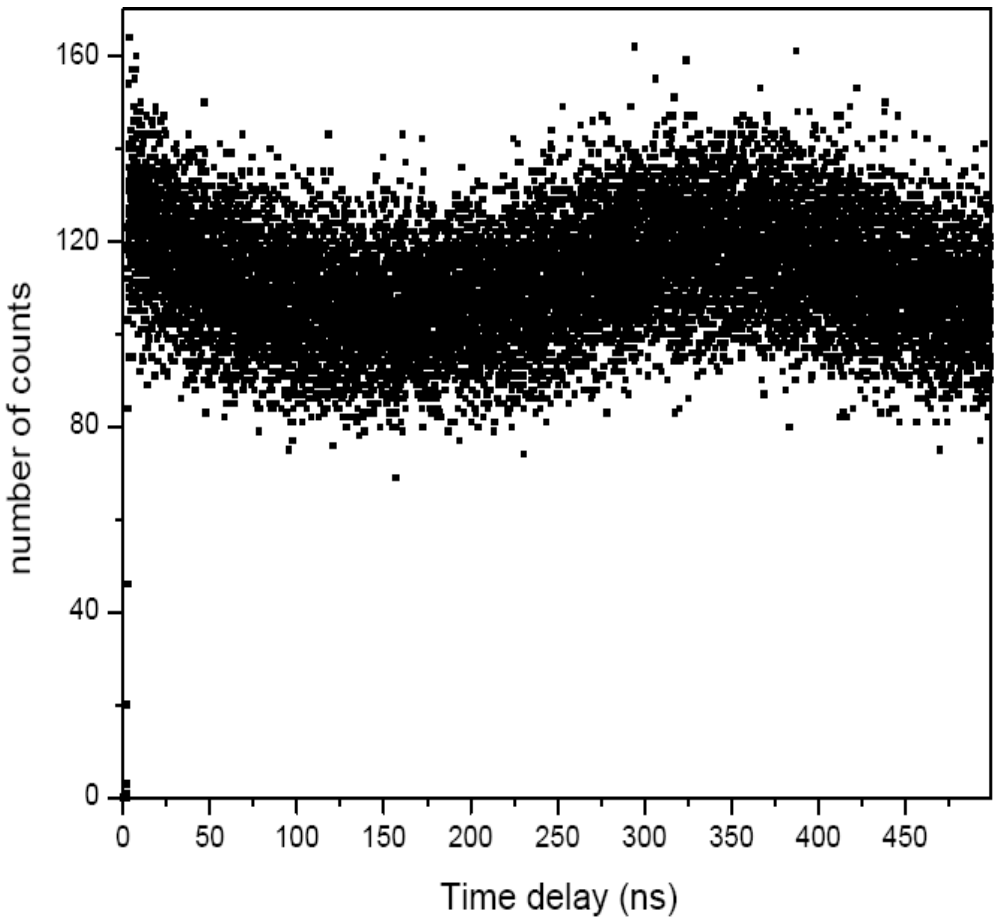

Figure 6.4 The spectrum of the number of counts of the photon arrivals at each of the detectors versus the time delay in nanoseconds for clearTria. There is a broad dip appearing at around 100 ns therefore this diamond approaches the behaviour of a single photon source. The broadness could be attributable to the effects of the other defects other than NV centres present in this diamond or may be due to the excitement of too many NV centres.

In Figure 6.4 we see that the cleaTria diamond sample also exhibited a dip, although broad, at the expected place on the time delay scale. The broadness of the dip and the fact that the number of counts was not as low as in the other sample may be due to a number of reasons. It could be that the excitation light was focused on a number of NV centres resulting in different decay rates or that the other defects present in the sample were interfering with the collection efficiency. This can be rectified by further improvements on the apparatus, that is, by devising a method to determine the number of centres that are being excited. The air gap between the sample and the microscope could also have not been at the right position for the optimal collection as the diamonds were moved with a mechanical xyz table which made it difficult to position the diamond at the right spot in front of the objective.

Chapter 7

Summary and Conclusion

The aim of this master's project was the identification of diamond samples with NV centres and the development of a single photon source based on the NV centre in the diamonds. The justification for this need has been explained in the discussion of Quantum Cryptography in Chapter 1. It has been explained in that chapter that encoding messages using single photons is a secure method of transmitting the key in QKD. This project began by first studying the properties of diamond and the NV centre. These have been presented in Chapter 2. Diamond can be classed depending on their impurity content. The common impurities in diamond are among others nitrogen and boron. Diamond also contains other defects, and the NV centre is one of them.

Experimental studies began with a suite of twenty seven diamond samples from which we searched for those samples that have defects through the use of Ultraviolet-Visible-Near infrared, Infrared, Electron Spin Resonance and Photoluminescence spectroscopic techniques which enabled us to narrow down the number of samples that are potential candidates for single photon generation, that is, those diamonds that contain NV centres or nitrogen. The samples that turned out to have nitrogen in some form or the other as a defect were eleven out of the twenty seven.

The experimental set-up to generate single photons using the NV centre in diamond was constructed in the laboratory on an optical table. This was based on a confocal microscope arrangement. A laser beam was focused onto a selected point on the diamond by means of a microscope objective. The fluorescence light from the NV centre was collected by the same objective and passed on for further processing. Using the HBT interferometer, the second order autocorrelation function of the fluorescence light was computed. This enabled us to

determine if the fluorescent light displayed single photon characteristics. The number of diamond samples showing characteristic behaviour of single NV centres, there is, a dip in the autocorrelation at zero time interval between the arrivals of photons at the detector was further reduced to two.

A number of experimental difficulties were encountered during the setting up of this experiment. The major difficulty was the precise alignment of the apparatus. However, even after overcoming this, the consistent measurement of data was still difficult. The experiment was trial and error, and obtaining the right gap between the sample and the microscope objective was difficult. The backlash in the homemade xyz stage also presented a challenge as well as the environment in which the NV centres were positioned in the diamond crystal as this was unknown to us.

Because the samples had other defects in them, the collection of fluorescence from NV centres was affected. The other contributing factor could be the bulk properties, for example, internal reflections, of diamond contribute somewhat to the collection efficiencies. These challenges could be improved by changing the environment in which the NV centres are located in diamond by acquiring an ultra-pure diamond and fabricating NV centres whose spatial distribution we can estimate as well as by using a better microscope objective.

Appendix A

CAXBD97 decomposition spreadsheet fits

This appendix presents the fits obtained from the FTIR spectra using the Diamond Trading Company's CAXBD97 Excel program as explained below. The decomposition spreadsheet is designed to be used to decompose the single phonon region of a diamond infrared absorption spectrum in order to determine the concentrations of nitrogen present in various aggregation states. The centres that are fitted are:

C-centres: single substitutional nitrogen (neutral charge state)

A-centres: nitrogen pairs

B-centres: 4 nitrogen atoms plus a vacancy

N^+-centres: single substitutional nitrogen (positive charge state)

D-component: platelet-related

Nitrogen concentrations are determined from absorption coefficient values at particular wave-number positions for the various components. The spreadsheet uses the following figures from literature [65].

Single nitrogen

$$[N_C] = 25 \times \mu_C\ (1130\text{cm}^{-1}) \qquad \text{(A-1)}$$

A-centres

$$[N_A] = 16.5 \times \mu_A\ (1282\text{cm}^{-1}) \qquad \text{(A-2)}$$

B-centres

$$[N_B] = 79.4 \times \mu_B\ (1282\text{cm}^{-1}) \qquad \text{(A-3)}$$

N^+-centre

$$[N^+] = 5.5 \times \mu_{N+}\ (1332\text{cm}^{-1}) \qquad \text{(A-4)}$$

where [N] is the nitrogen concentration in parts per million (ppm) and μ is the absorption coefficient in cm^{-1} at the stated wave-number value for the chosen component.

The decomposition of the single phonon region is achieved using Excel's solver tool to carry out a least squares fit for the components and constraints determined by the user.

8.1.1 Layout of the Excel Workbook

The CAXBD97 workbook consists of two sheets: "data" where data is read in and the fit is carried out, "graph" where the resultant spectra are plotted and the nitrogen concentrations are listed for printing out.

8.1.2 Preparation of Spectra

A number of manipulations to the data must be carried out before reading it into the spreadsheet. The exact steps required will depend on the software used to acquire the data. The final format required for the raw data column has been chosen to be as simple as possible (i.e. absorption coefficient values corresponding to a wavenumber range of 1001 to 1399 cm^{-1} with a data spacing of 1 cm^{-1}).

The infrared absorption spectrum to be analyzed must first be converted to absorption coefficient in cm-1. The intrinsic diamond absorption is then subtracted from this (i.e. a spectrum from a type IIa diamond with no defect induced single phonon absorption features). The single phonon region (at least 1000 to 1400 cm^{-1}) is then saved in .csv format if possible. There is a macro on the spreadsheet that will interpolate such a data set and paste it into the raw data column – this is run via the "ReadInData" button on the "data" spreadsheet. Alternatively, a means can be found of producing a single column of absorption coefficient values (in cm^{-1}) corresponding to a wavenumber range of 1001 to 1399 cm^{-1} with a data spacing of 1 cm^{-1} and this can be pasted into the raw data column.

8.1.3 Spectral Decomposition

CAXBD97.XLS uses the solver tool built into Excel to carry out a least squares fit. This can be opened via the menu (route: Tools>Solver…). The solver dialogue box for fitting A, B and D components is shown below

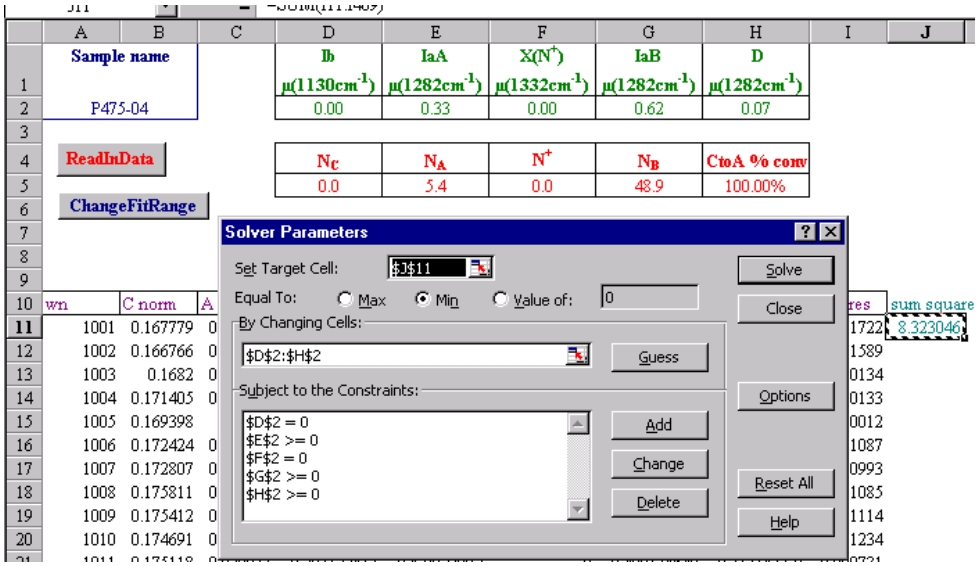

Target cell J11 is the sum of the squares of the differences between the raw data and the fit. This is minimized by varying the multiplication factors for the various components (cells D2:H2). With the set-up shown the constraints only allow the A, B and D components to fit as only cells E2, G2 & H2 can be non-zero. These constraints can be altered to fit other components by clicking on the constraint then the change button. This can also be used to set a component to a particular value. This is useful when the single nitrogen concentration is low and has been determined more accurately from the 1344 cm-1 peak. The absorption coefficient value at 1130 cm-1 corresponding to this can be set as a constraint for D2 and the rest of the components fit as usual.

Once the constraints have been set click on the Solve button. A least squares fit is carried out with the result that cells D2:H2 contain the best fit absorption coefficient values and cells D5:G5 the corresponding nitrogen concentration values. These values are also reproduced on the "graph" spreadsheet, where the fit can be viewed graphically and where there is also a plot of the residual spectrum (i.e. the raw data minus the fit).

The solver can be run manually as described above, or it is called automatically from the macro "ReadInData". There is also a button that runs the macro "ChangeFitRange": this is used to vary the data range used in the least squares fit and is useful in cases where part of the single phonon region is saturated. In this Appendix we present the results of this program for all the samples studied using Infrared spectroscopy.

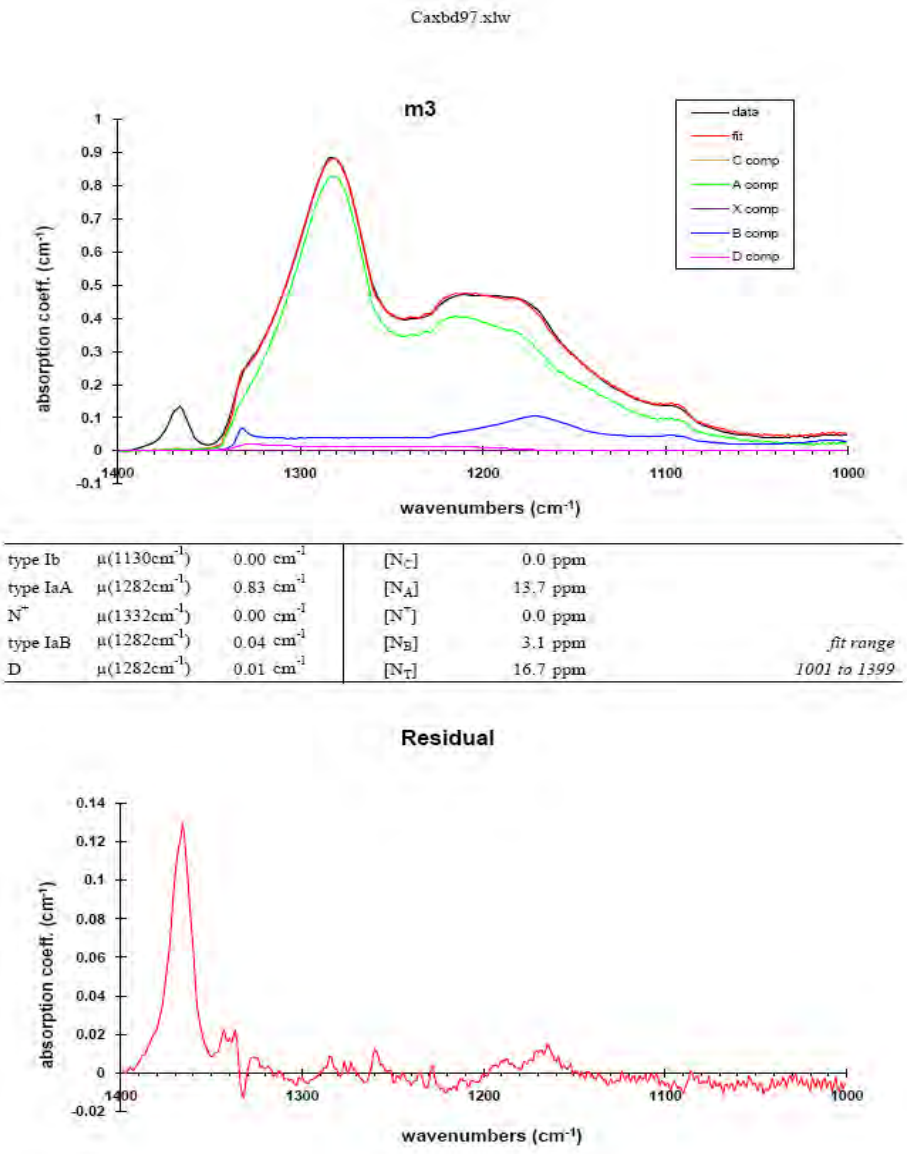

type Ib	$\mu(1130cm^{-1})$	0.00 cm^{-1}	$[N_C]$	0.0 ppm	
type IaA	$\mu(1282cm^{-1})$	0.83 cm^{-1}	$[N_A]$	13.7 ppm	
N^+	$\mu(1332cm^{-1})$	0.00 cm^{-1}	$[N^+]$	0.0 ppm	
type IaB	$\mu(1282cm^{-1})$	0.04 cm^{-1}	$[N_B]$	3.1 ppm	*fit range*
D	$\mu(1282cm^{-1})$	0.01 cm^{-1}	$[N_T]$	16.7 ppm	*1001 to 1399*

Figure A-1 IRspec-CAXBD94 decomposition spreadsheet fits used in the FTIR spectrum of sample m3 to determine the concentration of nitrogen defects present. The sample contains the platelet defects in high concentration followed by the A centre with a concentration of 13.7 ppm.

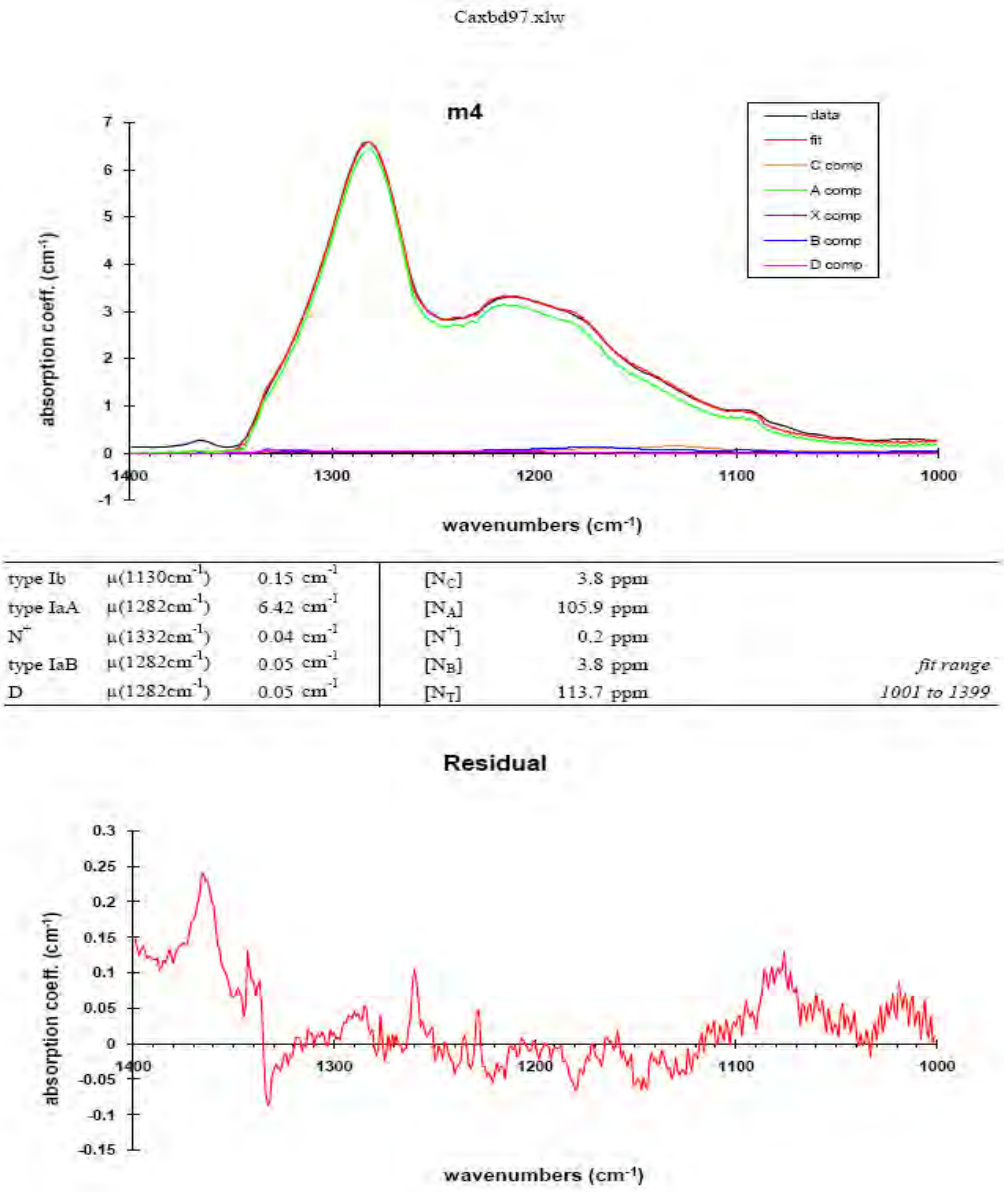

Figure A-2 IRspec-CAXBD94 decomposition spreadsheet fits used in the FTIR spectrum of sample m4 to determine the concentration of nitrogen defects present. The sample contains the platelet defects in high concentration followed by the A centre with a concentration of 105.9 ppm.

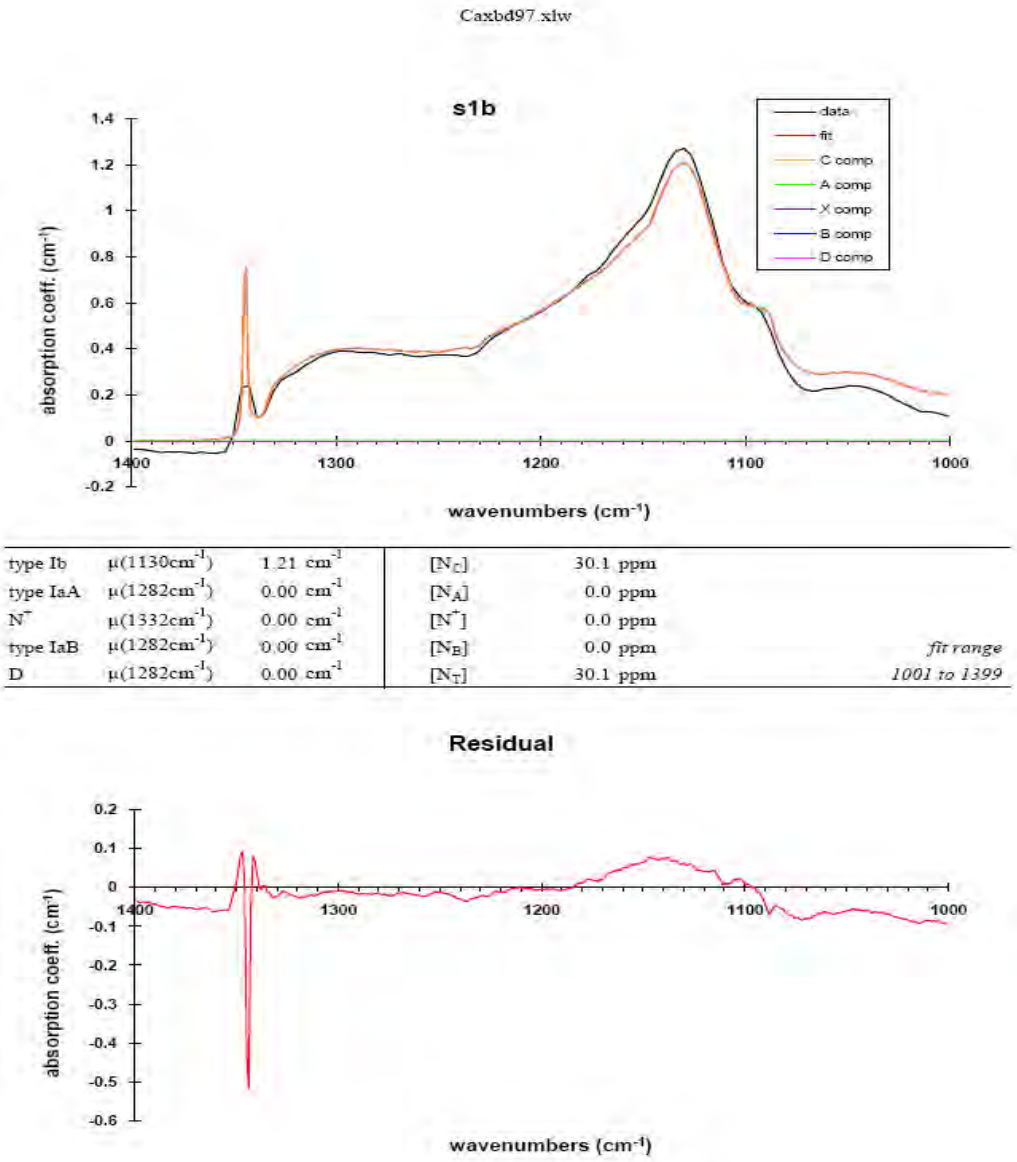

Figure A-3 IRspec-CAXBD94 decomposition spreadsheet fits used in the FTIR spectrum of sample s1b to determine the concentration of nitrogen defects present. The sample contains only the platelet defects and the single substitutional nitrogen both with a concentration of 30.1 ppm.

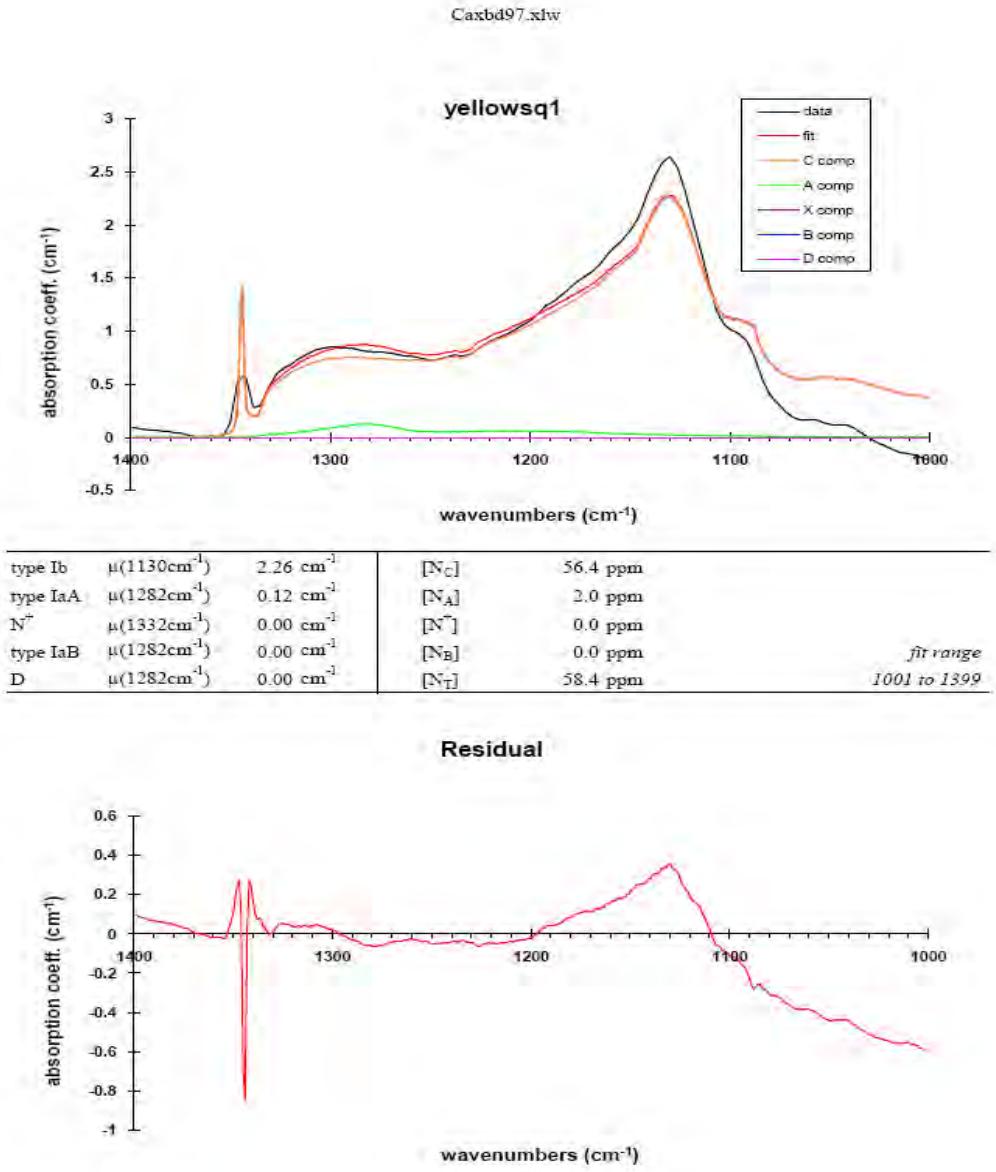

Figure A-4 IRspec-CAXBD94 decomposition spreadsheet fits used in the FTIR spectrum of sample yellowsq1 to determine the concentration of nitrogen defects present. The sample contains the platelet defect and the single substitutional nitrogen with concentration of 58.4 ppm and 56.4 ppm respectively.

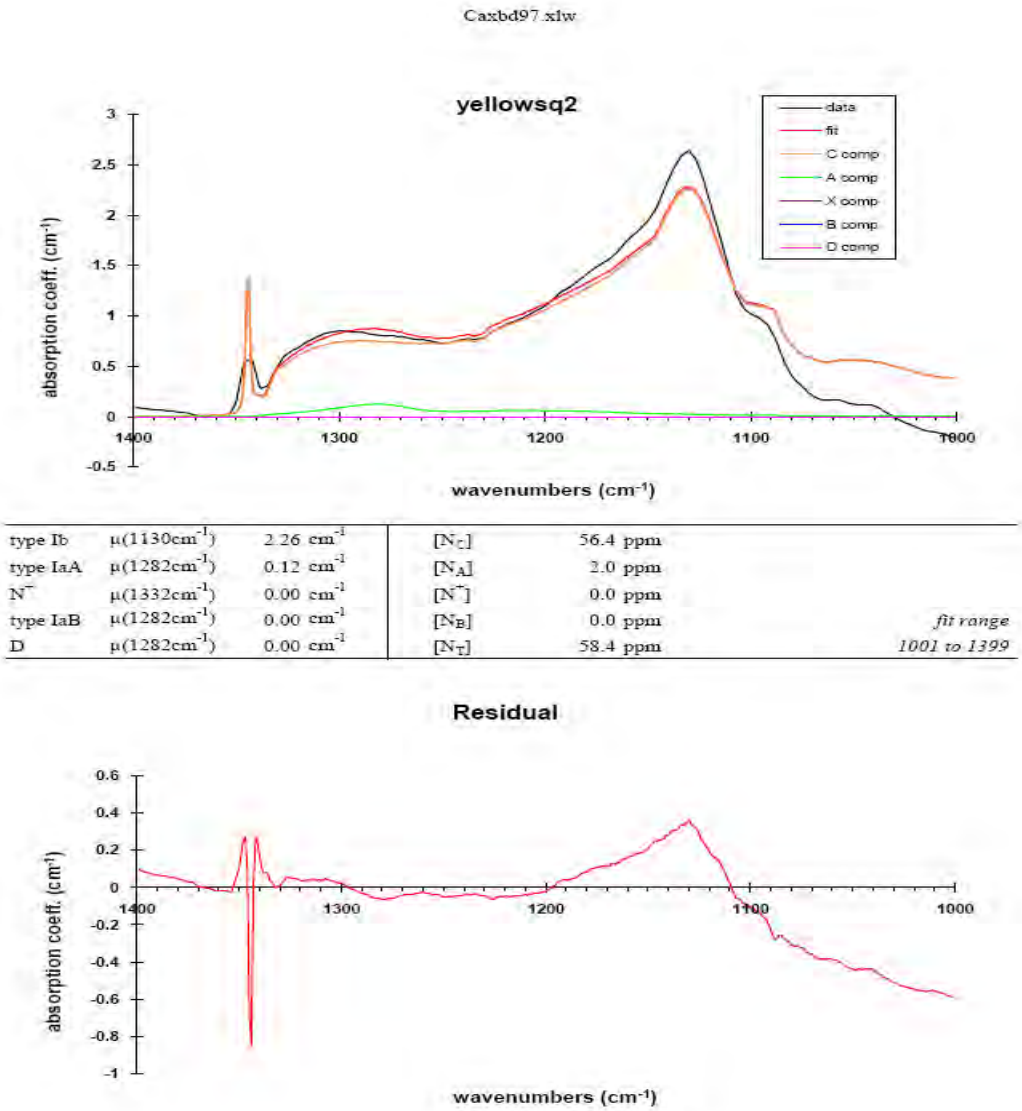

Figure A-5 IRspec-CAXBD94 decomposition spreadsheet fits used in the FTIR spectrum of sample yellowsq2 to determine the concentration of nitrogen defects present. The sample contains the platelet defect and the single substitutional nitrogen with concentration of 58.4 ppm and 56.4 ppm respectively.

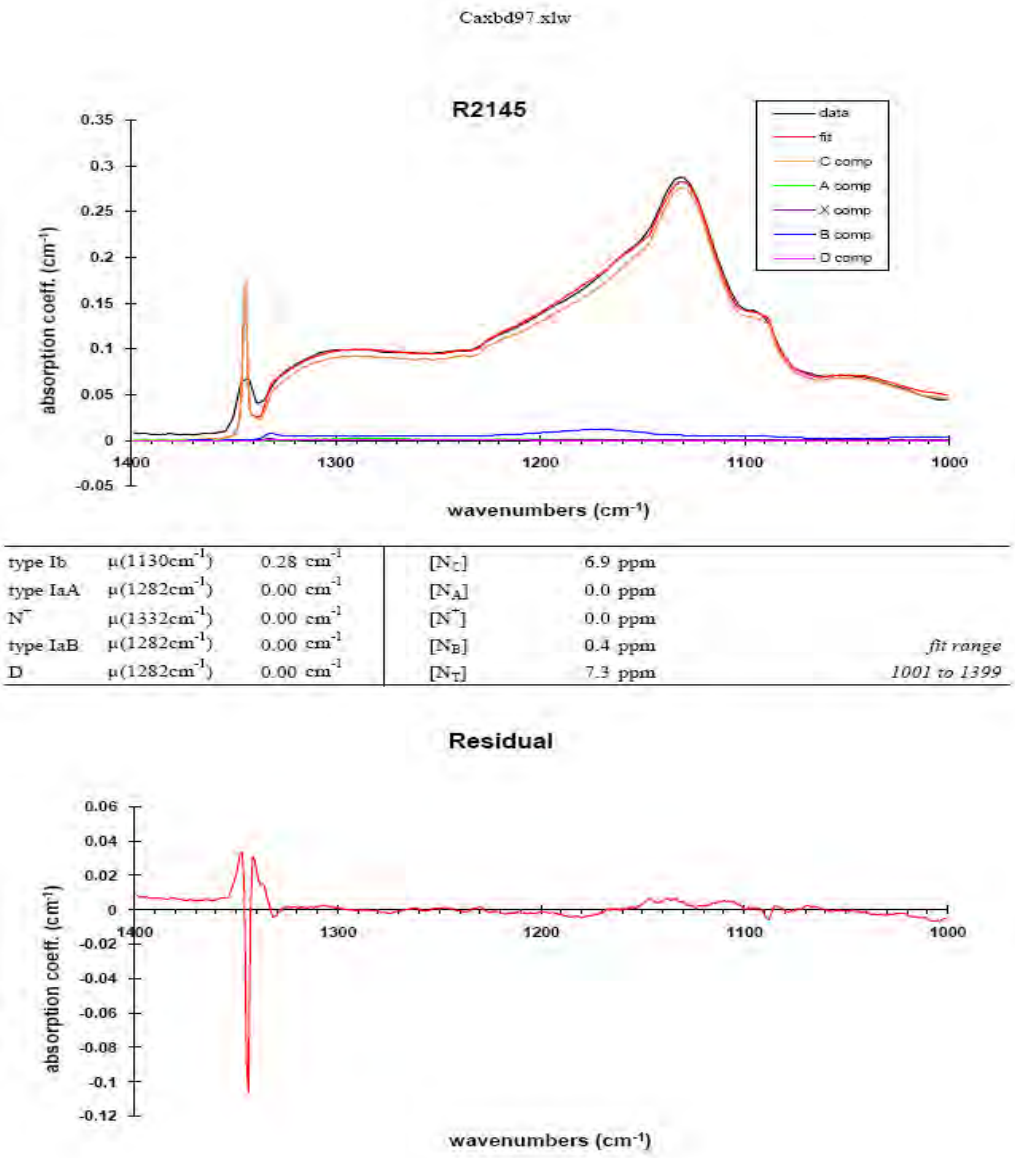

Figure A-6 IRspec-CAXBD94 decomposition spreadsheet fits used in the FTIR spectrum of sample R2145 to determine the concentration of nitrogen defects present. The sample contains the lowest concentration of the B-centre (0.4 ppm) compared to the other defects in it.

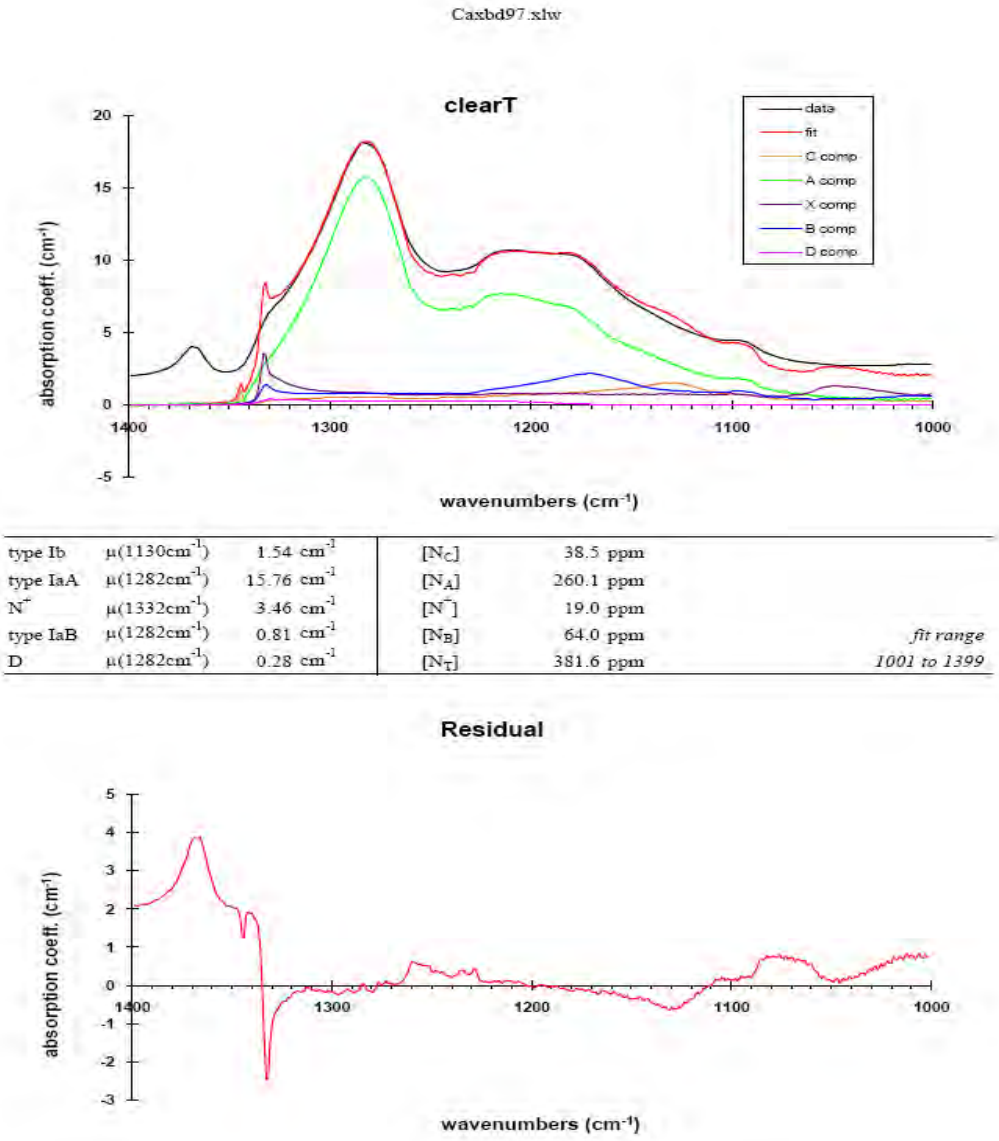

Figure A-7 IRspec-CAXBD94 decomposition spreadsheet fits used in the FTIR spectrum of sample clearTria to determine the concentration of nitrogen defects present. The sample contains the all of the defects it was tested for in different concentrations with the highest being the platelet defect and the A-centre.

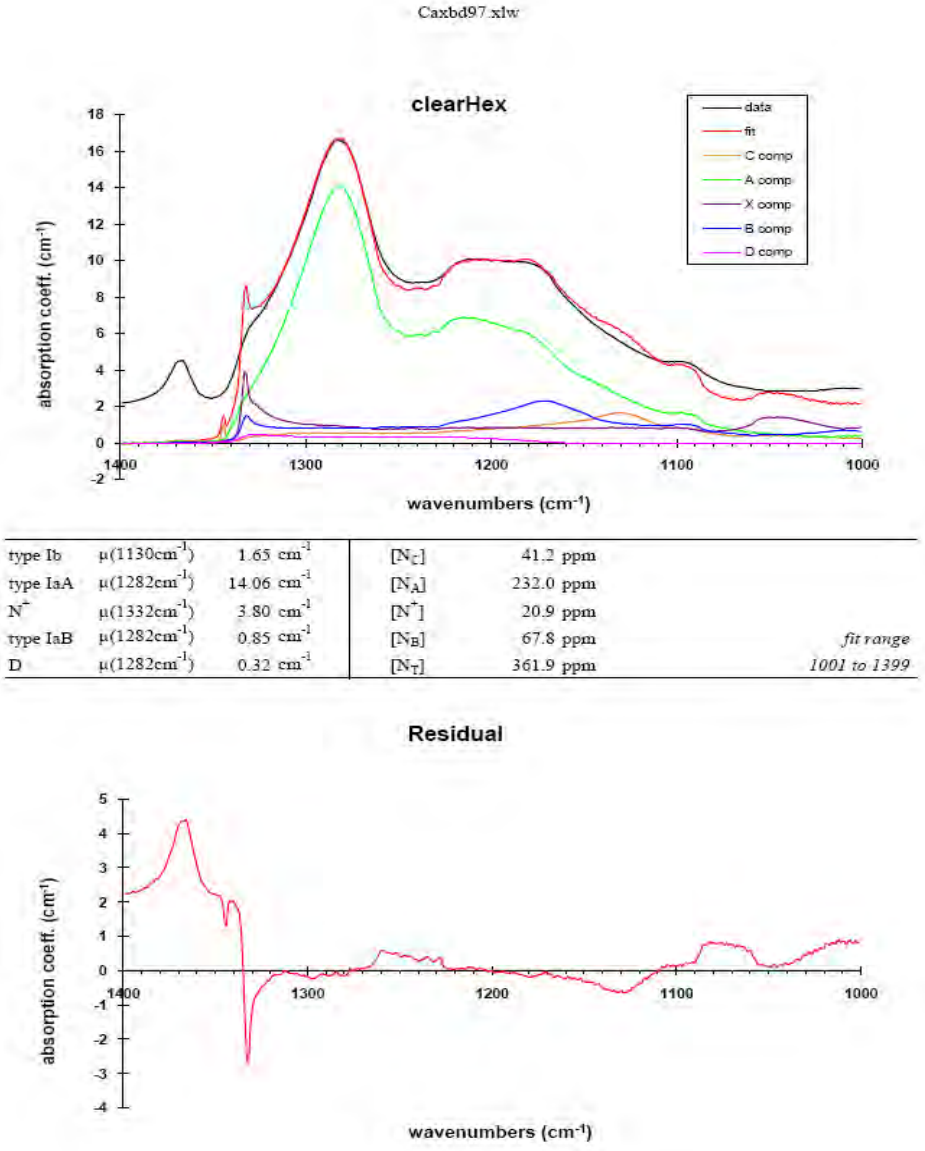

Figure A-8 IRspec-CAXBD94 decomposition spreadsheet fits used in the FTIR spectrum of sample clearT to determine the concentration of nitrogen defects present. The sample contains the all of the defects it was tested for in different concentrations with the highest being the platelet defect and the A-centre.

Appendix B

Laue measurements

The Laue method [73] is a technique in which the orientation of single crystals can be obtained. It involves shining a white (X-ray beam) radiation onto a sample where it can be transmitted or reflected from the crystal. The crystal is kept in a fixed position during the whole experiment, thus making this method sensitive to any imperfections in the crystals, e.g. due to slip which is a plastic deformation occurring when interatomic bonds are fractured and reformed. Figure B-1 and Figure B-2 show respectively a schematic of the transmission and reflection processes.

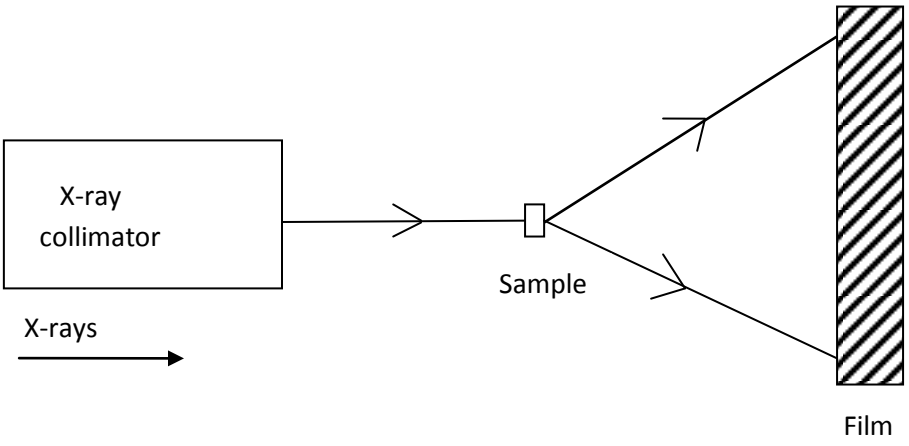

Figure B-1 A simple schematic of the transmission method of the Laue measurements. X-rays that are generated by the machine are directed onto the sample and transmitted through the sample onto the film.

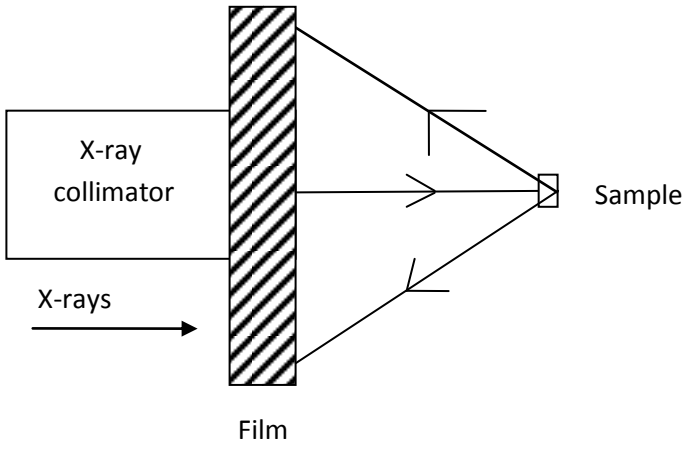

Figure B-2 A simple schematic of the reflection method of the Laue measurements. X-rays that are generated by the machine are directed onto the sample and reflected back to the film as shown.

The diffracted beams from the sample form an array of spots which are recorded onto a film placed behind the crystal for the transmission method (see Figure B-1) or the film can be placed in between the X-ray source and the sample (Figure B-2). The diagrams or pictures on the film show the relative positions of the various lattice planes and therefore enabling the determination of the internal symmetries of the crystal. Each spot on the diagram corresponds to one family of lattice planes.

For our experiments, we placed the each diamond sample in a transmission Phillips X-ray machine (Current = 20 mA, voltage = 40 kV), for about a minute and the resulting Laue pictures are shown below.

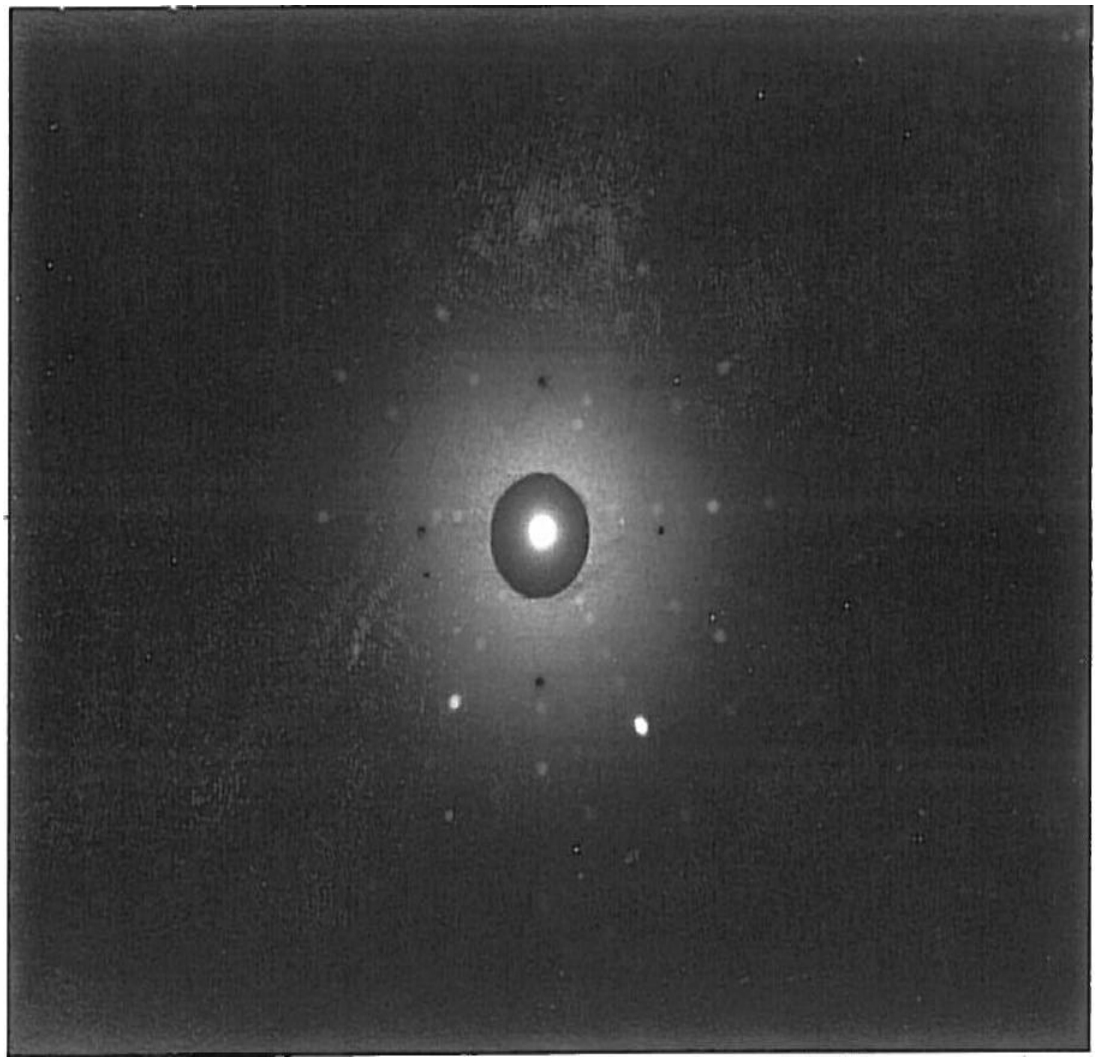

Figure B-3 A Laue photograph of sample M3. From this the face of the diamond was determined as <111>.

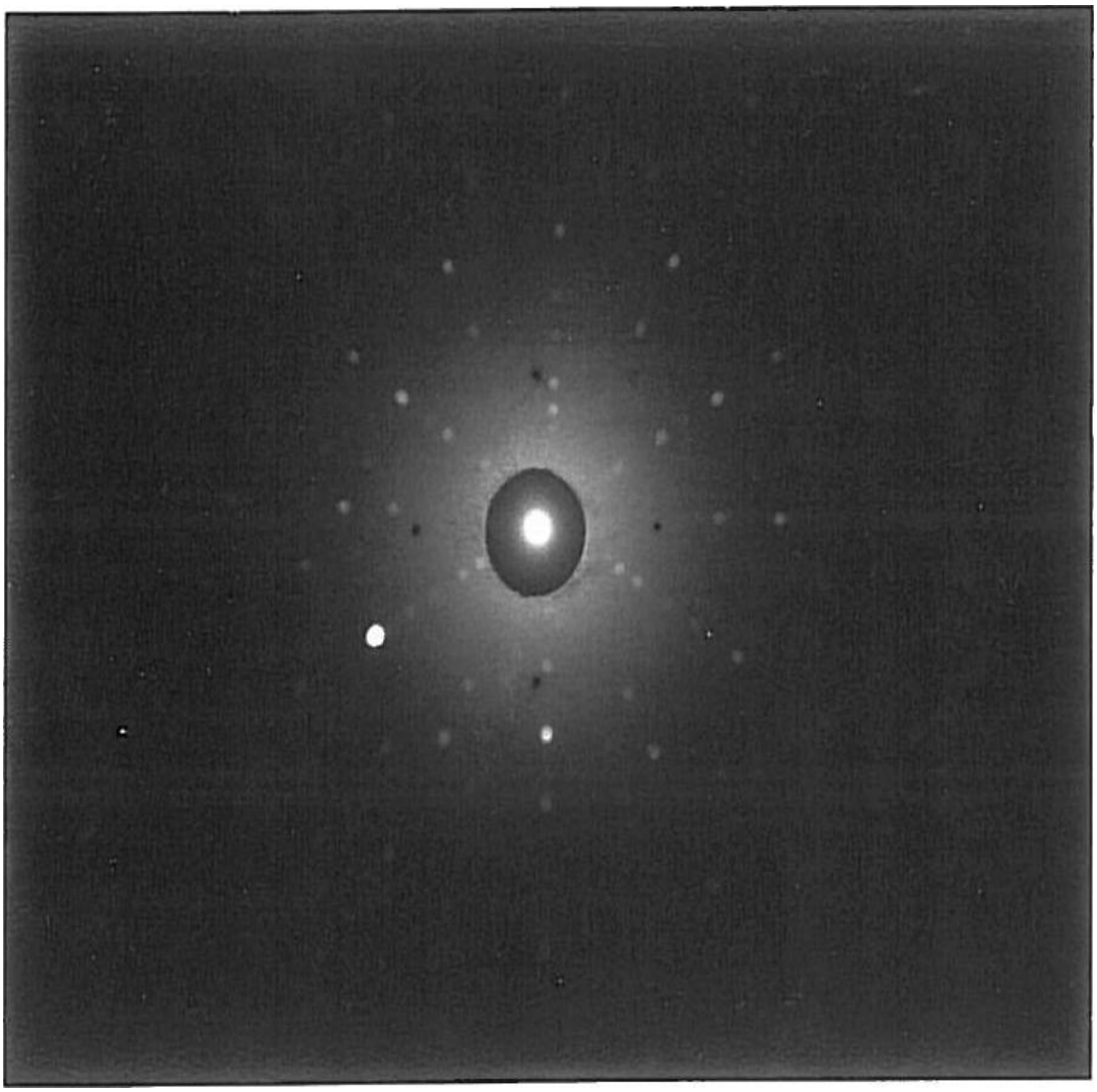

Figure B-4 A Laue photograph of sample M2. From this the face of the diamond was determined as <111>.

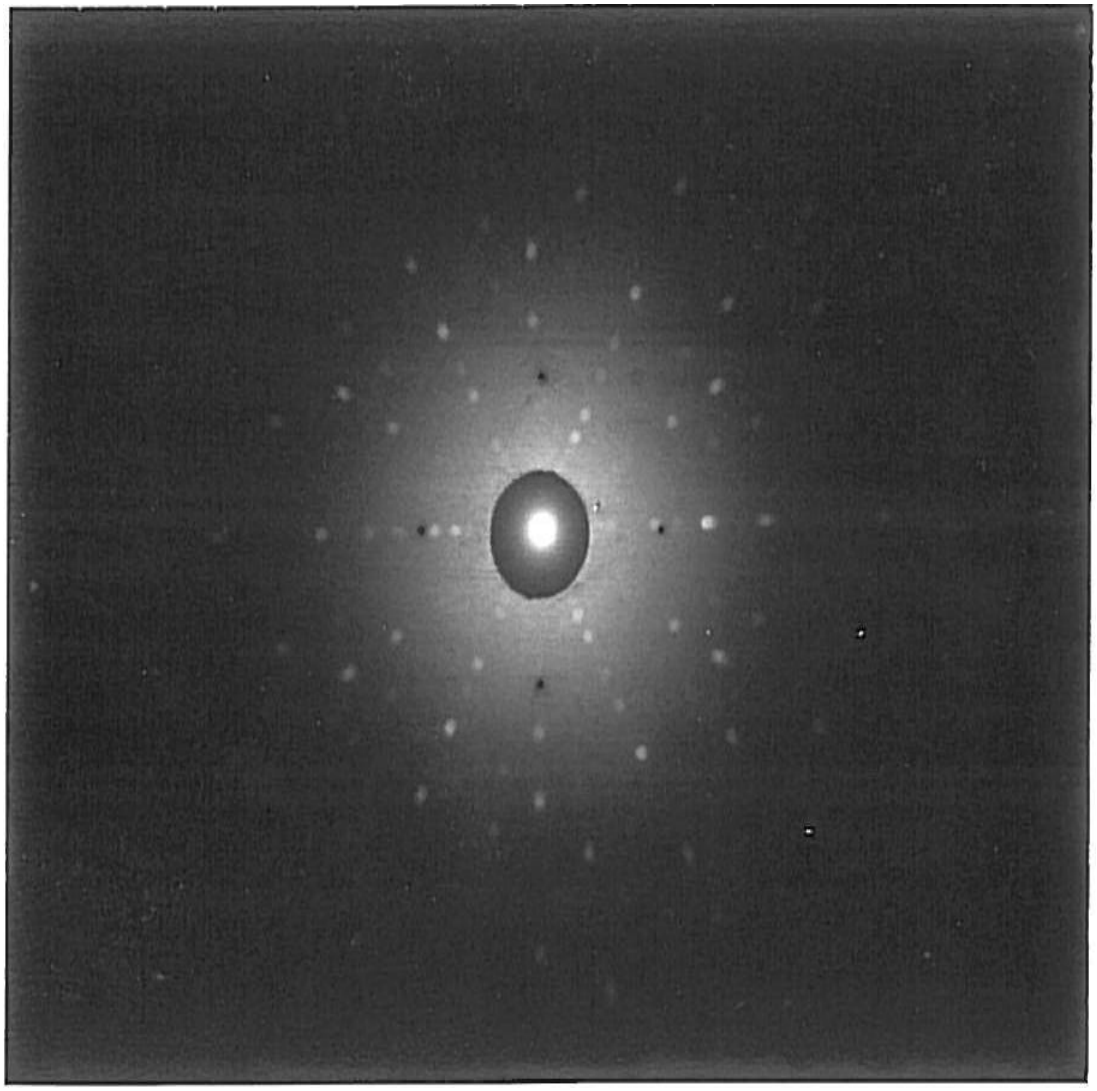

Figure B-5 A Laue photograph of sample M4. From this the face of the diamond was determined as <110>.

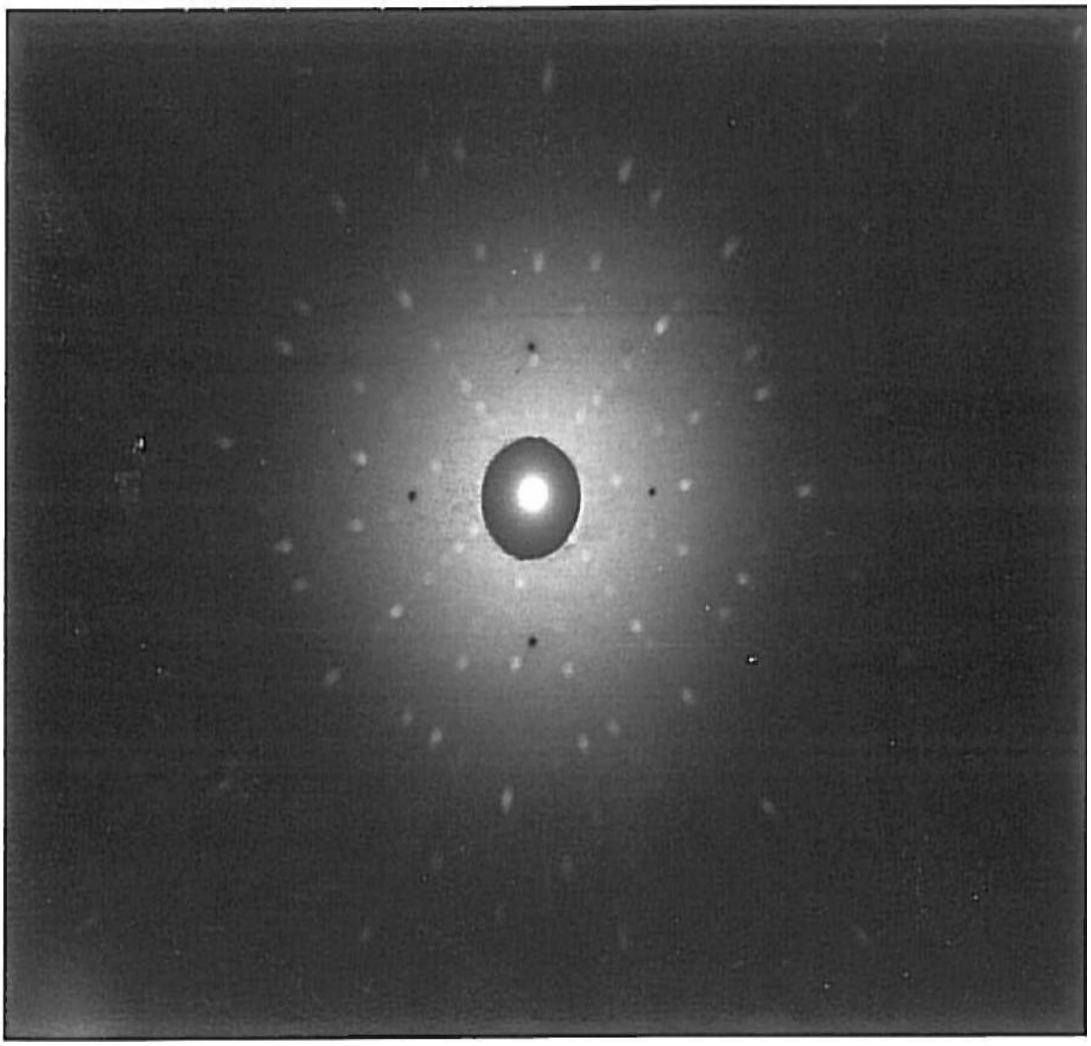

Figure B-6 A Laue photograph of sample S1b. From this the face of the diamond was determined as <100>.

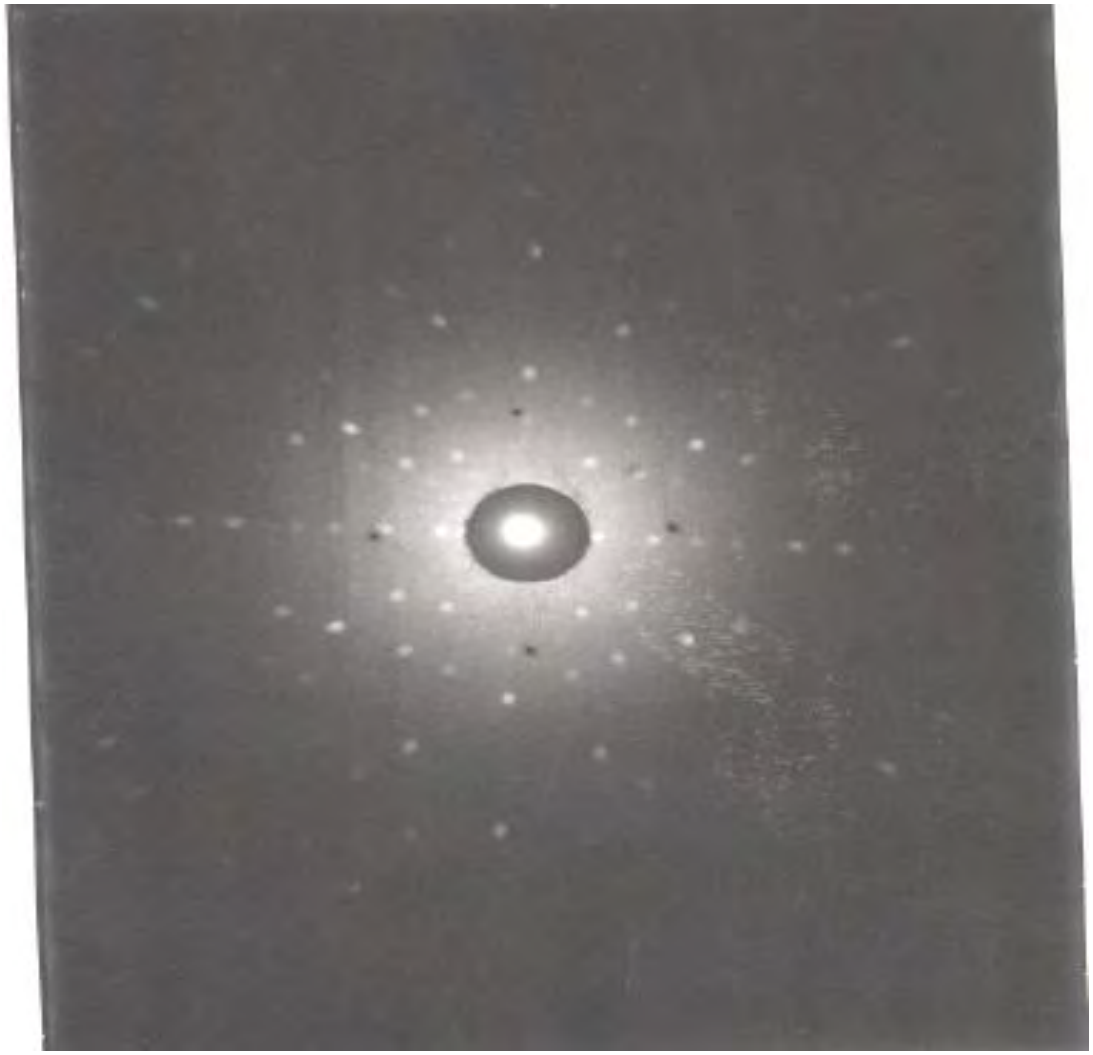

Figure B-7 A Laue photograph of sample clearHex. From this the face of the diamond was determined as <110>.

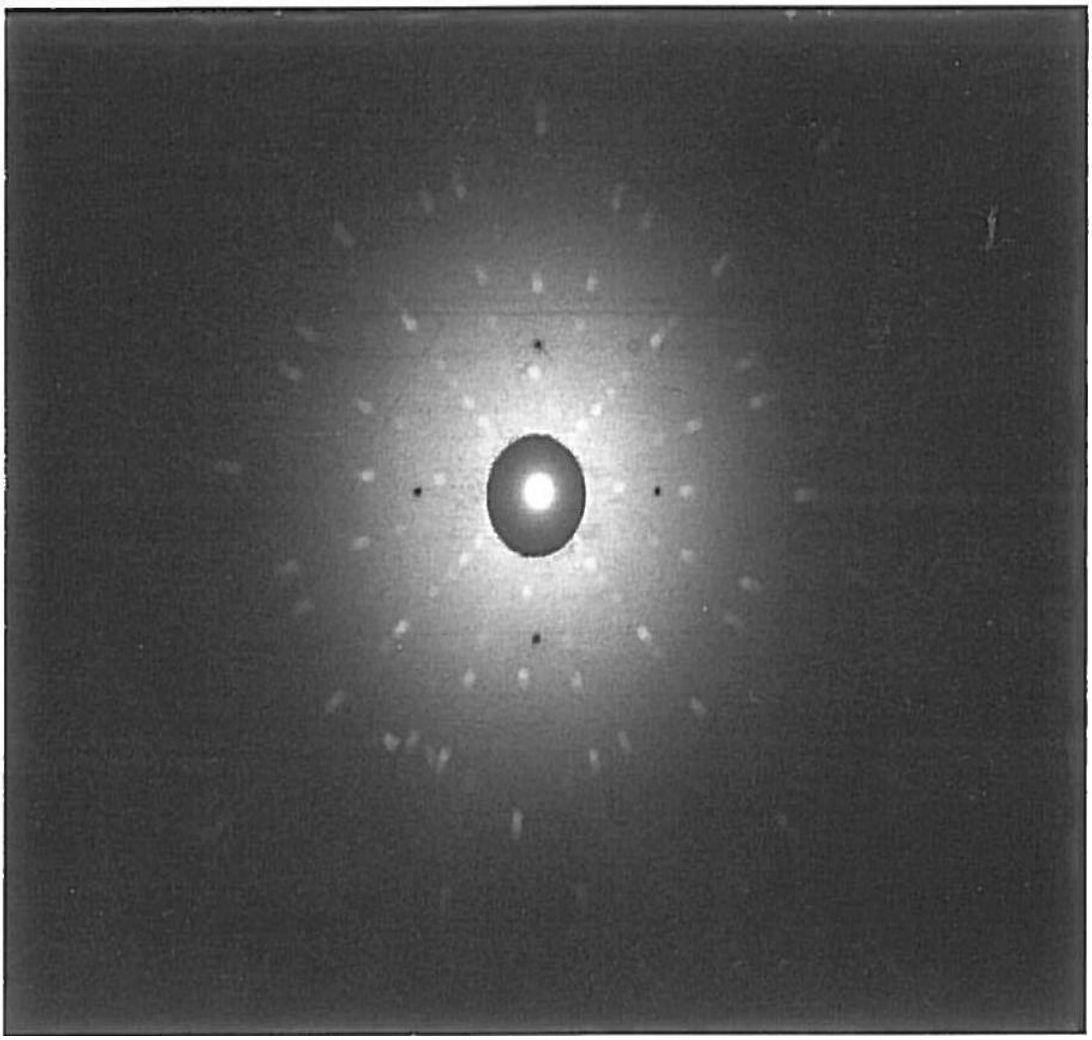

Figure B-8 A Laue photograph of sample R2145. From this the face of the diamond was determined as <100>.

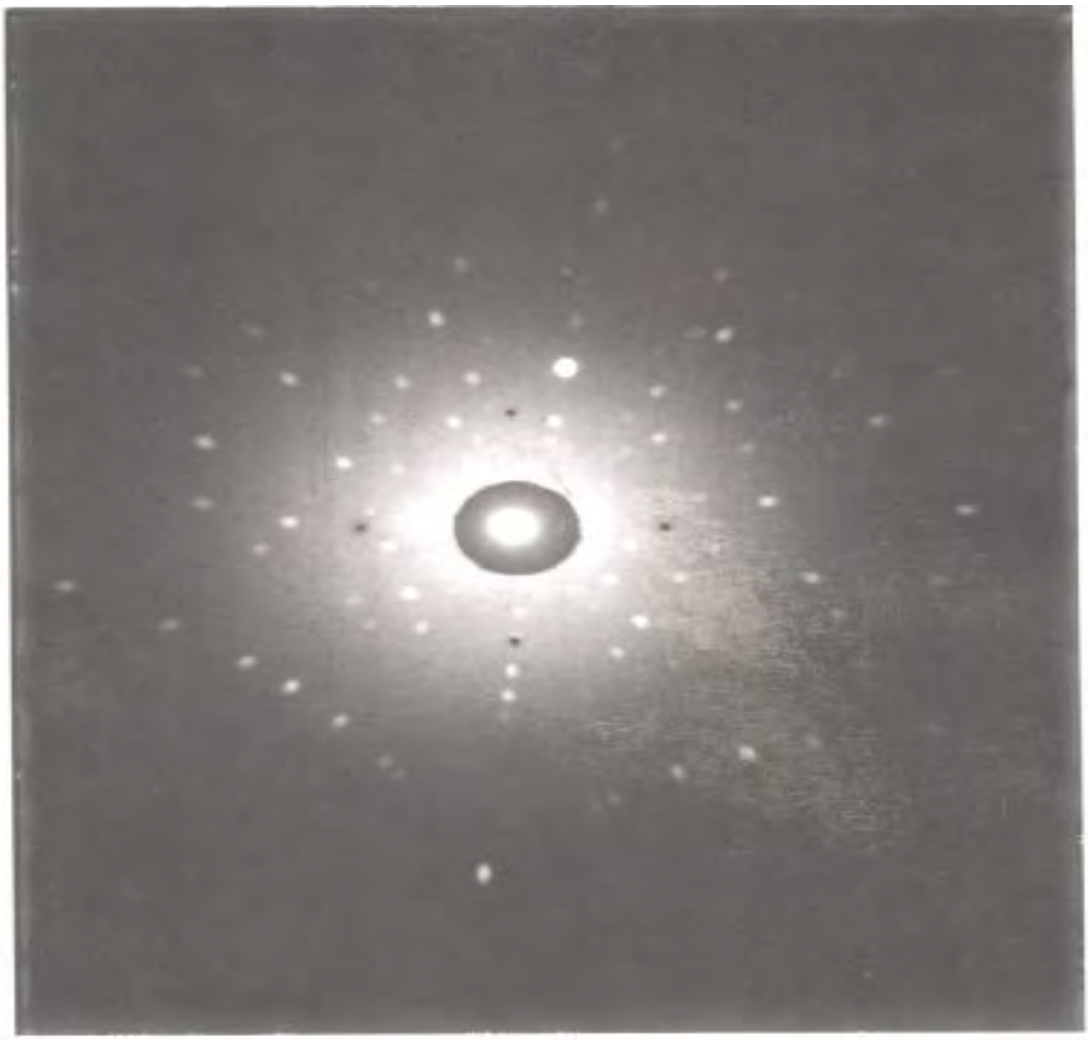

Figure B-9 A Laue photograph of sample clearTria. From this the face of the diamond was determined as <110>

Acknowledgements

I wish to thank Dr. Govender and Professor Petruccione for their immense support and supervision throughout this project. I would like to especially acknowledge the assistance provided by Dr Govender in setting up and testing of the single photon apparatus at the University of KwaZulu-Natal. I also wish to thank the Department of Physics (University of Witwatersrand, Johannesburg), Element Six and Ithemba Labs (Gauteng) for allowing use of their facilities. In particular I would like to thank Professor S. Connell for overseeing all the experiments in Johannesburg with the help of Dr. J. Keartland, Mr. R. Erasmus, Dr. M. Naidoo and Dr. M. Madhuku. Lastly, I wish to acknowledge that the construction and testing of the Hanbury-Brown Twiss electronics were done by another Master's student (Lucien Nzuzi Mbenza).

I wish to thank the **Innovation Fund** for ongoing financial support for the duration of this project.

References

[1] K. G Paterson, F. Piper and R. Schack, Why Cryptography? *e-print: arXiv: quant-ph/0406147v1* (2004)

[2] N. Gisin *et al,* Quantum Cryptography. *Reviews of Modern Physics,* **74**:145 (2002)

[3] W. Wooters and W. Zurek, A single photon cannot be cloned. *Nature*, **299**: 802 (1982)

[4] M. Dusek, N. Lutkenhaus and M. Henrych, Quantum Cryptography. *e-print: arXiv: quant- ph/060120v3* (2006)

[5] http://www.idquantique.com

[6] G. Brassard, N. Lutkenhaus, T. Mor and B. Sanders, Limitations on practical Quantum Cryptography. *Physical Review Letters*, **85**: 1330-1333 (2000)

[7] C. H. Bennett and G. Brassard, Quantum Cryptography: Public key distribution and coin tossing. *Proceedings of IEEE International Conference on computer systems and signal processing,* page 175 (1984)

[8] C. H. Bennett, Quantum Cryptography using any two non-orthogonal states. *Physical Review Letters,* **68**: 3121 (1992)

[9] A. K. Ekert, Quantum Cryptography based on Bell's theorem. *Physical Review Letters,* **67**: 661-663 (1991)

[10] A. K. Ekert, Practical Quantum Cryptography based on two photon interferometry. *Physical Review Letters,* **69**: 1293-1295 (1992)

[11] P. Michler *et al,* Quantum correlation among photons from a single quantum dot at room temperature. *Nature*, **406**: 968 (2000)

[12] P. Michler *et al,* A Quantum Dot Turnstile Device. *Science*, **290**: 2282-2285 (2000)

[13] S. Fasel *et al*, High quality asynchronous heralded single photon source at telecom wavelength. *New Journal of Physics*, **6**: 136 (2004)

[14] H. J Kimble, M. Dagenais and L. Mandel, Photon antibunching in resonance fluorescence. *Physical Review Letters*, **39**: 691-695 (1977)

[15] Th. Basché et al, Photon antibunching in the fluorescence of a single dye molecule trapped in a solid. *Physical Review Letters*, **69**: 1516-1519 (1992)

[16] C. Kurtsiefer, S. Mayer, P. Zarda and H. Weinfurter, Stable solid-state source of single photons. *Physical Review Letters*, **85**: 290-293 (2000)

[17] M. A Reed, Quantum Dots. *Scientific American*, **268**: 118-123 (1993)

[18] J. Kim, O. Benson, H. Kan and Y. Yamamoto, A single photon turnstile device. *Nature,* **397**: 500-504 (1999)

[19] T. Aichle, G. Reinandi and O. Benson, Separating cascaded photons from single quantum dot: Demonstration of multiplexed Quantum Cryptography. *Physical Review B,* **70**: 235329 (2004)

[20] M. Benyoucef *et al,* Enhanced correlated photon emission from a pillar microcavity. *New Journal of Physics,* **6**: 91 (2004)

[21] M. Pelton *et al*, Efficient source of single photons: A single quantum dot in a micropost cavity. *Physical Review Letters*, **89**: 233602 (2004)

[22] P. G. Kwait, K. Mattle, H. Weinfurter and A. Zeilinger, New high-intensity source of polarization entangled photon pairs, *Physical Review Letters*, **75**: 4337-4341 (1995)

[23] B. Lounis and M. Orrit, Single photon sources. *Reports on Progress in Physics,* **68**: 1129-1175 (2005)

[24] S.A. Castello and R.E. Scholten*,* Heralded single photon sources: A route towards quantum communication technology and photon standards. *The European Physical*

Journal: Applied Physics, **41**: 181-194 (2008)

[25] A. Kuhn, M. Hennrich and G. Rempe, Deterministic single photon source for distributed quantum networking. *Physical Review Letters*, **89**: 067901 (2002)

[26] K. Matthias *et al,* Continuous generation of single photons with controlled waveform in an ion trap cavity system. *Nature*, **431**: 1075-1078 (2004)

[27] B. Darquie et al, Controlled single photon emission from a single trapped two level-atom. *Science* **309**: 454-456 (2005)

[28] B. Lounis and W. E Moerner, Single photons on demand from a single molecule at room temperature. *Nature*, **407**: 491-493 (2000)

[29] F. Treussart, R. Alléaume, J.-M Courty and J.-F Roch, Emission properties of a single photon source. *Physica Scripta,* **T112**: 95-98 (2004)

[30] C. Brunel, B. Lounis, P. Tamarat and M. Orrit, Triggered source of single photons based on controlled single molecule fluorescence. *Physical Review Letters*, **83**: 2722-2725 (2002)

[31] A. Beveratos, R. Brouri, J.-P. Poizat and P. Grangier, Bunching and antibunching from single NV's in diamond. *e-print: arXiv: quant-ph/0010044v1* (2000)

[32] T. Gaebal, I. Popa, A. Gruber, M. Domhan, F. Jelezko and J. Wrachtrup, Stable single photon source in the near infrared. *New Journal of Physics,* **6**: 98 (2004)

[33] K. Johnston and A. Mainwood, Properties of nickel nitrogen complexes in diamond: stability and electronic structure. *Diamond and Related Materials*, **12**: 516-520 (2003)

[34] J. R. Rabeau, Fabrication of single nickel nitrogen defects in diamond by chemical vapor deposition. *Applied Physics Letters*, **86**: 131926 (2005)

[35] E. Wu *et al*, Room temperature triggered single photon source in the near infrared. *New Journal of Physics,* **9**: 434 (2004)

[36] H. Sternschulte, K. Thonke, R. Saue, P. C. Münzinger and P. Michler, 1.681-eV luminescence centre in chemical vapor deposited homo-epitaxial diamond films. *Physical Review B*, **50**: 14554 (1994)

[37] C. Wang, C. Kurtsiefer, H. Weinfurter and B. Burchard, Single photon emission from SiV centres in diamond by ion implantation. *Journal of Physics B: Atomic, Molecular and Optical Physics,* **38**: 37-41 (2006)

[38] H. Hanzawa *et al,* Disorder effects of nitrogen impurities, irradiation-induces defects

and ^{13}C isotope composition on the Raman spectrum in synthetic Ib diamond. *Physical Review B*, **54**: 3793-3799 (1996)

[39] A. T. Collins, M. F. Thomaz and M. B. Jorge, Luminescence decay time of the 1.945 eV centre in Type Ib diamond. *Journal of Physics C: Solid State Physics*, **16**: 2177 (1983)

[40] A. Beveratos, R. Brouri, J.-P. Poizat and P. Grangier, Photon antibunching in the fluorescence of individual colour centres in diamond. *e-print: arXiv quant- ph/0010044v1* (2000)

[41] J. N. Murrell, S.F.A. Kettle and J. M. Tedder, *Valence Theory, 2nd edition,* page 80, Wiley and Sons Ltd (1970)

[42] http://en.wikipedi.org/wiki/Diamond_cubic

[43] W. Kaiser and W. L. Bond, Nitrogen: a major impurity in common Type I diamond. *Physical Review,* **115** : 857-863 (1959)

[44] A. Mainwood, Substitutional impurities in diamond. *Journal of Physics C: Solid State Physics*, **12**: 2543-2549 (1979)

[45] K. LAkoubovskii, Optical study of defects in diamond. *PhD Thesis*, Katholieke University Leuven (2000)

[46] http://www.diamondlab.org

[47] A. C. Jones and M. Hitchman, *Chemical Vapor Deposition: Precursors, Processes and Applications* : 1-36, Royal Society of Chemistry, Cambridge (2009)

[48] J. A. van Wyk, Carbon-12 hyperfine interaction of the unique carbon of P2 (ESR) or N3 (optical) centre in diamond. *Journal of Physics C: Solid State Physics*, **15**: L981(1982)

[49] G. Davies *et al*, Vacancy related centres in diamond. *Physical Review B*, **46**: 13157-13170 (1992)

[50] J. Walker, Optical absorption and Luminescence in diamond. *Reports on Progress in Physics,* **42**: 1605-1659 (1979)

[51] http://www.xqp.physik.uni-muenchen.de

[52] Y. Mita, Change of absorption spectra in Type -1b diamond with heavy neutron irradiation. *Physical Review B*, **53**: 11360 (1996)

[53] J. Meijer *et al*, Generation of single colour centres by focused nitrogen implantation. *arXiv: cond-mat/0505063* (2005)

[54] J. Rabeau *et al,* Implantation of labeled single NV centres in diamond using ^{15}N. *arXiv: cond-mat/0511722* (2005)

[55] N. B. Mason, J. P. Harrison and M. J. Sellars, Nitrogen vacancy centre in diamond: model of the electronic structure and associated dynamics. *Physical Review B*, **74**: 104303 (2006)

[56] F. Jelezko and J. Wrachtrup, Read-out of single spins by optical spectroscopy. *Journal of Physics: Condensed Matter*, **16**: R1089 (2004)

[57] J. M. Hollas, *Modern Spectroscopy*, *4th edition*, page 33, Wiley and Sons Inc (2004)

[58] G. R. Fowles, *Introduction to Modern Optics,* page 80 Holt, Rinehart and Winston Publication (1975)

[59] J. A. Weil, J. R. Bolton and J. E. Wertz, *Electron Paramagnetic Resonance: Elementary theory and applications,* page 21, Wiley and Sons Inc (1994)

[60] W. V. Smith, P. P. Sorokin, I. L. Gelles and G. J. Lasher, Electron Spin Resonance of Nitrogen Donors in Diamond. *Physical Review*, **115**: 1546 (1959)

[61] M. D. Lumb, *Luminescence Spectroscopy,* page 93 Academic Press (1978)

[62] A. Gruber, A. Dräbenstedt, C. Tietz, L. Fleury, J. Wrachtrup and C. von Borczyskowski, Scanning confocal optical microscopy and magnetic resonance on single defect centres. *Science*, **276**: 2012-2014 (1997)

[63] A. T. Collins, A spectroscopic survey of naturally-occurring vacancy-related colour centres in diamond. *Journal of Physics D: Applied Physics,* **15**: 1431-1438 (1982)

[64] C. A. Klein, T. M. Hartnett and C. J. Robinson, Critical-point phonon frequencies of diamond. *Physical Review B,* **45**: 12854-12863 (1992)

[65] S.C. Lawson, D. Fisher, D. C. Hunt and M. E. Newton, On the existence of positively charged single substitutional nitrogen in diamond. *Journal of Physics: Condensed Matter*, **10**: 6171 (1998)

[66] T. Hainschwang, F. Notari, E. Fritsch and L. Massi, Natural, untreated diamonds showing the A, B and C infrared absorptions (" ABC diamonds"). *Diamond and Related Materials* **15**: 1555-1564 (2006)

[67] N. A. Nadolinny *et al,* EPR spectra of separated pairs of substitutional nitrogen atoms in diamond with high concentration of nitrogen. . *Physical Review B*, **60**: 5392 (1999)

[68] W. V. Smith, P. P. Sorokin, L. L. Gelles and G. J. Lasher, Electron-Spin Resonance of

nitrogen donors in diamond. *Physical Review*, **115**: 1546-1553 (1959)

[69] http://www.olympusfluoview.com

[70] R. Hanbury Brown and T. Q. Twiss, Correlation between photons in two coherent beams of light. *Nature*, **177** :27-29 (1956)

[71] A. Beveratos, R. Brouri, T. Gacoin, J-P Pizat and P. Grainger, Non-classical radiation from diamond nanocrystals. *Physical Review A*, **64**: 061802 (2001)

[72] J. P. D. Martin, Fine structure of excited ^{3}E state in nitrogen vacancy centre of diamond. *Journal of Luminescence*, **81**: 237 (1999)

[73 L. Amoros, *The Laue method.* Academic Press (1975)